Autogenous Shrinkage of Alkali-Activated Materials

Zhenming Li, Farid Benboudjema, Brice Delsaute, Vilma Ducman, Zhangli Hu, Maïté Lacante, Ning Li, Tianshi Lu, Yang Lv, Yuwei Ma, Zhengyao Qu, Jesus Rodriguez-Sanchez, Stéphanie Staquet, Babak Vafaei, Guang Ye, Hailong Ye, Kangting Yin, Zuhua Zhang, Xiaohong Zhu, and Lea Žibret

Abstract Alkali-activated materials (AAMs), as eco-friendly alternatives to Portland cement (PC), have attracted increasing attention of researchers and users in the past decades. Despite the eco-friendly nature of AAMs, doubts about these materials as an essential ingredient of concrete exist, regarding, for example, their volume stability. One possible volume change concerns autogenous shrinkage. Autogenous

Z. Li (✉) · K. Yin
School of Intelligent Civil and Ocean Engineering, Harbin Institute of Technology, Shenzhen, China
e-mail: zhenmingli@hit.edu.cn

Z. Li
Guangdong Provincial Key Laboratory of Intelligent and Resilient Structures for Civil Engineering, Harbin Institute of Technology, Shenzhen, China

F. Benboudjema
CentraleSupélec, ENS Paris-Saclay, CNRS, LMPS-Laboratoire de Mécanique Paris-Saclay, Université Paris-Saclay, Gif-Sur-Yvette, France

B. Delsaute · M. Lacante · S. Staquet
BATir Department, Université Libre de Bruxelles, Brussel, Belgium

V. Ducman · L. Žibret
ZAG –Slovenian National Building and Civil Engineering Institute, Ljubljana, Slovenia

Z. Hu
School of Materials Science and Engineering, Southeast University, Nanjing, China

N. Li
Department of Civil Engineering and Management, University of Manchester, Manchester, UK

T. Lu
School of Civil Engineering and Geomatics, Southwest Petroleum University, Chengdu, China

Y. Lv · Z. Qu
State Key Laboratory of Silicate Materials for Architectures, Wuhan University of Technology, Wuhan, China

Y. Ma
Research Center for Wind Engineering and Engineering Vibration, Guangzhou University, Guangzhou, China

G. Ye and F. Dehn (eds.), *Mechanical Properties of Alkali-Activated Materials*, RILEM State-of-the-Art Reports 46, https://doi.org/10.1007/978-3-032-07116-3_10

shrinkage is the self-created volume reduction of materials due to chemical reactions without the need for substance or heat exchange with the environment. If the autogenous shrinkage of a binder material is too large, cracking might happen, which will seriously impair the durability of concrete. The aim of this chapter is to provide a state-of-the-art review on the autogenous shrinkage of AAMs. The different characteristics and mechanisms of autogenous shrinkage of different AAMs are reported. Corresponding shrinkage-mitigating strategies are summarized. Existing models to simulate and predict the autogenous shrinkage of AAMs are reviewed. Remarks are then given on testing methods of autogenous shrinkage, which link back to the determination of the magnitude of autogenous shrinkage of AAMs. Connections between autogenous shrinkage and other deformations such as drying shrinkage, thermal deformation and creep are also discussed. Research gaps and outlook on future research in this field are given in the end.

Keywords Autogenous shrinkage · Alkali-activated materials · Mechanisms · Mitigation · Modelling

1 Introduction

Poor volume stability has been recognized as one main reason why AAMs have not been widely used in civil engineering. While various types of shrinkages can be shown by binder materials and concrete, autogenous shrinkage is a critical one because it develops fast at the early age when the binder material remains weak under tension [1]. Moreover, autogenous shrinkage is a type of deformation that is more "intrinsic" compared to drying shrinkage, carbonation shrinkage, creep, and

J. Rodriguez-Sanchez
Kingspan Innovation Centre IKON, Kingscourt, County Cavan, Ireland

B. Vafaei
Department of Civil, Architectural and Environmental Engineering, University of Miami, Coral Gables, USA

G. Ye
Section Materials and Environment, Department of 3Md, Faculty of Civil Engineering and Geosciences, Delft University of Technology, Delft, Netherlands

H. Ye
Department of Civil Engineering, The University of Hong Kong, Pokfulam, Hong Kong, China

Z. Zhang
Key Laboratory of Advanced Civil Engineering Materials of Ministry of Education, Tongji University, Shanghai, China

X. Zhu
Key Laboratory of Urban Security and Disaster Engineering of Ministry of Education, Beijing University of Technology, Beijing, China

thermal shrinkage, since autogenous shrinkage is a self-created phenomenon associated with on-going chemical reactions and internal stress [2]. Under drying conditions or thermal shock where drying (and possibly carbonation) shrinkage or thermal deformations are involved, autogenous shrinkage still exists and will be coupled with these deformations. Hence, having a clear understanding of the autogenous shrinkage behaviour of AAMs is vital for the evaluation and prediction of the performance of these materials in engineering.

However, significant variety exists in not only the precursors but also the activators to synthesise AAMs [3]. This results in the fact that different shrinkage characteristics are exhibited by different AAMs [4, 5]. It is challenging to comprehensively clarify the mechanisms of autogenous shrinkage of AAMs made from different raw materials. Yet, that is necessary, otherwise the development of shrinkage-mitigating strategies for AAMs would be mainly in a "trial and error" manner due to the absence of clear guidance. That is the reason why a relatively big expert team was formed to write this chapter, aiming to cover all kinds of AAMs and to provide a state-of-the-art review of the autogenous shrinkage behaviours of these materials.

This chapter is organized in a way shown in Fig. 1, with the autogenous shrinkage characteristics and mechanisms of each system reviewed at first. From the perspective of subject, the autogenous shrinkage behaviours will be reviewed for alkali-activated ground granulated blast furnace slag (AAS), alkali-activated fly ash (AAFA), alkali-activated MK/calcined clay (AAMK), AAMs made from other raw materials, blended AAM systems, and one-part AAMs, individually. A short summary and comparison of the shrinkage behaviours of these systems will be given after these sub-sections. The section after is focused on the mitigating strategies of the autogenous shrinkage of AAMs. Modelling and prediction are then discussed. Review and remarks on the testing methods of autogenous shrinkage-related properties are given in the next section. In addition, special attention is paid to the connections between autogenous shrinkage and other deformations, highlighting the important role of autogenous shrinkage in the volume stability of AAMs. Conclusions and perspectives are given in the end of this chapter. Cracking proneness induced by restrained shrinkage is so important that it is reviewed not here but in a separate chapter (Chap. "Restrained Shrinkage of Alkali-Activated Materials").

2 Autogenous Shrinkage of AAMs

2.1 Alkali-Activated Slag

Characteristics. It has been reported by Bakharev et al. [6], Kumarappa et al. [7], and Chen et al. [8] that the autogenous shrinkage of AAS materials was about 5–7 times compared with that of PC. The shrinkage of AAS concrete is dependent on the characteristic of the mixing components (i.e., composition [9] and fineness of the slag [10, 11], type and dosage of activator [11–16] and modulus of water glass

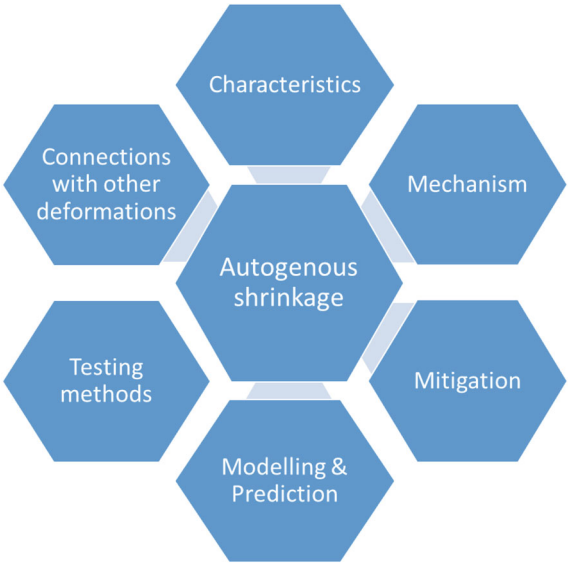

Fig. 1 Outline of this Chap. "Classification, Terminology and Abbreviations" Autogenous shrinkage of AAMs

solution [17]), curing conditions [11, 18, 19], aggregate stiffness, aggregate to slag ratio [17], and the hydration process [20]. Factors affecting the shrinkage of the AAS have been summarized in the following review papers [17, 21–26].

The reactivity and strength of AAS materials are strongly influenced by the particle size and fineness of slag. Smaller slag particles, particularly those below 20 μm, react rapidly within the first 24 h, enhancing early strength [3, 27, 28]. Greater fineness (higher specific surface area) increases water demand and accelerates setting [22], and particles in the 2–30 μm range lead to higher long-term strength [29]. Finer slag particles, typically with a specific surface area above 3500 cm^2/g, improve early strength and long-term compressive strength due to reduced porosity and increased surface density [30–32]. However, excessive fineness beyond 4000 cm^2/g has limited benefits for 28-day strength and may even decrease that due to increased porosity [33, 34]. Optimal fineness for maximum strength is reported between 4000 and 5500 cm^2/g, depending on the slag type [35, 36]. A few cases, for example, that need rapid hardening may need finer slag particles.

Despite a large number of studies of the effect of slag fineness on the reactivity, flowability, workability, setting time, and compressive strength of alkali-activated slag pastes, a few studies exist in the literature on its influence on autogenous shrinkage. Nevertheless, relatively larger number of publications have investigated the effect of GGBFS fineness in slag cement pastes, where GGBFS were used as the replacement of cement at different percentages [37–40].

Alkali hydroxide (ROH), nonsilicic salts of weak acids R_2CO_3, R_2S, RF, or silicic salts of the $R_2O \cdot nSiO_2$, are the most effective materials to activate aluminusilicates such as GGBFS and fly ash (FA), etc. where R represents an alkali metal ion such as sodium, potassium, and lithium [30]. Among different activators, sodium hydroxide

(NaOH), potassium hydroxide (KOH), sodium carbonate (Na_2CO_3), and sodium silicates (also known as water glass) $Na_2O \cdot nSiO_2 \cdot mH_2O$ are the most common alkaline activators reported in the literature. Depending on the type of alkaline activators used to produce concrete/paste, the short-term and long-term properties of concrete/paste vary. For example, Brough and Atkinson [41] compared degree of reaction, microstructure, and strength of sodium silicate and KOH-activated mortars. They reported that mortars activated by KOH resulted in higher 1-day strength, however, the subsequence strength development was much lower than the mortars activated by sodium silicate. Despite the lower strength of KOH-activated mortars, the degree of reaction was obtained 57% higher than that for activation of the same slag with sodium silicate. Compared to sodium silicate-activated mix, the microstructure of mix activated by KOH was much more heterogenous with more porosity and interfacial porosity [41].

Many studies have recently investigated the effects of the alkaline type and concentration on the mechanical properties of shrinkage of AAS systems. Recent studies [42–45] showed that decreasing alkaline content and alkali-activated modulus (M_s, corresponding to the molar ratio of SiO_2/Na_2O) can effectively alleviate drying and autogenous shrinkages in AAS systems because of the reduced hydration reaction. More specifically, by increasing the M_s and alkaline dosage, the porosity or the pore structure within the AAS matrix is densified. Chen et al. [45] attributed the increase in autogenous shrinkage when alkali dosage and M_s increases to the enhanced capillary pore pressure and syneresis of C–A–S–H gels, caused by the enhanced reaction degree under a high alkaline environment.

In their research, Kang and Kim [46] illustrated the pore size distribution versus alkaline concentration. Their results showed that the reduction in alkaline concentration lowered the portion of the medium capillary (0.05–0.01 μm) and gel (~<0.01 μm) pores and increased the large capillary pores (10–0.05 μm) content, resulting in a reduction in shrinkage magnitude [16, 19, 47]. Kumarappa et al. [7] further confirmed that a higher amount of both M_s and Na_2O resulted in larger capillary stress, leading to greater autogenous shrinkage. However, although decreasing M_s and alkaline contents reduces the shrinkage, the reduction is unbeneficial to AAS systems for the development of strength [48]. This was further confirmed by Zhang et al. [49], who investigated the effects of M_s and Na_2O-to-binder ratio by weight, N/B on the mechanical behaviour and drying shrinkage of AAS mortars made with seawater and coral sand. They found that reducing M_s from 1.6 to 1.0% and N/B ratio from 6.0 to 3.0% decreased drying shrinkage by approximately 44% and 15%, respectively, though compressive and flexural strength were not improved. The optimal values for balancing shrinkage and strength were an M_s of 1.2 and an N/B of 4% according to them. Fang et al. [86] further observed that increasing M_s enhances compressive strength and reduces chloride penetration, though it also raises drying shrinkage and lowers flexural strength.

Hu et al. [50], explored the effect of M_s on autogenous and drying shrinkage of alkali-activated slag mortars. Their results showed that with the increase of M_s from 0 to 0.5, the autogenous shrinkage of AAS mortars increased, and reduced when the ratio increased up to 1.5. Cartwright et al. [51] reported that lowering Ms and

alkali dosage in NaOH-activated slag mortars reduced both autogenous and drying shrinkages, with a more significant reduction in autogenous shrinkage.

The shrinkage of the AAS system varies notably with curing conditions (i.e., curing temperature, methods, and humidity). The typical curing technics are thermal curing, sealing, steaming, and water immersion [11]. Humad et al. [52] investigated the impact of different curing regimes on the shrinkage of AAS concretes, using four curing procedures: heat-treatment and no-heat-treatment, in both sealed and unsealed conditions. They found that combined heat-treatment with sealed curing reduced the shrinkage by 30–50%, whereas non-heat-treated and unsealed samples exhibited higher shrinkage. This shrinkage reduction is attributed to an enhanced polymerization reaction, leading to a denser microstructure with greater tensile strength. Sealed curing creates a dense structure that resists volumetric changes and limits microcracking, preventing drying shrinkage. Additionally, heat treatment promotes a coarser matrix, lowering tensile strain from pore water evaporation and reducing shrinkage. Bakharev et al. [53] also demonstrated that higher curing temperatures promote intense reaction products around slag particles, limiting further dissolution and solidification reactions.

Cai et al. [54] examined the impact of early-age curing methods, including elevated-temperature water curing (20, 40, and 60 °C) and CO_2 curing, on the shrinkage of alkali-activated slag concrete (AASC) with target strengths of C30 and C50. They found that, under the same conditions, C30 concrete exhibited higher shrinkage than C50, due to its higher water-to-binder ratio and greater free water content. Water and CO_2 curing were more effective in reducing shrinkage than air curing, with heat curing at 60 °C reducing shrinkage by up to 80%. CO_2 curing reduced drying shrinkage by 49% in C30 and 53% in C50 due to decalcification of C–A–S–H gels, which decreased porosity and altered pore size distribution. High-temperature water curing proved most effective, followed by CO_2 curing, while air curing was the least effective and increased shrinkage. Similarly, Chi [55] noted that the lowest shrinkage occurred in AASC cured in a heat room at 60 °C with 80% relative humidity (RH), followed by limewater and air curing, as the reduced water content in C–S–H gel formed during heat curing helps to lower shrinkage.

Ye et al. [56] observed that increasing RH from 30 to 85% led to a 30–35% reduction in shrinkage in samples activated with various activators and alkali content. High RH conditions promote hydration, resulting in more hydration products and reduced desiccation of the pores [20]. Under high RH, AAS exhibits lower capillary pressure, but it still shows visco-elastic/visco-plastic behavior leading to irreversible shrinkage [57].

In a recent review paper, Zhang et al. [58] summarized and tabulated the effect of various curing conditions on the shrinkage of AAS mortars, pastes, and concrete reported in the literature, including curing methods, curing temperature, RH, activator type, alkaline content, M_s, and shrinkage values. It can be concluded that water curing is the most effective curing method, and air curing achieved the least shrinkage-reducing effect. In addition, high-temperature curing, and heat treatment can effectively mitigate the shrinkage of AAS systems. The shrinkage-reducing effect of heat treatment is more pronounced when the samples are under sealed conditions.

Mechanisms. Although various assumptions were made regarding the reasons behind the higher magnitude of the shrinkage of AAS compared to PC, most of them have attributed this to the microstructure of AAS and PC. More specifically, a lower pore volume is generated in AAS than PC at the same degree of hydration, but the pore size distribution of AAS is characterized by a higher volume of gel pores [59]. Therefore, it can be indirectly understood that AAS shrinkage is largely associated with the reaction products and RH, although shrinkage is a complex phenomenon and depends on several factors such as, hydration degree, RH, modulus of elasticity, viscoelastic and viscoplastic properties, and possibly internal microcracks [60–62]. More details are discussed in the following.

Pore structure. Yang et al. [63] measured the total porosity of AAS pastes using Mercury Intrusion Porosimetry (MIP). Their results showed that the volume percentage of mesopores in AAS pastes was 91.1%, 91.2%, and 89.9% at 3, 7, and 28 days, respectively. The larger proportion of mesopores volume in AAS pastes compared to PC was further confirmed in [12, 59, 63–66]. The small pore size creates greater capillary tension compared to larger pore sizes. Because of the fine pore structure, a certain chemical shrinkage would make a small radius of the meniscus in the AAS pastes, resulting in a high pore pressure [1, 57]. In other words, the higher percentage of mesopores in AAS leads to higher capillary stress, resulting in higher shrinkage during the drying process. According to Shi et al. [12], PC mortars demonstrate a continuous pore distribution, with pore sizes ranging from 50 to 12,000 Å. In contrast, the diameters of pores in AAS mortars are under 100 and over 2000 Å. Moreover, Aydın et al. [67] reported that in addition to the water loss in the mesopores, the size of the mesopores plays an important role since the size of the macropores determines the ease of water removal from the mesopores. Loss in the mesopores, the size of the mesopores plays an important role since the size of the macropores determines the ease of water removal from the mesopores. Melo Nito [59] reported that the presence of lower total porosity and higher mesopores volume directly relates to the content of the activator. They showed that this characteristic is linked to a high degree of hydration and a predominant presence of C–S–H in the hydrated products.

Hydration products (1. Silica-rich gel). Some researchers pointed out that AAS concretes based on water glass often experience greater shrinkage caused by forming silica or silica-rich gel during hydration [17, 68, 69]. According to Glukhowsky et al. [70], in alkali-activated slag, the initial phases are rich in silica hydrosilicates and silica acid. The silica acid can then be polymerized into silica gel. At alkaline environment, the ease of silicic acid to condense is increased when it is slightly dissociated or in a molecular state and takes place within only a few minutes. The silica gel with a high-water content begins to shrink and expel water from the mass. The shrinkage begins with this syneresis process when free liquid enmeshed in the gel is spontaneously expelled. This syneresis ends when the water content of the gel is still high (~90%). On further drying, the structure of the gel continues to shrink, and the number of particle-to-particle bonds in the structure gradually breaks. The formation of silica or silica-rich gels in the hydration products and its role in the lager shrinkage of AAS pastes than PC pastes was further confirmed by Krizan et al.

[71], who reported that in dry conditions, silica gel with high water content easily dehydrates, producing a relatively large shrinkage of the pastes.

Hydration products (2. C–S–H gel). The C–S–H phases in PC and AAS pastes demonstrated differences in terms of morphology, crystallinity, and chemical composition [72–75]. Yang et al. [63] observed a loose density reticular C–S–H and dense rod like C–S–H gels in the morphology of hydration products of AAS pastes. In contrast, a needle-like C–S–H phase forms in PC pastes with a low Si content [75–77]. To measure the surface area of the pastes, Tennis et al. [78] conducted nitrogen sorption and classified C–S–H gels into low-density and high-density C–S–H gels [78]. The hydration products of alkali-activate slag pastes possess a higher specific area, compared with PC pastes. This indicates that in AAS pastes low-density C–S–H dominates a higher fraction of hydration products than PC pastes. In addition, a lower Ca/Si ratio was obtained in hydration products of C–S–H gels in AAS pastes (Ca/Si = 1.1) than PC pastes (Ca/Si = 2.0). The shrinkage is mainly caused by the formation of low-density C–S–H gels in hydration products of pastes and tends to take place in C–S–H gels with a low Ca/Si ratio [12, 63, 75, 79]. This type of C–S–H gel has a structure similar to that of 1.1 nm tobermorite, possessing a poor water-retaining property [80]. Consequently, moisture inside AAS paste would be eliminated easily and rapidly, resulting in fast shrinkage [81].

Hydration products (3. Presence of other crystalline phases in PC but their absence in AAS pastes). Regardless of the formation of C–S–H gels, other phases (i.e., portlandite, ettringite, monosulfate, Aft, and AFm) are formed in PC pastes. However, these crystals were undetectable in AAS pastes [72, 82]. The main hydration products of AAS are C–A–S–H with a low Ca/Si ratio and hydrotalcite [41, 72] (the formation of AFm phase in AAS pastes activated by NaOH was reported by Wang and Scrivener [72]). The mentioned crystalline structures in PC pastes barely generate shrinkage under drying conditions; however, these crystals serves as fine aggregates in the paste structures, leading to partially alleviating the drying shrinkage of the pastes [83]. By contrast, there is a lack of crystalline phases that can resist the "sliding" of C–A–S–H gel in AAS pastes, which would induce viscoplastic deformation [62].

Hydration products (4. Rearrangement of C–A–S–H gel). Ye and Radlińska [43] investigated the effectiveness of three shrinkage mitigation strategies (i.e., high-temperature curing, sulphate-enrichment, and calcium-enrichment) in mitigating the shrinkage of AAS pastes. According to them, the autogenous shrinkage of AAS pastes highly depends on the internal RH, and the capillary pressure was confirmed as the main driving force for AAS shrinkage at RH >~ 50%. It was reported that the autogenous shrinkage is regardless of the moisture loss. The moisture loss of cementitious materials at a given RH varies depending on the pore structure and physicochemical properties of pore solution [43]. The generation of capillary pressure due to the formation of menisci in pores as the main driving force for shrinkage in cementitious materials was previously studied by [84–87]. Moreover, they showed that the cause of large shrinkage in AAS is due to the high viscoelastic/viscoplastic compliance (i.e., low creep modulus) of alkali-enriched C–A–S–H. Under a constant magnitude of effective capillary pressure, the AAS porous body shows a compliant

viscoelastic/viscoplastic response to that stress. In other words, the main component of shrinkage in AAS pastes is the time-dependent of C–A–S–H. Under pore pressure, C–A–S–H can be rearranged/reorganized, exhibiting pronounced viscous characteristics in AAS pastes [58]. The viscous characteristics of AAS was further confirmed by Ye et al. [88], indicating that AAS is a viscoelastic/viscoplastic material with low creep modulus. Characterizing the shrinkage of AAS at various RH could be a potential way to illuminate different shrinkage mechanisms of AAS. It should be noted that at different RH ranges and over various sizes of pores, different shrinkage mechanisms may dominate [87].

Ye et al. [88] characterized the shrinkage performance of AAS at four different levels of RH. They reported a higher mass loss and slower shrinkage kinetics in AAS compared to PC at similar RH. They showed that the ultimate shrinkage of AAS mixtures depends not merely on the RH or mass loss, but on the drying rate and drying history. In addition, they concluded that it is the high viscoelastic/viscoplastic compliance (low creep modulus) of its solid skeleton that is the cause of high-magnitude shrinkage in AAS mortar rather than a higher driving force.

Further, the incorporation of alkali metal cations in C–A–S–H gel weakens the regularity of the arrangement of C–A–S–H layers [89], leading to the collapse and redistribution of C–A–S–H during drying [86]. As such, this results in the large shrinkage of AAS pastes [90].

2.2 Alkali-Activated FA

As introduced in Chap. "Conventional Precursors and Activators" already, FA is a mixture of spherical particles consisting of both amorphous and crystalline constituents, primarily calcium, silicon, aluminium, and iron oxides. FA itself does not have hydraulic properties, but the addition of alkaline activators such as NaOH, KOH and $Ca(OH)_2$ into FA can greatly stimulate the pozzolanic activity of FA and make it interact with alkaline solution. Elevated temperature curing is normally applied on AAFA synthesis in order to achieve relatively high early age strength. Given a proper mix proportion and curing condition, the general engineering properties of AAFA mixtures can be equal or even superior to Portland cement-based mixtures.

Although AAFA or FA-based geopolymer have demonstrated outstanding mechanical characteristics in construction in comparison to conventional PC composites, there are still challenges in the widespread utilization of this material. The most striking difficulty is their volumetric instability (i.e., high shrinkage) [91]. The high shrinkage rate of AAFA is closely related to the nature of the raw material, the type of alkali activator, the pore structure and the reaction product of the pasty matrix.

Characteristics. Research on the autogenous shrinkage of AAFA is limited. More attention is paid to the drying shrinkage of AAFA, as well as the autogenous shrinkage of alkali-activated slag-containing system in previous studies. Since a relatively high temperature (e.g. 40, 60 or 80 °C) is normally applied during the initial curing

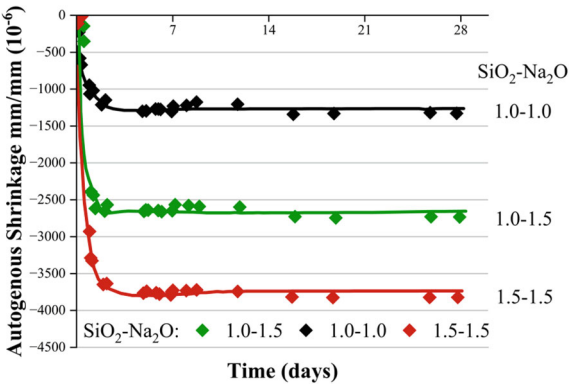

Fig. 2 Autogenous shrinkage of AAFA pastes with different SiO_2 and Na_2O content, 40 °C (corrugated tube method, measurement started after the time of final setting) [92]

of AAFA, the measurement of autogenous shrinkage in the early age is difficult. The autogenous shrinkage of AAFA (class F fly ash) with different activator content (Na_2O and SiO_2 content) was studied at the curing temperature of 40 °C [92]. Figure 2 shows the autogenous shrinkage of AAFA pastes measured by the corrugated tube method (the autogenous shrinkage was the mean value of three replicates for each specimen in Fig. 2 and the standard deviations are also shown in this figure). At an elevated curing temperature, most of the autogenous deformation of AAFA mixtures happened in the first 1–3 days. After 3 days, the autogenous shrinkage value kept almost constant. The specimens with the highest sodium and silica content (SiO_2–Na_2O = 1.5–1.5) exhibited the highest autogenous stain, followed by specimens 1.0–1.5 and 1.0–1.0.

Generally, the autogenous shrinkage of AAFA pastes is important for the internal tensile stress developed in the matrix. If a large autogenous strain is developed under the restrained condition, there is a (high) possibility of cracking for the samples. It is noticed in Fig. 2 that the autogenous strain was very high for the three AAFA mixtures (e.g. around 3800 μm/m for mixtures SiO_2–Na_2O = 1.5–1.5). However, this large strain did not necessarily lead to an early age cracking of the samples. As shown in the ellipse ring tests (Fig. 3), no cracks were observed on the surface of the three AAFA mixtures after sealed curing at 40 °C for 7 days (Fig. 3). It indicates that the stress caused by the autogenous strain is lower than the tensile strength of the AAFA pastes, which can be related to two reasons: a low elastic modulus of the AAFA mixtures at the very early stage and/or a large creep with relaxation.

Mechanisms: As known for cement paste, the autogenous shrinkage happens (after setting) because of the self-desiccation of the hydrating mixtures. The capillary pressure has been widely acknowledged as the main driving force for autogenous shrinkage. Samples with a higher capillary pressure show a larger magnitude of autogenous shrinkage. The generation of capillary pressure is associated with the drop of internal RH. For AAFA pastes, the relationship between the internal RH and autogenous shrinkage appears to be very different from PC paste. The measured internal RH of a typical AAFA paste SiO_2–Na_2O = 1.5–1.5 at curing temperature of 40 °C is shown in Fig. 4. The internal RH of the samples shows a fast increase in the

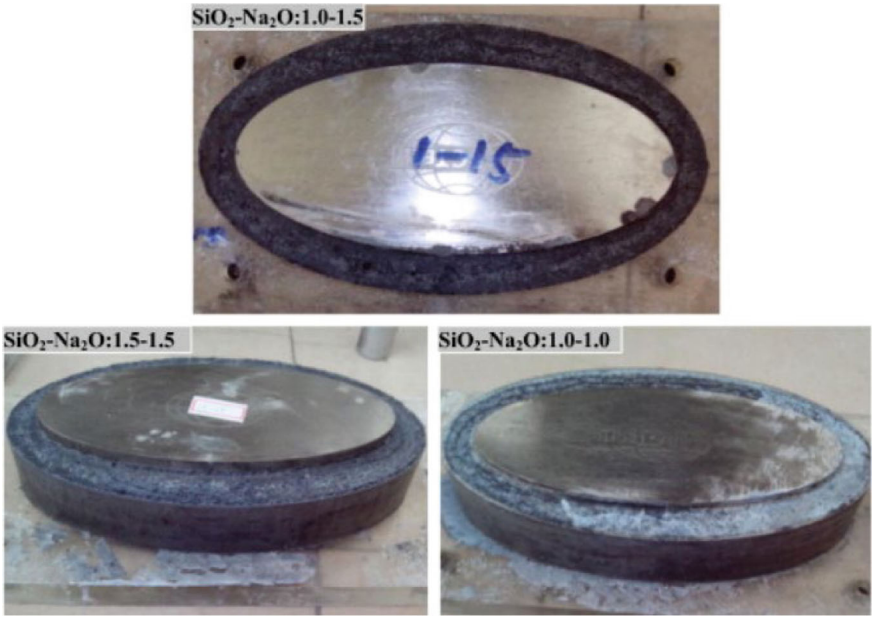

Fig. 3 Ellipse ring test for AAFA pastes after sealed cured at 40 °C for 7 days (demolded): cracking was not observed on the surface of all AAFA pastes

first 1–2 h from roughly 80% to about 90%. After that, the RH gradually increased with time. At later age, a high internal RH (>98%) was reached and kept constant. This phenomenon is very different from PC paste, of which the internal RH may drop to 70–80% for the PC paste with a lower w/c ratio.

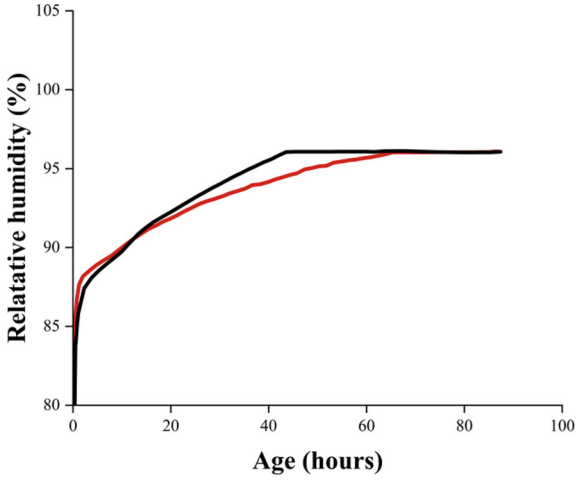

Fig. 4 Measured internal RH with curing time for two samples of AAFA pastes 1.5–1.5 (curing temperature 40 °C) [92]

The increase of the measured RH in the first 40 h may be caused by two processes: (1) The moisture equilibration process between the RH sensor and the specimens. (2) The decrease of salts content (Na^+ and Si^{4+}) in the activating solution with progress of the reaction. In the beginning, the activating solution contains a certain amount of silica and sodium. Due to these salts, the initial RH is lower than 100% (86% calculated according to Raoult's law [1]. During the alkali activation, the alkali and silica ions react with the FA particles and will become incorporated in the reaction products. The concentration of these ions in the pore fluid decreases, which in turn leads to an increase of internal RH with time (Fig. 4). Hu et al. [93] investigated the internal RH evolution of AAFA (activated by NaOH and by Na_2SiO_3) at different curing temperature. They also observed the internal RH of AAFA stared with a low value and increased with age. They agreed that that the initial low RH in AAFA is caused by the high ion concentration in the pore solution. Since the trend of RH can indicate the consumption rate of ions, a method based on this to estimate the reaction kinetics of AAFA was then proposed [93].

From the results, it is clear that in AAFA pastes, the internal RH did not decrease with the with the ongoing reaction process. Even at longer curing age, the non-evaporable water content in AAFA mixtures was kept almost unchanged (Fig. 5). The non-evaporable water content is much lower than that in cement paste, where a value of 12–16% was normally reported, depending on the degree of hydration.

The results indicate that the autogenous shrinkage of AAFA paste is not caused by such "self-desiccation" process that happens in PC pastes. Water is limited consumed and chemically bonded into the gel phase in AAFA. The different state of water in these two systems can be explained if we look to the different chemical reactions that happen in these two materials. In PC paste, water reacts with cement particles, producing C–S–H gel. Part of the water in PC paste is chemically bonded in the C–S–H gel and the calcium hydroxide [94]. In the system of AAFA paste, the reaction product is a highly connected aluminate (AlO_4) and silicate (SiO_4) tetrahedral

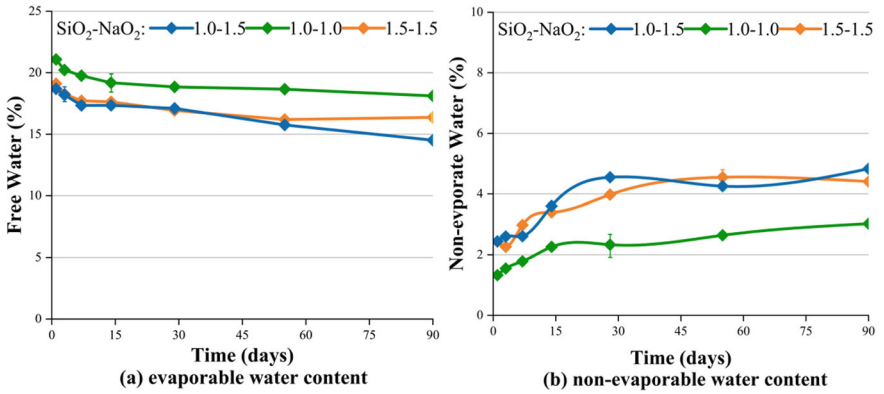

Fig. 5 Evaporable and non-evaporable water content of AAFA pastes (weight percent with respect to original solid) [92]

network, with the negative charge balanced by the alkali metal cations [3]. Most of the water is not chemically incorporated (or, weakly bounded) in the aluminosilicate gel. More than 75% of the water, i.e. 15% by the weight of the original solid in Fig. 5a, was still free water even after 90 days of curing. Similar findings were also proposed by Duxson et al. [95]. They proposed the conceptual reaction model of AAFA and indicated the formation of two types of gel (Al-rich gel and Si-rich gel) during the geopolymerization. As stated in previous chapters, the reaction of AAFA consists of the following steps: dissolution of FA, speciation equilibrium, gelation (condensation), reorganization and polymerization of reaction products. The presence of OH^- ions (provided by NaOH) initiates the rupture of Si–O–Si, Al–O–Al and Al–O–Si bonds in original FA particles, producing silicon and aluminum species (e.g. $Si(OH)_4$ and $Al(OH)_4^-$). The formation of more silicon and aluminum species enhances the contact among these species, forming a coagulated structure, where the hydroxyl groups (e.g. $Si(OH)_4$ and $Al(OH)_4^-$) become connected to produce new Si–O–Si and Si–O–Al bonds [96]. This type of reaction can continue to build larger and larger molecules, forming a continuous inorganic polymer network [97]. It is suggested that water, normally consumed during the dissolution process, is released during the gelation process. Thus, water plays a role of a reaction medium and resides in pores in the gel. Therefore, the internal RH in AAFA remains at a high value during the reaction. It is proposed that the autogenous shrinkage of AAFA is not caused by a self-desiccation process as it happens in cement paste. The reaction happened in AAFA is analogous to the sol–gel process, in which the fine colloidal particles (the sol) links together to form a continuous solid phase (the gel). The aluminosilicate gel also undergoes the reorganizations and polymerization with the elapse of time, transforming into a denser gel. The reorganization process is supported by the formation of two types of gel, i.e. Al-rich gel and Si-rich gel, as well as the formation of crystalline phases, e.g. zeolites [95]. The continuous reorganization and polymerization of the aluminosilicate gel structure are more likely to cause the autogenous shrinkage of AAFA.

It is found that AAFA samples with a finer pore structure had a higher autogenous shrinkage. In Fig. 6 the pore structure obtained from both the MIP and nitrogen adsorption tests of three 7 days old AAFA pastes are presented. Mixtures SiO_2–Na_2O = 1.5–1.5 (The amount of SiO_2 and Na_2O substances in one kilogram of FA is 1.5 mol) exhibited the finest pore structure. This mixture also showed the highest autogenous shrinkage (Fig. 2). For mixtures SiO_2–Na_2O = 1.0–1.5 and 1.0–1.0, a lower autogenous shrinkage was found (Fig. 2) for the mixtures with a coarser pore structure (Fig. 6). This finding indicates that there might be a relationship between the autogenous shrinkage and the pore structure of AAFA systems. The finer pore structure of AAFA may be attributed to a higher degree of polymerization of the gel structure at early age, resulting in a denser matrix with smaller volume. This will then be observed as autogenous shrinkage.

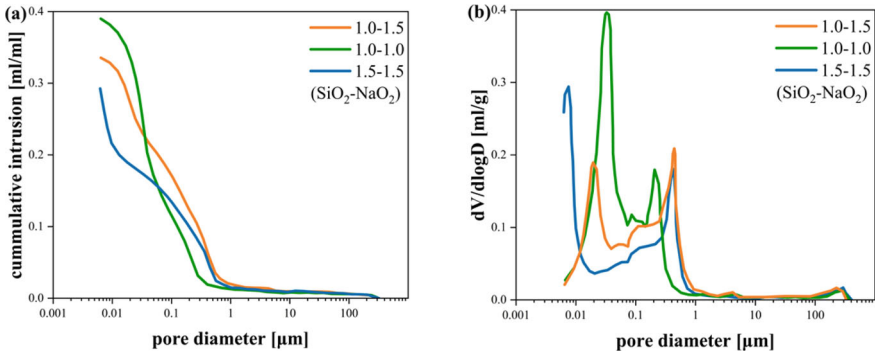

Fig. 6 Pore size distribution of 7 days old AAFA pastes derived from MIP [92]

2.3 Alkali-Activated Metakaolin/Calcined Clay

Metakaolin (MK) with its characteristic disordered structure, is the most common precursor of low-calcium alkali-activated materials (AAMs) [89]. It has high reactivity in alkaline environment, even at ambient temperature.

Rapid dissolution of amorphous aluminosilicates results in supersaturated solution and condensation of oligomers into large networks and thus formation of gel. The initial gel network is further reorganized into 3-D aluminosilicate network, a similar process to what has been observed for AAFA as discussed in Sect. 2.2. Low calcium AAMK is based on structurally disordered strongly cross-linked N-A-S-(H) gel, which has chemical composition similar to zeolites [89, 98]. Consequently some nucleation and crystallization of the nanocrystalline zeolites can also take place [98]. It was demonstrated that in immediately available silica systems the mineralization process is affected by alkali content [99]. The type and characteristics of the gel formed in alkali-activated systems depend on factors such as pH value, calcium concentration, nature of raw materials, curing conditions, Si/Na ratio, and liquid to solid ratio (L/S) [100]. The formation of gel causes a reduction in pore solution, resulting in autogenous shrinkage. An overall shrinkage in MK based AAMK can be up to 3.5 times higher than in PC matrix; for example Mastali et al. reports shrinkage to be up to 3800 µm/m depending on the composition of AAMK comparing to app. 750 µm/m in PC [16]. Palumbo et al. [101] reported that the autogenous deformation of alkali activated MK pastes after 24 h of curing at 40 °C reached ±400 µm/m. AAMK systems exhibits large drying shrinkage, which is ascribed to the high water demand caused by the large surface area and particle shape of MK [16], and what subsequently contributes to the crack formation [102, 103]. On the other hand, autogenous deformation of alkali activated MK can be characterized by shrinkage or by expansion, depending on the precursor, the activator type and the curing age [104, 261]. The early-age chemical expansion in AAMK has been reported in several studies [105, 106] and is attributed to low content of confined water within the molecular structure of N–A–S–(H) gel [106]. Confined water content is

proportional to Si: Al ratio [103] and chemical expansion of AAMK decreases with increased Si: Al ratio [106]. Li et al. [107] described three main stages of chemical deformation for alkali activated MK. The initial deformation is chemical shrinkage caused by dissolution of precursor. In this stage the crucial parameter is the type of raw material [104], namely alkali activation of MK with higher density results in smaller volume reduction during dissolution [107]. The second stage of chemical deformation is expansion, induced by growth of Al-rich (nano) zeolites, which can be accelerated by elevated curing temperature or the use of pure NaOH [98]. The third reported stage of chemical deformation is shrinkage, caused by formation of Si-rich gel. The expansion of AAMK is commonly followed by monotonic autogenous shrinkage, which appears after 1–2 days of reaction and is evident only at macroscale [106]. Lolli et al. [106] reported that autogenous deformation of geopolymers is driven by a combination of chemical expansion during N–A–S–H gel formation and cross-linking, which is accompanied by water rearrangement. According to the possible chemical expansion a small addition of MK to AAS can be used to mitigate the autogenous shrinkage of AAS [108–110].

The concentration of alkali, such as sodium or potassium ions, significantly influences the shrinkage behaviour. Studies have shown that increasing alkali concentration can lead to higher drying and autogenous shrinkage in AAMs [48]. The alkali concentration affects the dissolution rate of solid aluminosilicates, and the balance between the dissolution rates of aluminium and silicon species is crucial for controlling shrinkage. Moreover, the Si/Al ratio in the alkali-activated system has been found to be an important factor in shrinkage behaviour [111]. By adjusting the Si/Al ratio, it is possible to modulate the formation and structure of the geopolymeric gel. Another important factor which influences shrinkage is SiO_2/Na_2O molar ratio where lower ration result in a denser matrix with reduced shrinkage rates, as it promotes the formation of a more rigid and less porous structure [112]. The choice of alkali source also impacts the shrinkage characteristics [113]. Sodium hydroxide (NaOH) and sodium silicate (Na_2SiO_3) are commonly used as alkaline liquids in geopolymerization, but potassium hydroxide (KOH) and potassium silicate (K_2SiO_3) can also be utilized. It has been reported by Kuenzel [103] that change of sodium ion to potassium requires lower amount of structural water and consequently makes paste more stable in terms of shrinkage. The effect is ascribed to the fact that»larger K^+ ion presents a relatively lower charge density and thus, in an aqueous environment, creates a sphere(s) of polar water molecules around the ion that are comparatively easier to remove than with a Na^+ ion [103]. The type of alkali source also affects the dissolution of aluminate silicate precursors and the subsequent reaction kinetics, which can influence the shrinkage behaviour of AAMs [113, 114]. Additionally, it was found that the total quantity of cations, and mostly the stability of (cation: AlO_4^-) pairs in the paste are responsible for the prevention of excessive drying shrinkage at ambient temperature.

2.4 Blended Systems

Slag and FA blended systems. FA and slag are the most commonly used raw materials of AAMs. The reaction of AAFA is quite slow but it can be accelerated by blending the precursor with slag. In contrast, AAS reacts fast but is subject to high autogenous shrinkage. In comparison to ordinary Portland cement (PC), shrinkage has been reported up to ten times higher for AAS [115, 116]. The blending of slag and FA to make alkali-activated slag/FA (AASF) has often been used and investigated to reduce the drawbacks of AAFA and AAS for practical applications [117, 118].

The first parameter that has been investigated is the proportion of FA and slag used in the mix design. Ma et al. [119] examined the autogenous shrinkage of AASF paste for FA/slag proportions (FA/S) equal to 0/100, 30/70, 50/50, 70/30 and 100/0. The water/precursor ratio w/p was 0.4, the silicate ratio M_S was 1.5, and the alkalinity coefficient n was 4.0 (g Na_2O/100 g precursor). They found that higher slag content induced higher autogenous shrinkage, from 1500 μm/m after 7 days for 0% slag content to 8000 μm/m for 100% slag content. Nedeljkovic et al. [31] studied the autogenous shrinkage of AASF paste for the following FA/S: 30/70, 50/50, 70/30 and 100/0. The liquid/precursor ratio was 0.5, M_S was 1.45, and n was 4.8. They found that increasing the slag amount increases the autogenous shrinkage from 2000 μm/m for the mix with 30% slag to 6000 μm/m for the mix with 100% slag, as seen in Fig. 7. Uppalappati et al. [120] investigated mortars with FA/S equal to 0/100, 25/75, 50/50, 75/25 and 100/0. The water/binder (w/b) ratio was 0.53, n was 7.5 and M_S was 1.28. They also observed that autogenous shrinkage increases with the slag amount. The autogenous shrinkage of the mix with 100% slag was around eight times higher than for the mix with 0% FA. These observations were also made by Lee et al. [64], Hojati et al. [86] and Fang et al. [121] for high FA amounts, and Humad et al. [122] for high slag amounts.

Uppalapatti et al. [120] also studied the influence of reduced n and w/b on autogenous shrinkage, for M_S equal to 1.28. They found that for a slag amount of 70%,

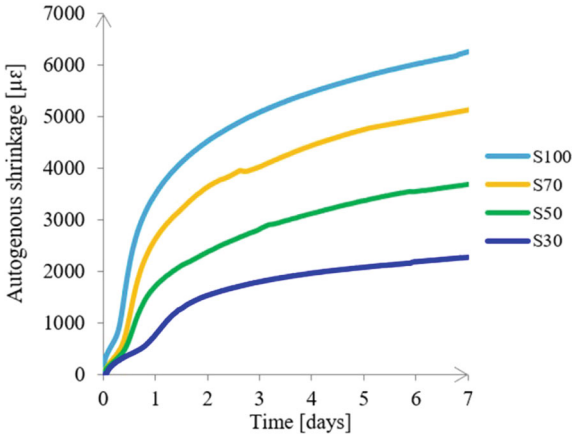

Fig. 7 Influence of the FA/S ratio on autogenous shrinkage. Results from [31]. *Note* S70 corresponds to alkali-activated slag/FA blends with FA/S = 30/70

autogenous shrinkage was decreased, but for lower amounts of slag, autogenous shrinkage increased. Other studies show that for 100% slag content, lower n decreases autogenous shrinkage [7], while for 100% FA content, lower n increases autogenous shrinkage [123]. This is coherent with the results of Uppalapatti et al. [120]. Hojati et al. [86] studied AASF pastes with two different alkali solutions with different n but the same amount of SiO_2 in the solution. This means that for higher n, M_S was decreased and vice versa. M_S varied between 1.13 and 1.44, while FA/S varied between 80/20 and 90/10. The results indicated that higher n and lower M_S decreased autogenous shrinkage. In contrast, Lee et al. [64] found that for FA/S of 80/20 and M_S equal to 2.18, higher alkalinity of the solution caused increased autogenous shrinkage. Humad et al. [122] showed that for mixes with FA/S of 20/80, concrete with M_S equal to 1.0 had higher autogenous shrinkage than concrete with M_S equal to 0.5. Thus, the optimum alkali solution to obtain the lowest autogenous shrinkage of AASF depends on FA/S.

For AASF activated with NaOH, Uppalapatti et al. [120] found that the autogenous shrinkage decreases drastically with a higher amount of FA. The results are shown in Fig. 8. Conversely, the heat of reaction decreases with a higher amount of FA. This is coherent with the results from Puertas et al. [124] who found that mechanical properties decrease with higher FA/S.

The autogenous shrinkage of AASF has often been linked to the reaction kinetics of the system. In [31] and in [120], it was found that the higher the heat of reaction, the higher the autogenous shrinkage. In particular, the heat of reaction varies greatly with FA/S. Higher FA/S induces lower heat of reaction. Li et al. [116] observed that the heat of reaction is higher when FA/S is equal to 0/100 than when it is equal to 20/80 and this is correlated to a higher shrinkage. When different FA/S ratios are studied, the higher autogenous shrinkage observed for lower FA/S could be explained by a higher chemical shrinkage. For instance, Lee et al. [64] studied mixes with FA/S varying from 70/30 to 90/10. They observed that the chemical shrinkage is four times lower after 42 h for the mix with the most FA in comparison to the mix with the most slag, as

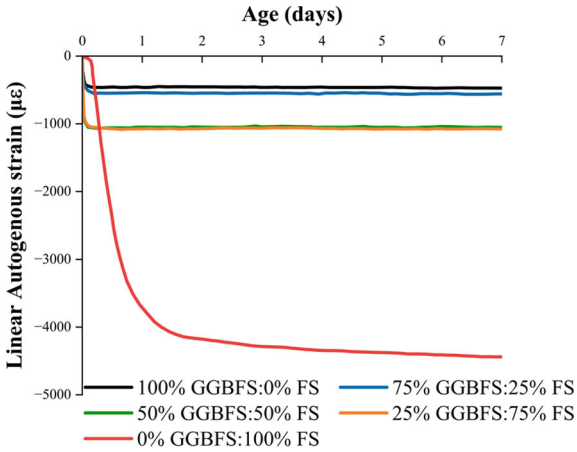

Fig. 8 Autogenous shrinkage of blended slag/FA mortars with sodium hydroxide. Results from [120]

seen in Fig. 9. For this system, lower chemical shrinkage induced lower autogenous shrinkage. Nevertheless, it can be seen that the chemical shrinkage of cement is seven times higher than the one with *FA/S* = 70/30 but has the same autogenous shrinkage. The chemical shrinkage of slag/FA systems has been investigated for other ranges of *FA/S* in the literature. Fang et al. [121] studied ratios between 0/100 and 40/60, Hojati et al. [86] between 80/20 and 90/10 and Li et al. [116] between 0/100 and 20/80. In all cases, the higher the amount of slag, the higher the chemical shrinkage.

Due to chemical shrinkage, self-desiccation takes place to generate autogenous shrinkage. In this case, the contraction depends on the stiffness of the materials and thus on the reaction products. Puertas et al. [125] found that the polymerization of C–A–S–H increases over time for AASF. Also, the gel product is rich in aluminum and sodium in comparison to pure slag systems. In addition, an amorphous alkaline aluminosilicate product with a 3D structure develops around the FA particles. These differences could explain the change in the stiffness of the matrix. Uppalappati et al.

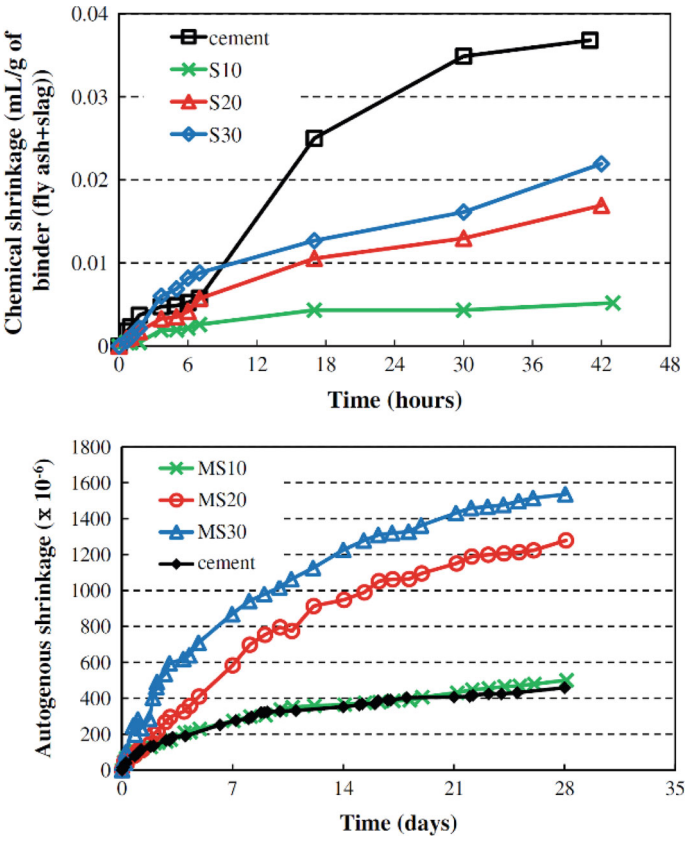

Fig. 9 (Up) Chemical shrinkage of alkali-activated FA/slag pastes with different amounts of slag and (Down) autogenous shrinkage of corresponding mortars. Results from [64]

[120] detected N–A–S–H gel as well as hydrotalcite in AASF. The former could be characterized when FA/S was higher and the last one when FA/S was below 75/25 and when sodium hydroxide was used.

Another significant parameter to explain autogenous shrinkage is pore structure. Lee et al. [64] found that when FA/S increases from 70/30 to 90/10, the number of pores increases and this increase is correlated to lower autogenous shrinkage. Li et al. [108] showed that the incorporation of MK in AASF coarsens the pore structure and is associated with a smaller autogenous shrinkage following the pore pressure theory. Nevertheless, according to Uppalappati et al. [125], the capillary pressure theory coupled with the elastic behaviour is not sufficient to explain the autogenous shrinkage and other mechanisms should be taken into account to explain the viscoelastic behaviour or creep induced by the capillary pressure.

In conclusion, the autogenous shrinkage of AASF depends mainly on the FA/S ratio. Higher slag content induces higher autogenous shrinkage. The optimum alkali solution to reduce autogenous shrinkage depends on FA/S. Higher alkalinity will increase the reaction rates of slag and FA. On the one hand, higher slag reaction increases greatly autogenous shrinkage. On the other hand, higher FA reaction increases stiffness properties and reduces shrinkage.

Other blended systems. Dependent upon the proportion of particular precursors in binder, AAMs blended systems can usually be classified into the following three categories: (1) High-calcium system (e.g., alkali-activated slag); (2) Low-calcium system (e.g., alkali-activated Type F fly ash or MK); and (3) Middle-calcium system (e.g., alkali-activated slag-FA mixtures). Besides FA, slag and MK, other precursors or wastes can also be used to synthesize AAMs. However, most of them were used as additives to AAS, AAFA or AASF systems, rather than used solely, primarily due to the limited reactivity of these materials. Table 1 summarizes the characteristics and mechanisms of autogenous shrinkage of alkali-activated blended systems, except for AASF system that has been discussed in the previous section. The working mechanisms of different precursors are summarized as follows: (1) dilution effect caused by the reduced binder content, such as limestone, glass wool; (2) internal curing effect, such as rice straw ash, waste concrete powder; (3) delayed reaction due to low reactivity, such as ferronickel slag, steel slag, municipal solid waste incinerator bottom ash; (4) delayed reaction by providing additional Si and Al, such as MK; (5) formation of expansive hydration products, such as cement kiln dust; (6) modified reaction and pore structure by providing additional reactive composition, such as MK, circulating fluidized bed combustion (CFBC) ash, calcium carbide residue, and waste concrete powder; (7) acting as inert components such as $CaCO_3$ and calcium carbide residue. In general, the incorporation of these materials can mitigate the autogenous shrinkage of AAMs. However, the efficacy of the mitigation is strongly dependent upon the content of those materials and the activator types. However, the incorporation of less than 30% limestone increases the autogenous shrinkage of AAS, which is related to the accelerated reaction of limestone [126]. However further increasing the limestone content to 50% suppressed the autogenous shrinkage of the AAS at 12-day. Conversely, the addition of less than 25% municipal solid waste incinerator bottom ash to AAFA was able to inhibit autogenous shrinkage

by approximately 20% [127]. Whereas the addition of over 25% municipal solid waste incinerator bottom ash increases the autogenous shrinkage because of the reaction between metallic aluminium particles in municipal solid waste incinerator bottom ash and sodium silicate, which results in the formation of damaging foaming [127]. For ferronickel slag, the addition of the AAS is in favour of reducing the early autogenous shrinkage (first 3 days), while the long-term autogenous shrinkage is impacted to some extent, which is dependent on the activator type [128]. For instance, the autogenous shrinkage is mitigated with NaOH-based activator; while the use of sodium silicate would increase the autogenous shrinkage [128].

2.5 AAMs Made from Other Raw Materials

Apart from slag, FA and MK, there are fewer studies on the autogenous shrinkage of AAMs from sole raw material systems. Wang et al. [138] found that the alkali-activated blast furnace ferronickel slag concrete exhibited much lower autogenous shrinkage at 7 days when compared to the alkali-activated GGBFS concrete, which can be reduced by 7.8–10.5% and 25.2–69% when using NaOH and sodium silicates as the activator, respectively. This was explained by the lower reactivity of ferronickel slag than GGBFS, which leads to a slower reaction kinetic by using the same activator. The reaction rate significantly influences the self-desiccation and chemical shrinkage that contributed to the overall autogenous shrinkage. Navarro et al. [139] investigated the autogenous shrinkage of alkali activated ground Si–Mn slag mortars with different types of aggregates (silica sand, limestone sand, and recycled sand). A higher shrinkage (both drying and autogenous shrinkage) was identified in mortars activated with sodium silicate (when compared to those activated by NaOH), although autogenous shrinkage was low for all types of activators and aggregates, except for recycled concrete aggregates.

2.6 One-Part AAMs

Problems linked to the corrosive aspect of the alkaline solutions needed for the alkali activation, from their transportation to their storage, including their handling, make it harder for AAMs to be commercialised and used widely, especially when highly concentrated solutions are used. To overcome these challenges to both the workers and the environment, the one-part or "just add water" AAMs equivalents represent an interesting alternative to the two-part AAMs [140].

In one part AAMs, both the (aluminosilicate) precursor and the alkali-activator are in dry solid form, and they are dry blended along with other admixtures before water is added to start the reaction and hardening of the material [141]. As it has been reported in [142] most of the interest has been given in the last years to their

Table 1 Characteristic of autogenous shrinkage of blended AAMs systems, except for AASF, and working mechanisms of different materials

Main precursors	Mixed precursors	Activators	Content (%)	Increase or reduction degree		Working mechanism	References
Slag	Limestone	Na_2CO_3	≤30	+30.8 to 32.7%		Intensified and accelerated reaction	[126]
			50	−3%		Dilution effect caused by the reduced slag content	
	Rice straw ash (RSA)	NaOH modified sodium silicate	5	−23.8%		Internal curing effect of RSA	[129]
			10	−41.9%			
	Glass wool	NaOH modified sodium silicate	25	−30 to 56%		Dilution effect caused by the reduced slag content	[130]
			50	−78 to 90%			
	MK	NaOH modified sodium silicate	10	−14.3 to 40%		By providing additional Si and Al, and decreasing the pH of the pore solution, the incorporation of MK retards the formation of C–A–S–H gels. The chemical shrinkage and pore refinement are consequently mitigated, resulting in a substantial reduction in the pore pressure	[109, 110, 131]
			20	−20.5 to 50%			
			30	−37.5%			
	Ferronickel slag	NaOH, sodium silicate	20	Early shrinkage within 3 days: 10–80%	NaOH: −14.8%, Na_2SiO_3: +8.2%	Low reactivity FNS, the reaction of AAM is delayed The reason for the late increase in autogenous shrinkage of sodium silicate activated FNS is unknown	[128]
			40		NaOH: −39.2%; Na_2SiO_3: +9.4%		
			60		NaOH: −63.1%; Na_2SiO_3: +12.2%		

(continued)

Table 1 (continued)

Main precursors	Mixed precursors	Activators	Content (%)	Increase or reduction degree	Working mechanism	References
		NaOH modified sodium silicate	50	−102.1%		[132]
	Steel slag	NaOH modified sodium silicate	50	−132.4%	Low reactivity steel slag, the reaction of AAMs is delayed	[132]
	Cement kiln dust	NaOH	5	−8.3%	Formation of expansive hydration Products like portlandite and hydrotalcite during the first 24 h	[133]
			15	+15.9%		
			25	−9.7%		
			50	−12.4%		
	Circulating fluidized bed combustion (CFBC) FA	NaOH modified sodium silicate	10	−7%	Higher sulfate content in circulating fluidized bed combustion decreased the pH of the pore solution and led to a retarded reaction. The anhydrite and portlandite in Circulating fluidized bed combustion resulted in the size and volume of the pores in the AAMs matrix increased	[134]
			20	−15.4%		
	CFBC bottom ash	NaOH modified sodium silicate	10	−16.9%		
			20	−15.4%		
FA	Municipal solid waste incinerator bottom ash	NaOH modified sodium silicate	25	−2.3%	Low reactivity municipal solid waste incinerator bottom ash, the reaction of AAMs is delayed	[127]
			50	+147%	Metallic aluminum particles in municipal solid waste incinerator bottom ash reacted with Na_2SiO_3 to formation of damaging foaming	
			75	+180%		
	Calcium carbide residue	NaOH	30	626–788 με	$Ca(OH)_2$ in calcium carbide residue promoted the C–A–S–H and N–A–S–H in AAM; $CaCO_3$ in calcium carbide residue acted as micro-aggregate filler in AAMs	[135]
		NaOH modified sodium silicate	15	390 με		[136]
			30	70 με		
			45	335 με		

(continued)

Table 1 (continued)

Main precursors	Mixed precursors	Activators	Content (%)	Increase or reduction degree	Working mechanism	References
Slag/FA 50/50	Waste concrete powder	NaOH modified sodium silicate	1	−11.6%	Internal curing effect of waste concrete powder; pore structure of AAMs was refined with the waste concrete powder addition	[137]
			3	−21.6%		
			6	−30.7%		
			9	−37.8%		

microstructural level analysis and compressive strength. The different steps of the preparation and mixing of one-part AAMs is illustrated in [142].

One possible application of one-part AAMs is 3D-printing as reported in [142]. The general good pumpability and thixotropic characteristics (ability of a material to lose and recover viscosity when shear stresses are applied and then removed) make one-part AMM a very good candidate for such applications. However, 3D-printing structures are very sensitive to cracking due to the partial restrained of the shrinkage during the construction process [143]. For this reason, the study of the volume change of such materials is of major importance. However, very limited quantity of study exists in the literature.

Often, GGBFS is used as the main precursor for one-part AAMs. However, since it is also used in the cement industry for the production of CEM III for example [144], other secondary materials (by-products or wastes) are being investigated to partly replace the most common GGBFS.

It has been seen in [145] and in [116] that two-part AAS exhibits autogenous shrinkage going up to 1900–2200 μm between 24 h of age and 7 days whereas for one-part AAS it is 1100 μm/m (Fig. 10, where the control sample is AAS and the RSA samples have 5 and 10 wt% replacement dosages with rice straw ash). Compared to PC, it is however still 2 times higher [129]. Little data can be found regarding the comparison between the autogenous shrinkage of one-part AAMs and PC in mortar and concrete scale, thus not discussed here.

Chemical shrinkage is a key factor influencing autogenous shrinkage. In [146], the chemical shrinkage of thermally treated asbestos cement residues (precursor) and solid sodium metasilicate (activator) has been investigated. As asbestos is potentially carcinogenic, it undergoes a process to make it inert thanks to a heat treatment to be

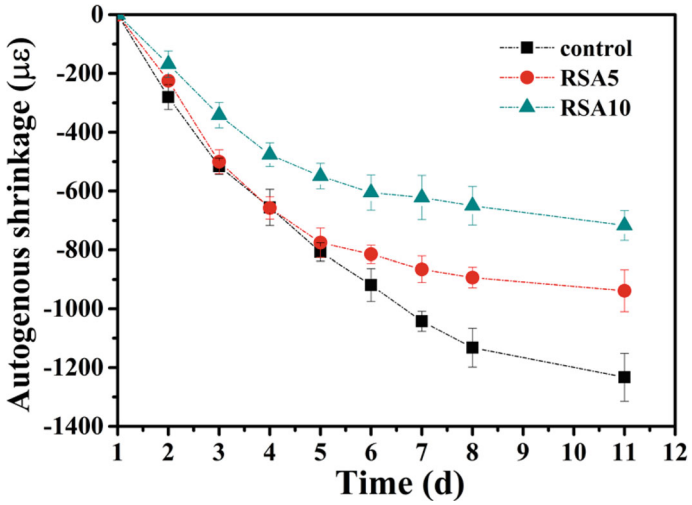

Fig. 10 Autogenous shrinkage of different one-part mixtures [129]

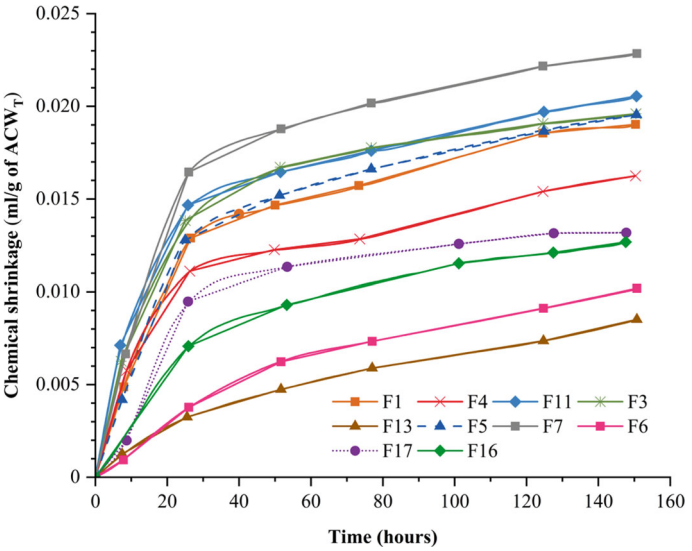

Fig. 11 Chemical shrinkage of one-part alkali-activated pastes during the first seven days of hydration [146]

used without any risk. The influence of the mass fractions of the residue (ranging between 0.600 and 0.700), of sodium metasilicate (range between 0.000 and 0.106) and of water (range between 0.294 and 0.360) have been studied. The chemical shrinkage of these compositions is presented on Fig. 11.

The chemical shrinkage significantly depends on the variation of the mass fractions. The different compositions show an increase of the chemical shrinkage before stabilising. This is explained by the reaction between the asbestos cement residue and the sodium metasilicate because compositions F6 and F13 which do not contain alkaline activator, do not show this behaviour. However, the small chemical shrinkage that can be observed for those compositions is explained through the presence of ettringite (which has an expansive effect and consequently a reducing effect on the chemical shrinkage) and portlandite shown through the XRD results. An increase in the rate of reaction of the alkaline activation results in more significant chemical shrinkage due to its contribution to the hydrated phases formation (ex: hydrotalcite). In fact, the chemical shrinkage can also increase with an increase of the amount of calcium-rich precursor and sodium silicate because this induces more formation of C–N–A–S–H phases [146].

The chemical shrinkage of one-part alkali-activated materials is similar to that of two-part AAMs which is between 0.01 and 0.03 ml/g of precursor. In addition, the chemical shrinkage of AAMs (paste scale) is lower than that of ordinary Portland cement which is around 0.035 ml/g of cement [64].

3 Summary and Comparison of the Autogenous Shrinkage of Different AAMs

This section systematically shows the magnitude, influencing factors and mechanisms of autogenous shrinkage of different AAMs. As illustrated in the previous parts, the value and kinetics of autogenous shrinkage differ with the types of precursors, alkali activators and the curing conditions. It becomes challenging to directly assess the value of the shrinkage for different AAMs. The influencing factors ranging from the type of precursors, the type of activators, the liquid to solid ratio, the modulus and curing temperature, were mentioned in different studies though never being quantitively analysed. To date, no study provides the conclusive results. Therefore, after regressing the data extracted from the references, the correlation of the different factors/features and the autogenous shrinkage of AAMs is examined.[1] The weight of the influencing features is calculated using optimized XGBoost regression [147] and the best fitting parameters are determined with network grid, and the weight ranking for comparative magnitude of 28d-autogenous shrinkage within common alkali activated systems is present in Fig. 12. Some conclusions, therefore, can be safely drawn.

Shrinkage behaviours in AAMs with different types of commonly used precursors can be compared. For alkali-activated slag or slag dominating systems, one general consensus is that the autogenous shrinkage of the AAMs is higher than that of PC [64, 148]. The main difference in the deformation is spotted at the early ages before 28 days, driven by the increasing capillary pressure due to the more intense reaction and larger number of mesopores in the [7, 50]. Noteworthy that the chemical shrinkage of the AAMs is however lower than that of PC [64]. Meanwhile, the gel-like properties of the reaction products in slag dominating systems, C–A–S–H and N–A–S–H, contribute to the water consumption, thereafter amplifying the autogenous shrinkage [64, 110, 121]. In slag-FA/-MK blended AAMs, higher autogenous shrinkage is observed with the higher amount of slag. The added FA and MK decrease the formation C–A–S–H of slag and modify the pore networks. As can be seen in Fig. 12, the FA content plays the most important role on autogenous shrinkage, compared to other raw materials. Therefore, apart from the common methods for mitigating shrinkage used in PC, e.g., the internal curing with SAP and LWA which can also be functioned in AAMs, employing higher amount of FA and MK is also efficient [110]. When it comes to AAFA or AAMK, the autogenous shrinkage turns to be similar and even lower than that of PC [92]. The main underlying mechanism is found to be the polymerization of the reaction products N–A–S–H instead of self-desiccation. In such cases, internal RH hardly indicates the evolution of shrinkage, given the dissolution of the FA and MK increasing the alkalinity (geopolymerization) and the RH of the pore solution.

[1] Statistical analysis on 231 data points of autogenous shrinkage of AAMs collected from the references were carried out. The datasets can be provided as a supplementary material if necessary. After data cleaning, optimized XG-Boost regression algorithm was used for predicting the 28 days autogenous shrinkage with different factors and weight ranking was obtained.

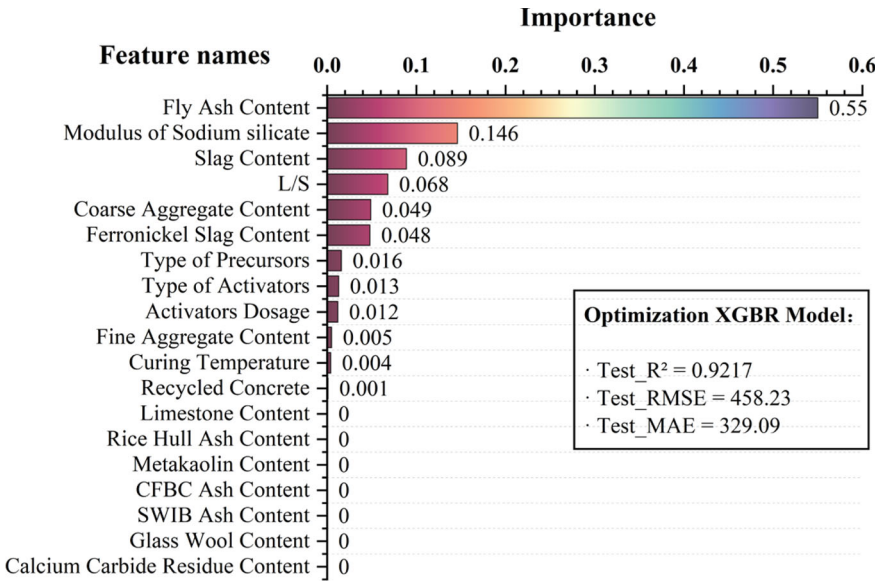

Fig. 12 Weight of influencing factors on shrinkage magnitude (28 days) obtained with optimized XGBoost regression algorithm (the higher the importance value, the higher the impact level of the factor)

Shrinkage behaviour in AAMs prepared with different widely used activators can be also concluded. The lowest autogenous shrinkage of AAMs is claimed in that with sodium carbonate. While being activated with sodium silicate, attributed to the extreme reaction rates both the magnitude and the kinetics of the autogenous shrinkage increased significantly. The key features for determining the autogenous shrinkage are Na_2O content and the alkali-activated modulus SiO_2/M_2O, the higher which the larger the autogenous shrinkage. As with the analysed weight ranking of influencing factors, the modulus of sodium silicate is the second important feature for autogenous shrinkage. The content of alkali activators can be quantified as the liquid to solid ratio (L/S), which is also key for the magnitude of the deformation.

Intensive studies on driving force of AAMs autogenous shrinkage are carried out, while the resistance part of the deformation is yet uncertain. Except the elastic modulus and compressive strength, which is always high in AAMs, the contribution of the viscoelastic behaviour of the matrix on shrinkage is not trivial. Being known for decades, half of the autogenous shrinkage is attributed to the viscoelastic behaviour of PC, surely the impacts of which also depends on the components. However, there is still little knowledge on the effect of viscoelastic behaviour of AAMs on the total autogenous shrinkage. The study by Li et al. [119] considered this issue and concluded that the viscoelastic part outweighs the elastic part for total autogenous shrinkage in AAMs. Concerning the viscoelastic properties, creep of AAMs should be focused on. Studies with basic creep tests and nanoindentation shown that for slag-dominating AAMs, the creep is 4–5 times higher than that of PC when activated

with sodium silicate solutions, led by amount of the partly-active, non-activated slag or non-activated compact glass phases [149, 150]. With FA being imbedded, the basic creep is reduced with the increasing amount of FA [149]. Therefore, the higher amount of shrinkage could be part of the results of higher creep. The benefits on lower cracking risks, though, are also due to the higher viscoelastic behaviour (relaxation in AAMs) [151].

A simplified knowledge graph based on the extraction of all considered influencing factors and the autogenous shrinkage magnitude was drawn (Fig. 13). The arrows between the factors and the autogenous shrinkage reveals the influencing weight, with the bolder the linking line indicating the stronger correlation of the autogenous shrinkage and the features (entities). The weight of the influencing features is calculated as in Fig. 12.

As a summary, wider range of raw materials can be applied in AAMs in recent years, which calls for a general criterion for assessing shrinkage deformation. Together with the phenomenal experimental results, more investigations should cover the mechanisms, not only lying on the porosity and hydration kinetics but also on the characteristic of primary and secondary products. Further investigations should

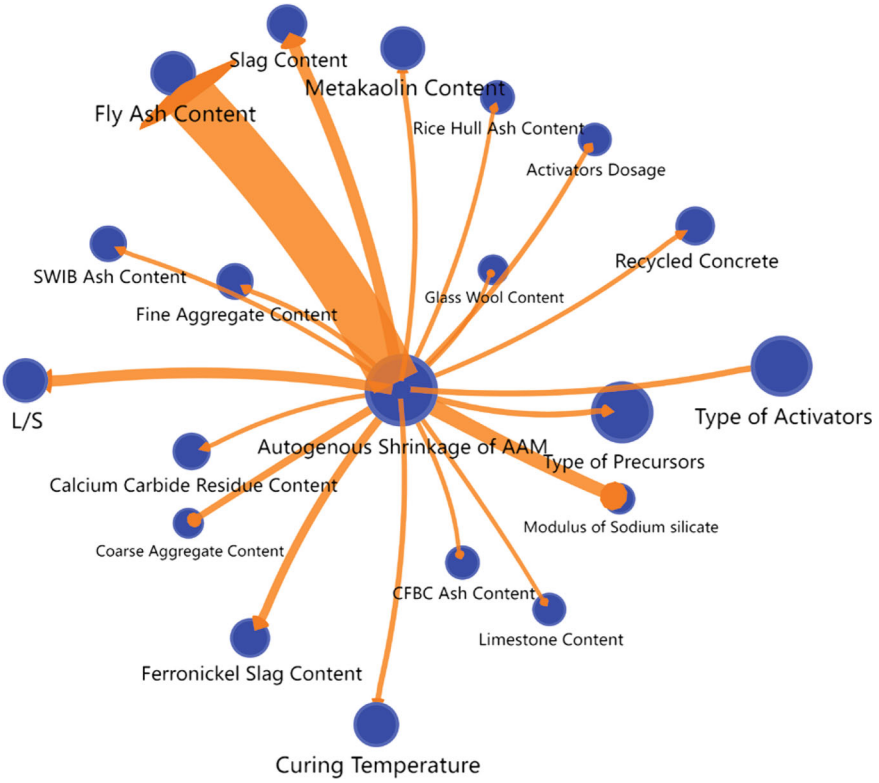

Fig. 13 Correlations between influencing factors and the autogenous shrinkage

be done on effect of multi-scale structures and the abovementioned viscoelastic behaviours, which can trigger larger applications of AAMs.

4 Mitigation Strategies

4.1 Shrinkage Reducing Admixtures (SRAs)

In this part, we will discuss the different strategies that have been proposed to mitigate the autogenous shrinkage of AAMs (AAS, AAFA and AAMK). The first strategy is to use admixtures that can mitigate shrinkage, such as shrinkage-reducing agents (SRAs). SRA is a special type of chemical product, i.e., surfactants, based on neopentyl glycol ($((CH_2)_2–C–(CH_2OH)_2$) or other similar products [152]. As classified as surfactants SRA is made of a hydrophilic and a hydrophobic part [7, 153–155].

When surfactant is dissolved in water, the hydrophobic part breaks the hydrogen bonds between water molecules and rearrange the water molecules around the surfactant. Some of the surfactant molecules are expelled to the interfaces between water and air so as to minimize their contact with the water molecules. A layer of surfactant molecules with their hydrophobic part primarily point to air covers the surface of water [156] (Fig. 14. The common substance of the hydrophobic part of surfactant is long-chain hydrocarbon residue and the hydrophilic part of surfactant is an ionic or highly polar group [157]. Depending on its nature, surfactants can be classified as several different types, namely anionic, cationic, zwitterionic and non-ionic [158].

The effect of SRA on shrinkage reduction originates from decreasing the surface tension of the pore solution and then the autogenous shrinkage. Some examples of SRAs that have been tested in AAS including polyethylene glycol [153] and poly ethers [154]. When 7.5% SRA was added in to AAS mortars, the autogenous shrinkage of AAS mortars was reduced by 77% [7]. The addition of SRAs can also delay the hydration of AAS, which is needed to be taken into account depending on the specific product and the project requirements for AAS.

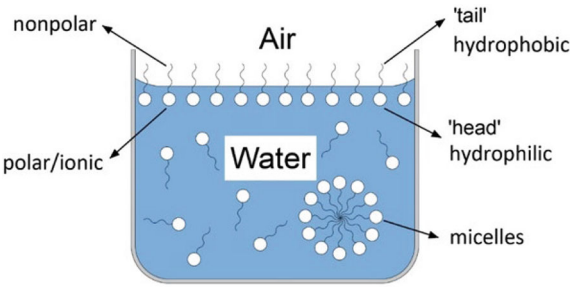

Fig. 14 Schematic representation of working mechanism of surfactant (after [156, 159])

According to the literature [48, 160], the autogenous shrinkage of AAFA is different to that of PC or AAS paste. The cracking proneness of AAFA due to autogenous shrinkage is not significant. Therefore, cracking related to autogenous shrinkage is not considered as a major problem of AAFA and no specific investigation is given to it.

4.2 Water Repelling Agents

Another usually used admixture to reduce the autogenous shrinkage of cement paste is water repelling agent [161]. The most commonly used water repelling agent includes silane, siloxane and saturated fatty acid [161]. Water repelling agent can change the wetting behaviour of the pore wall of cementitious materials and the contact angle between water and pore wall [162].

Take silane as an example, it reacts under alkaline conditions and forms a thin layer of polymer resin on the pore wall of cement paste. The reaction of silane mainly includes two steps, i.e., hydrolysis and condensation [163]. At the 'hydrolysis' step, the alkoxy groups of silane are replaced with hydroxy groups and silanols are generated. Then during the 'condensation' step, silanol reaction product reacts with siloxane and silicon-oxygen bonds form. Due to the silicon-oxygen bonds, the 3D network of polymer resin takes shape [96]. The polymer resin is of siloxane species and water repellent. The change of the contact angle will significantly affect the internal force related to the self-desiccation, e.g., capillary tension, and autogenous shrinkage [36]. It is found that the combination of 20% waterborne epoxy resin and 1% silane coupling agent by mass of the starting materials (slag cement/OPC) reduced the autogenous shrinkage of MK-based geopolymer by 131.2% [164]. The addition of 5% polydimethylsiloxane reduced the autogenous shrinkage of AAMK by 91.2% [165].

4.3 Expansive Agents

The third strategy proposed to mitigate autogenous shrinkage of AAMs is adding expansive agent, due to which expansive reaction products can form during the hydration [166, 167]. As a result, crystallization pressure is generated within the matrix and the autogenous shrinkage can be compensated [168–170]. Typical expansive agents encompass sulfoaluminate, calcium oxide, and magnesium oxide expansive agents [171, 172]. In addition, the addition of inorganic admixtures such as nano-titanium dioxide [63] and calcium hydroxide ($Ca(OH)_2$) [81] can also mitigate the autogenous shrinkage of AAMs.

Akturk et al. [173] showed that the addition of $Ca(OH)_2$ enabled AAS to achieve comparable performance to PC while reducing shrinkage strain. Gypsum is another type of expansive additive. It was found that the incorporation of gypsum coarsened

the pore structure of AAS and triggered the formation of expansive sulphate-rich phases, e.g., ettringite [43]. Therefore, the early-age autogenous shrinkage of AAS was partially compensated. However, the early-age expansion was insufficient to offset the subsequent long-term shrinkage [43].

Calcium sulfoaluminate-based expansive additive was also tested by Choi et al. [174] in AAFA. They observed that this expansive additive at dosages up to 7.5% by mass of the binder reduces slightly the autogenous shrinkage and that it was linked to an increase in stiffness properties.

The use of chemical admixtures such as expansive agents, shrinkage-reducing admixtures, superabsorbent polymers and nano-particles (NPs) helps to reduce shrinkage by densifying the structure, changing the pore size distribution and/or initiating the formation of certain crystalline phases (i.e. calcium hydroxide, AFt, and AFm) [175].

4.4 Curing Techniques

Another strategy to control autogenous shrinkage in AAMs is the application of different curing techniques [176–178]. Curing refers to the process of maintaining a moist environment around the materials during setting and hardening process [58]. This helps to keep internal RH high thus reducing internal RH drop due to hydration, allowing the AAS to mitigate the autogenous shrinkage. As found by Liu et al. [179], sealed curing contributes to desirable mechanical properties and durability of AAS mortars but results in high early shrinkage. Fog and water curings are highly effective at mitigating early shrinkage in AAS mortars. Their study underlines the significance of curing condition to shrinkage evolution of AAMs. To mitigate autogenous shrinkage, internal curing is usually efficient, with the use of porous materials like lightweight aggregates (LWA) [129] or superabsorbent polymers (SAP) [177]. These internal curing agents have the ability to provide extra water during the hydration of AAMs, which in turn, decreases the pore pressure to mitigate the autogenous shrinkage.

It has been reported that the application of 0.3% SAP can decrease the autogenous shrinkage of AAS up to 80% compared with the referral sample [180]. However, the internal curing agents could result in voids in the AAS matrix after water release which can lead to the reduction of mechanical performance and durability [110]. Tu et al. [181] showed that the addition of SAPs could reduce drastically autogenous shrinkage at different dosages of binder content for FA/S equal to 75/25. The autogenous shrinkage is reduced by a factor of 2 for a dosage equal to 0.2% and by a factor of 6for a dosage equal to 0.5%, as seen in Fig. 15. Reasons for that could be a reduction of the chemical shrinkage as well as delayed reaction kinetics. In [182], Li et al. studied a reference mix with $FA/S = 50/50$. They found that a dosage of 0.32% of SAP was effective to decrease long-term autogenous shrinkage. Besides, their results also indicate that the replacement of 10% slag by metakaolin allows the reduction of autogenous shrinkage at early-age. The combination of SAP

and metakaolin reduces shrinkage at early-age and later-age, as observed in Fig. 16, and leads to concrete with less cracking potential. Among the solutions to reduce the autogenous shrinkage of alkali-activated slag/fly ash systems, adding SAP and metakaolin seems to be the most promising solution.

Besides the traditional internal curing agent, rice husk ash is considered as a potential alternative option and has drawn more and more attention due to its pozzolanic reactivity and porous structure in recent years. Yin et al. [129] found that the addition of RSA reduced the autogenous shrinkage of one-part alkali-activated slag. Yin et al. [129] reports that a substitution of 5% reduces the autogenous shrinkage by 21.1% and a substitution of 10% reduces it by 42.6% at 7 days of age, which is comparable to superabsorbent polymers. In addition, the mitigation through RSA has a decreasing effect on the heat flow and the hydration heat [129].

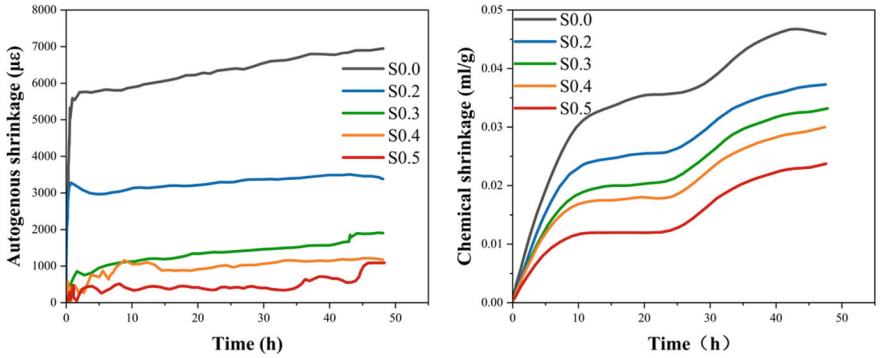

Fig. 15 (Left) autogenous shrinkage and (right) chemical shrinkage of alkali-activated slag/fly ash with different SAP dosages. S0.2 corresponds to an SAP dosage of 0.2% mass binder. Results from [181]

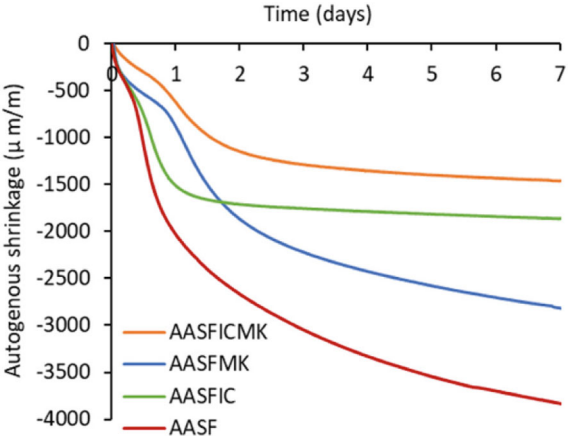

Fig. 16 Autogenous shrinkage of alkali-activated slag/fly ash paste with SAPs and/or MK. Results from [182]

In addition to internal curing, heat-curing and low temperature curing can also reduce the shrinkage of AAS. Thomas et al. [176] found that heat-curing can significantly reduce the shrinkage of AAS, which is even lower than that of PC sample. Xiang et al. [183] measured the shrinkage of AAS under room temperature curing and low temperature curing, and found that the shrinkage strain of AAS under low temperature curing conditions could be reduced by at least 16% compared with the shrinkage of AAS under room temperature curing conditions.

Numerous studies have demonstrated that the drop of RH can effectively mitigate the autogenous shrinkage of early-age cement pastes, for instance, through internal curing methods [184, 185]. Internal curing is typically achieved by incorporating pre-wetted or saturated reservoirs, such as superabsorbent polymers (SAPs) or lightweight aggregates (LWAs), into a binder or concrete [186–191]. The release of water from the reservoirs compensates for hydration-induced water consumption and slow the progress of self-desiccation. This process reduces capillary pressure caused by self-desiccation. Research indicates significant potential for internal curing to alleviate autogenous shrinkage in alkali-activated materials (AAMs), despite possible compromises on strength [177, 178, 181, 192, 193]. In addition to traditional internal curing agents, rice husk ash (RHA) has emerged as a promising alternative due to its pozzolanic reactivity and porous structure. RHA, derived from completely incinerated rice husks [194], primarily consists of amorphous silica (90–96 wt%) [195]. According to Tuan et al. [195], RHA exhibits a larger pore volume compared to many other pozzolanic materials of similar particle size. Due to its high porosity, RHA can be used as a water reservoir and provide internal curing for ultra-high-performance concrete (UHPC).

It was reported that elevated temperature curing at 60–80 °C was helpful to reduce the drying shrinkage of AAMs [53, 166]. The reduction was due to the fact that the visco-elastic/visco-plastic compliance of C–A–S–H gels was reduced at elevated temperatures. Since the autogenous shrinkage of AAMs is also critically influenced by the deformability of the gels [196], the elevated temperature curing may also be effective in mitigating the autogenous shrinkage. However, this strategy may be unsuitable for cast-in-situ concrete due to the high requirement for the curing condition.

4.5 Optimization of the Mix Design

The optimization of the mix design of AAS includes adjusting the type of activator, ratio of activator to slag, as well as the type and amount of mineral materials used [58]. By optimizing the mix design, it is possible to reduce the amount of autogenous shrinkage that occurs during the setting and hardening process. Mineral admixtures are generally incorporated into AAS by substituting slag either partially or completely. Commonly used mineral admixtures include FA, silica fume, limestone powder, and MK. Kim et al. [197] incorporated circulating fluidized bed combustion (CFBC) into sodium silicate-activated slag system. The results showed that

the autogenous shrinkage of AAS decreased at all ages, which can be attributed to the modification of the microstructure of the matrix by ash. Zhenming et al. [110] reported that the autogenous shrinkage of AAS can be reduced by 40 and 50% when replacing 10 and 20% slag with MK, which can be attributed to the refinement of micro chemical environment in the pore solution. The incorporation of limestone can also reduce the autogenous shrinkage due to the filler effect [198].

4.6 Fibres

In addition to using the above methods to inhibit the shrinkage of AAMs, some studies have explored incorporating fibres, latex, and biofilms, and have also achieved positive results. The effect of fibres on inhibiting the shrinkage of AAS depends on the type and content of fibres. Chen et al. [199] studied the shrinkage inhibition effect of polypropylene (PP) fibre and steel fibre on AAS. The results showed that both fibres can reduce the shrinkage of AAS, and steel fibre is more effective. The addition of PP fibres is also promising in AAFA [200]. Shrinkage and eventual cracks can be decreased also by change in curing regime, i.e. when samples undergo drying at later age, and after heat-curing [19]. However, a same effect of PP fibres on autogenous shrinkage of AAMs have not been reported.

Besides fibres, El-Yamany et al. [201] used two different latexes (Styrene-Butadiene rubber and acrylic ester) to reduce the shrinkage of AAS. The results showed that the shrinkage strain of AAS decreased significantly after the addition of the two kinds of latex, but the content of the two kinds of latex had little effect on the shrinkage inhibition effect. Qu et al. [145] proposed the application of biofilm to mitigate the shrinkage of AAS. The biofilm can hydrophobized the pore structure, which in turn, decreasing the pore pressure to mitigate autogenous shrinkage.

In conclusion, there are several strategies that can be employed to mitigate the autogenous shrinkage of AAMs. Each strategy has its own advantages and limitations, and the optimal approach will depend on the specific application and requirements of the AAMs. By carefully considering these factors and selecting the appropriate strategy, it is possible to overcome the challenges associated with shrinkage and achieve high-performance AAMs with excellent durability and strength.

5 Modelling and Prediction

5.1 Introduction

To prevent macro/micro-cracking issues in early age concrete that may compromise its mechanical performance and the long-term durability of the structure, it is essential to understand three key aspects: (1) the material's behaviour under free

conditions, (2) its mechanical properties, and (3) the level of restriction it experiences [202]. Consequently, several models have been developed to equip engineers with the necessary tools to calculate stresses induced by displacements restriction and ensure they remain within the strength limits of concrete. Among all the material parameters, the development of autogenous deformations exerts a pronounced influence, particularly in compositions featuring a low water-cement ratio such PC) or compositions based on AAMs.

Numerous studies have been conducted on the development of autogenous deformations. It is widely acknowledged that autogenous deformations are induced by variations in internal RH. However, despite these efforts, uncertainties still remain regarding the underlying mechanisms driving their deformation. Additionally, the discrepancies in test methods and protocols employed across different laboratories further contribute to significant variations in the measurement of autogenous deformations [203, 204]. Consequently, researchers use various mathematical expressions to reproduce experimental results. All these models were initially developed to define the evolution of autogenous deformations in concrete composed by PC. Several models were then used or modified for AAMs. This chapter section is organized as follows: The first part presents different models used for PC, while the second part focuses on various models used for AAMs. Finally, the third part explores several perspectives for predicting autogenous deformations of AAMs.

5.2 Models for PC

Numerous models have been developed to reproduce, analyse, or predict the development of autogenous deformations of PC. These models can be categorized into empirical and analytical models.

Empirical Models. Empirical models are derived either by directly reproducing a limited dataset dedicated to the study of specific concretes or materials (e.g., ultra-high-performance concrete [205], recycled aggregate concrete [206], internally cured concrete [207]), or by performing a regression analysis on a large set of test data. Engineers commonly employ predictive models that rely on a database of experimental data, such as the *fib* Model Code 2010 (Eq. 1), the JSCE model (Eq. 2), and the B4 model (Eq. 3). In these models, the autogenous deformations are defined using the Equations included on Table 2.

These predictive models establish correlations between autogenous deformations and material age by means of hyperbolic or exponential expressions. They encompass a multitude of concrete parameters, including its composition (e.g., water-to-cement ratio, cement type, aggregate content, and the presence of mineral additives) and the mechanical performance (compressive strength) of the material. The variables denoted in Eqs. 1–3 are comprehensively detailed in the respective references indicated in Table 2. The databases used to create the predictive models described above can also be used to predict autogenous deformations using machine learning methods [211, 212].

Table 2 Autogenous shrinkage models used in standards

Model	Equations	Influencing parameter	
MC2010 [208]	$\varepsilon_{as}(t) = \varepsilon_{as0}(f_{cm}, \alpha) \cdot \left[1 - \exp\left(-0.2 \cdot \sqrt{t}\right)\right]$	f_{cm}, strength class of cement	(1)
JSCE [209]	$\varepsilon_{as}(t) = \gamma \cdot \varepsilon_{as\infty} \cdot \left[1 - \exp\left\{-a \cdot (t - t_s)^b\right\}\right]$	Cement and admixture type, W/C, setting	(2)
B4 [210]	$\varepsilon_{as}(t) = \varepsilon_{as\infty} \cdot \left[1 + \left(\frac{\tau_{as}}{t+t_0}\right)^{\alpha}\right]^{r_t}$	W/C, cement type, aggregate/cement, age at environmental exposure	(3)

Moreover, the influence of temperature, T, can be effectively incorporated into these models through the application of Arrhenius' law, with a specific emphasis on the equivalent time principle as delineated in Eq. 4 [213].

$$t_{eq}(t, T) = \int_0^t \exp\left(\frac{E_a}{R} \cdot \left(\frac{1}{273 + T(s)} - \frac{1}{273 + T_r}\right)\right) \cdot ds \tag{4}$$

where E_a is the apparent activation energy expressed in J/mol, R is the universal gas constant (= 8.314 J/mol/K) and T_r is a reference temperature (generally 20 °C).

The development of autogenous deformation can also be characterized as a function of parameters such as heat release, Q, or degree of reaction, ξ, [214]. The heat release can be assessed through isothermal, quasi-adiabatic or adiabatic calorimetry [215–217]. The degree of reaction corresponds to the fraction of the cement that has reacted. A linear relation was used by Bendboudjema and Torrenti [214] to correlate autogenous shrinkage and degree of reaction as indicated in Eq. 5. In this Equation, ξ_0 corresponds to the reaction degree when the paste sets. This type of model inherently accounts for the maturity of the material. The parameter κ corresponds to the rate of autogenous shrinkage according to the degree of reaction and is expressed in μm/m.

$$\varepsilon_{as}(t) = \kappa \cdot (\xi - \xi_0) \tag{5}$$

However, single-term models assume a singular mechanism responsible for autogenous deformation development. Consequently, they are insufficient for capturing multiple mechanisms with distinct kinetics, such as swelling and self-desiccation shrinkage. To address this complexity, two-term models have been developed to separate and analyse different mechanisms. This approach is notably applicable to concretes comprising CEM III/A [218], those featuring a high water-to-cement ratio [219], or incorporating mineral additions [220, 221]. Each term within these models can be expressed as a function of either equivalent time or the degree of reaction. The swelling term can be represented through an exponential law based on equivalent time or an inverse exponential law with respect to the degree of reaction. Meanwhile, the self-desiccation term can be expressed as an exponential law concerning

equivalent time, or as a sinusoidal or linear function in relation to the advancement degree of reaction. Carette and Staquet [222] have further investigated the influence of temperature on the magnitude of swelling and shrinkage by incorporating an apparent absorption enthalpy term into the model. In the context of concrete composed of recycled aggregates, Delsaute and Staquet [206] has introduced a three-term model to account for initial swelling, self-desiccation shrinkage, and the internal curing effect induced by the high porosity of recycled aggregates. Each of these terms is represented by an exponential function with respect to equivalent time, as presented in Eq. 6.

$$\begin{aligned}\varepsilon_{as}(t) = & \underbrace{A_{sw} \cdot \exp\left[-\left(\frac{p_{sw}}{t_{eq}-t_{fs}}\right)^{r_{sw}}\right]}_{Initial\ swelling} + \underbrace{A_{sd} \cdot \exp\left[-\frac{p_{sd}}{t_{eq}-t_{fs}}\right]}_{self-desiccation} \\ & + \underbrace{A_{ic} \cdot \exp\left[-\left(\frac{p_{ic}}{t_{eq}-t_{fs}}\right)^{r_{ic}}\right]}_{internal\ curing}\end{aligned} \tag{6}$$

Analytical model. Analytical models are linked to the physical mechanisms involved in the development of autogenous deformations. As detailed in Sect. 2 of this chapter, numerous theories have emerged to explain the development of the autogenous deformation, with a predominant focus on the pressure stemming from the self-desiccation phenomenon within capillary pores. Capillary or pore pressure, denoted as σ (Pa), can be quantified using Laplace's law (Eq. 7), Kelvin's law (Eq. 8), and their combination (Eq. 10). Laplace's law establishes a relationship between capillary pressure, the surface tension of the pore solution γ (N/m), the meniscus radius r (m), and the contact angle of solid matter and water θ. Meanwhile, Kelvin's law relates the internal RH induced by meniscus formation, denoted as RH_K, to the molar volume of the interstitial solution V_W (m^3/mol), in conjunction with parameters γ, θ, r, R and T. The parameter RH_K can be derived through Eq. 9 [223], with RH representing the paste's RH, and RH_S is the RH change due to the water activity in the solution. The internal RH of the paste can be monitored directly by using adapted probe [224] while RH_S can be measured by extracting the pore solution at different ages [225].

$$\sigma = -\frac{2 \cdot \gamma \cdot cos\theta}{r} \tag{7}$$

$$\ln(RH_K) = \frac{2 \cdot \gamma \cdot V_W \cdot cos\theta}{r \cdot R \cdot T} \tag{8}$$

$$RH = RH_S \cdot RH_K \tag{9}$$

$$\sigma = -\frac{\ln(RH_K) \cdot R \cdot T}{V_W} \tag{10}$$

To establish a connection between capillary pressure and autogenous deformation of the paste, it is imperative to account for the mechanical behaviour of the material, particularly its elasticity. The elastic component can be determined using Eq. 11, assuming that the material is elastic and isotropic [226].

$$\varepsilon_{el} = \frac{S \cdot \sigma}{3} \cdot \left(\frac{1}{K} - \frac{1}{K_S} \right) \tag{11}$$

where S (−) is the saturation fraction and represents the ratio between the liquid content in the hardening phase V_l and the total pore volume of the paste V_p (Eq. 12). V_l can be calculated by subtracting the non-evaporable liquid content V_{nl} from the initial liquid content V_{il}. V_p can be calculated by adding the chemical shrinkage V_{cs} to V_l. K and K_S (Pa) are respectively the bulk modulus of the paste and the bulk modulus of the solid skeleton. K_S can be defined based on the composition of the solid skeleton [227]. According to Lura [2], the influence of K_S is limited and can be considered equal to 44 GPa for PC [116]. K is calculated using the modulus of elasticity, E (Pa), and the Poisson's ratio, υ (−), of the paste (Eq. 13). The evolution of the elastic modulus and the Poisson's ratio of the paste can be defined experimentally by means of repeated minute long loading test [228–230] or by means of ultrasonic pulse velocity test [231].

$$S = \frac{V_l}{V_p} = \frac{V_{il} - V_{nl}}{V_{il} - V_{nl} + V_{cs}} \tag{12}$$

$$K = \frac{E}{3 \cdot (1 - 2 \cdot \upsilon)} \tag{13}$$

Several researchers have noted that employing an elastic approach for calculating autogenous deformations tends to underestimate experimental measurements, particularly as RH decreases. According to [151, 232], the deformations induced by the creep of cement paste can be in the range of 2–3 times the elastic deformations. The relationship between creep deformations, elastic deformations, and the age at loading τ is described in Eq. 14.

$$\varepsilon_{cr}(t, \tau) = \varepsilon_{el}(\tau) \cdot \varphi(t, \tau) \tag{14}$$

Various models in the literature have been developed to characterize creep coefficient while accounting for material aging. As for autogenous deformation, the aging of the creep coefficient can be defined based on material age, equivalent age or degree of reaction. Numerous models are presented in the references [233]. The aging of the creep function can be experimentally characterized through a series of long duration creep tests [234] or a combination of long-term creep tests and repeated minute-long loading tests [228].

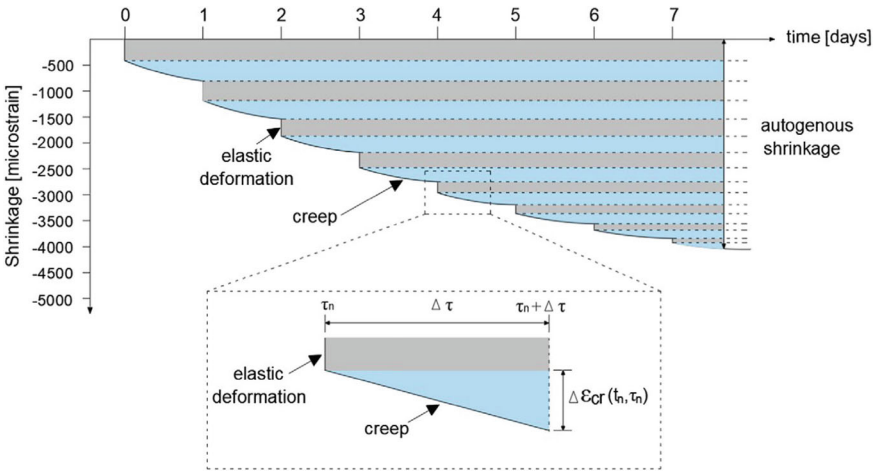

Fig. 17 Schematical representation of the incremental calculation of the autogenous shrinkage when considering creep [116]

As capillary pressure progressively increases during paste reaction, it becomes imperative to consider the aging of viscoelastic properties to accurately predict autogenous deformations. To address this, the calculation is incremental, conducted at different time or stress intervals. Figure 17 provides a visual representation of how deformations are calculated, accounting for the evolving viscoelastic properties.

As autogenous strain is influenced by processes at various scales, multi-scale modelling techniques can be employed to capture the behaviour accurately. These models integrate information from the micro-scale (e.g., cement hydration and capillary pores) to the macro-scale (e.g., aggregate-cement paste interface), to provide a comprehensive understanding of autogenous strain development. Autogenous deformations at the mortar or concrete scale can be reliably predicted through a comprehensive analysis based on measured or predicted autogenous deformations, along with the viscoelastic properties of the paste. Additionally, key factors contributing to these deformations include the properties of the aggregate, such as particle size distribution, content, elastic properties, absorption, and potentially inherent shrinkage, as well as the interaction between the paste and aggregates, particularly within the interfacial transition zone (ITZ). To account for the autogenous deformation restriction imposed by aggregates, the Pickett model [235] proposes an elastic calculation. The extended Pickett model [236] uses a viscoelastic calculation which allow more accurate prediction. For both approaches, the cement paste is conceptualized as a single shell surrounding the spherical aggregate and is described by Eq. 15 where $\varepsilon_{as,c}$ is the concrete autogenous strain (μm/m), $\varepsilon_{as,p}$ is the paste autogenous strain (μm/m) and β is the restraining factor (−) [236]. The restraining factor is not constant and change according to the age of the materials [237] and can be defined as a function of the aggregate elastic properties, the paste viscoelastic properties, the activation energy and the internal stress. This modelling strategy provides a comprehensive

framework for understanding and predicting autogenous deformations of concrete systems

$$\varepsilon_{as,c}(t) = \varepsilon_{as,p}(t) \cdot (1 - g)^{\beta} \tag{15}$$

As explained above, the development of the autogenous strain cannot always be reproduced by considering only capillary depression mechanism. For that reason, Pichler et al. [238] applied micromechanical modelling approach that incorporates the apparent swelling induced by ettringite formation. The representation of the cement paste is articulated across two distinct scales. The primary scale encapsulates the four clinker phases, including high-density CSH, low-density CSH, water, and air phases, with a specific emphasis on time-dependent behaviour exhibited solely by CSH. This scale operates within the dimensional range of 10^{-8}–10^{-6} m. On the other hand, the secondary scale delineates the anhydrous cement, gypsum, portlandite, and reaction products arising from celite (C_3A) and felite (C_4AF) hydration processes. This scale operates within the dimensional range of 10^{-6}–10^{-4} m.

Influential factors. As highlighted in Sect. 4.2.1, the models presented herein are established and validated utilizing experimental data. However, it is imperative to acknowledge that the measurement of autogenous strains is inherently influenced by the characteristics of the employed test apparatus and the associated testing protocols [203, 204]. Typically, autogenous strains are conventionally initialized to zero at the setting, period when the solidification of the skeleton occurs and restricts Le Chatelier contraction (or chemical shrinkage) [239]. The determination of the "time-zero" marking the initiation of autogenous deformations being set to zero is a subject of variation among researchers [240]. Some propose to set to zero the autogenous strain at the initial setting time while others consider the final setting time [240, 241]. These two criteria also depend on the method used to define them [242, 243]. These parameters can be defined based on resistance to penetration, ultrasonic pulse velocity, heat release, electrical resistivity, or the development of the mechanical properties [242]. Alternately, some researchers employ the first time derivative of autogenous deformations as a time to set the autogenous strain to zero [91, 222, 244]. Additionally, there are proponents for setting autogenous deformations to zero at the moment of peak swelling [244]. The nuanced selection of these criteria underscores the complexity inherent in defining and characterizing autogenous strains within diverse experimental contexts.

5.3 Models for AAMs

AAMs can consist of one or more solid or liquid components, further complicating the establishment of mathematical models capable of reproducing all the findings in the literature due to the vast number of potential combinations. Similarly, predicting the evolution of autogenous deformations becomes an even more challenging task. In contrast to PCs, several notable trends emerge [245]:

– Autogenous deformations exhibit significantly greater amplitudes.
– The progression of autogenous deformations unfolds over a more extended timeframe.

Empirical models. Numerous studies have demonstrated the inadequacy of predictive models designed for PC when applied to the prediction of autogenous deformations in AAMs [116, 246, 247]. This limitation stems from inherent differences in the microstructure of these materials. For instance, the Model Code 2010 (Table 2 and Eq. 1) correlates the amplitude of autogenous deformations with the characteristic strength achieved at 28 days for PC. However, the autogenous deformations of AAMs exhibit substantial variations compared to PC, even when considering an equivalent compressive strength. Certain calculation codes incorporate parameters such as the cement type, which may not be applicable to AAMs. Crucially, the distribution and volume of pores, despite their significant influence on autogenous deformation development, are not considered in these codes. Consequently, direct application of existing calculation codes for predicting autogenous deformations in AAMs is not feasible. Nevertheless, there is a need to explore potential adaptations of these models to align with experimental results and to ascertain whether a unified mathematical expression can effectively replicate the evolution of autogenous deformations across a diverse database.

As part of the investigation into the mechanisms and efficacy of various shrinkage reducers and expanding agents on the drying and autogenous deformations of AAS mortars activated by liquid sodium silicate, Hu et al. [50] conducted a comparative analysis of existing models to assess their capability in reproducing experimental results. Three types of models were examined: exponential, logarithmic and polynomial (degree 3). Among the four compositions studied, Eq. 16 emerged as the most adept at replicating experimental results. In this Equation, ε_s denotes autogenous deformations at infinite time, while A and a represent material parameters.

$$\varepsilon_{au}(t) = \varepsilon_s \cdot (1 - A \cdot exp(a \cdot t)) \tag{16}$$

However, it is important to note that this study is confined to a limited number of compositions and does not encompass all the models outlined in Sect. 5.2. To broaden this comparison and assess the ability of other models to replicate experimental results, data from Lacante et al. [248] on eight alkali-activated slag-FA-silica fume pastes are incorporated. These compositions vary in solution-to-binder ratio (B series) and silicate modulus (T series). Seven mathematical expression, inspired by previously presented models, are employed and outlined in Table 3. Given the lack of consensus on the initialization of autogenous deformations (see Sects. 5.2 and 5.3), no constraints are imposed on this aspect during the fitting process. In other words, all results can be translated on the autogenous deformations axis to achieve optimal fitting. Equation parameters are left unrestricted for each mathematical expression, and the error is calculated as the sum of squares of differences between experimental results and fitting. Each Equation and associated error are presented in Table 3.

Table 3 Mathematical expression used to reproduce the development of the autogenous strain

Serial number	Mathematical expression	Number of parameters	Error
1	$A \cdot \exp\left[-\left(\frac{p}{t_{eq}}\right)^{r}\right]$	3	3.4E + 06
2	$A \cdot \exp\left[-\left(\frac{p}{t_{eq}-\tau}\right)^{r}\right]$	4	2.3E + 06
3	$A \cdot \left(1 - \mathrm{B} \cdot \exp\left(\mathrm{C} \cdot t_{eq}\right)\right)$	3	1.7E + 07
4	$A \cdot \left[1 - \exp\left(-0.2 \cdot \sqrt{t_{eq}}\right)\right]$	1	7.0E + 07
5	$A \cdot \left[1 - \exp\left(-B \cdot \sqrt{t_{eq}}\right)\right]$	2	2.3E + 07
6	$A \cdot \left[1 - \exp\left\{-B \cdot \left(t_{eq} - \tau\right)^{r}\right\}\right]$	4	1.1E + 07
7	$A \cdot \left[1 + \left(\frac{p}{t_{eq}+\tau}\right)^{\alpha}\right]^{r}$	5	2.3E + 06

The analysis reveals that all mathematical expressions adequately reproduce experimental results. Notably, a factor of 30 separates the lowest error obtained with Eqs. 2 and 7 from the highest error obtained with Eq. 4. The correspondences achieved with Eqs. 2 and 4 are visually depicted in the Fig. 18.

Based on this comparison, it is observed that Eqs. 1, 2 and 7 consistently replicate results throughout the entire autogenous deformation development. Conversely, other Equations accurately capture deformations over extended durations but exhibit discrepancies within the initial 24 h.

While achieving the ability to replicate autogenous deformations is a crucial initial step, the subsequent challenge lies in establishing the relationship between model parameters and the micro- or macroscopic properties of the material. This task necessitates the creation of a comprehensive database and rigorous examination of the sensitivity of each parameter. In this regard, Li et al. [23] undertook a comprehensive study wherein they compiled a large volume of results available in the AAS literature. Their investigation focused on studying the sensitivity of various

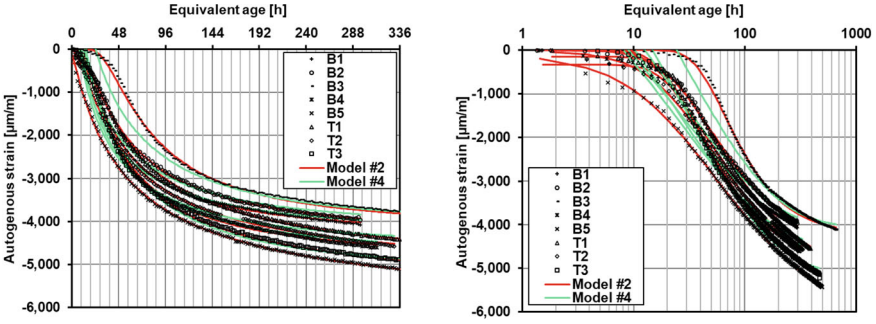

Fig. 18 Autogenous strain according to the equivalent age—linear scale (left) and logarithmic scale (right)—of AASF paste [248]. Continuous lines correspond to the mathematical expressions 10.2 and 10.4 from Table 3

material parameters, including Na_2O content, silicate modulus, water-to-binder (w/b) ratio, and activator type, in relation to the amplitude of autogenous deformations. Overall, their findings suggest that the amplitude of autogenous deformation tends to increase with higher alkali content, lower w/b ratio, and when the silicate modulus approaches 1.0. The influence of each parameter can also be investigated using machine learning methods, based on a comprehensive database. Shen et al. [249] examined the impact of composition through various algorithms to identify the factors that most significantly affect the autogenous deformations of AASF pastes.

Similar to PC, some researchers observe a linear correlation between autogenous strain development and heat release in pastes composed of AAS [62] and AASF [248, 250]. This simplistic modelling approach allows for the extrapolation of autogenous deformations when the heat release or degree of reaction is known over an extended duration. Notably, only two parameters—the degree of reaction at time zero ξ_0 and the factor κ—need to be determined for each composition. However, it is important to highlight that the availability of both types of data in the literature is limited, hindering the establishment of a comprehensive empirical model for predicting autogenous deformations across various types of AAMs. Additionally, it is worth noting that Lacante et al. [251] did not observe a linear relationship between the two parameters in pastes composed of AAS at an early age ($t_{eq} < 100$ h). This discrepancy can be attributed to the simultaneous action of two mechanisms contributing to the development of autogenous deformations, each operating with distinct kinetics and amplitudes.

Furthermore, other material properties have been correlated with autogenous deformation. For instance, Siva [246] observed a linear relationship between autogenous deformation and compressive strength, as well as bound water content in AASF pastes. In the same compositions, an exponential relationship was identified between autogenous deformation and P-wave velocity. These diverse correlations underscore the complex interplay of factors influencing autogenous deformation in AAMs.

Analytical model. As for PC, capillary pressure induced by self-desiccation is considered as the main driving force mechanism involved in the development of the autogenous shrinkage as explained in Sect. 2. Consequently, the same analytical approach utilizing poromechanics, employed in the context of PC (Sect. 4.2.2), has been applied to predict the autogenous shrinkage of AAM [62, 151, 246]. Notably, it has been observed by several researchers that an elastic calculation alone is insufficient for accurately predicting autogenous deformations. This underscores the pivotal role of early age creep in AAMs, with studies such as [252] demonstrating a significantly higher creep coefficient in AAMs mortar compared to PC at very early ages. Drawing upon rheological models [62] or empirical laws [116], it becomes feasible to incorporate creep and achieve highly accurate predictions. It is essential to highlight that the parameters of the creep models have been optimized to better fit with experimental results, although a direct comparison with creep tests is pending and remains imperative. Such comparisons are necessary to establish that creep, in isolation, accounts for the observed discrepancies in elastic calculations. Moreover, the substantial amplitude of creep must be duly considered to accurately reflect the restriction of paste deformation induced by the presence of aggregates.

Li et al. [253] have contributed valuable insights by demonstrating that the utilization of composite models neglecting creep (e.g., Pickett, Hobbs, Tazawa) yields unsatisfactory results. To address this, the authors employed the extended Pickett's model, incorporating considerations for the aging of elastic modulus and creep coefficient. This strategic approach proves effective in accurately predicting autogenous deformations in concrete, leveraging data obtained from AAS and AASF pastes.

Influential factor. Several studies have shown that the setting time of AAS vary also significantly according to the test method and the criteria used [254]. Notably, some researchers measure the setting time at very low degrees of reaction or well before the initiation of capillary depression [116, 255]. During this initial phase, the paste's stiffness is likely too low to support meniscus formation. Consequently, deformations measured during this period are more accurately attributed to Le Chatelier contraction rather than capillary depression [42, 181]. Therefore, it is more representative to consider zero time as the moment when internal RH begins to decrease [246] (if only self-desiccation causes autogenous strain). For certain compositions, the evolution of properties is rapid at the setting. A slight variation in the initialization of autogenous deformations can profoundly impact the evolution of stresses induced by the restriction of displacements. In this context, a criterion tied directly to the development of autogenous deformations, such as the knee-point method, appears more suitable and consistent for determining the progression of stresses induced by displacement restriction [251].

5.4 Prospects

Significant advancements have been achieved in recent years in modelling the autogenous deformations of AAMs. Nevertheless, several critical areas necessitate further research:

- Influence of curing temperature: investigate the impact of curing temperature on the amplitude of autogenous deformation [125] on the empirical and analytical models. This involves validating the model against realistic temperature histories.
- Consideration of additional mechanisms: explore the incorporation of other mechanisms identified in the literature, such as polymerization/syneresis of C–A–S–H gel and steric-hydration force into the modelling framework. This exploration could involve both analytical and empirical approaches.
- Definition of time zero: establish a universally accepted criterion for the initialization of autogenous deformations, fostering consensus within the scientific community.
- Integration of New Experimental Results: Consolidate and enrich existing databases by incorporating new experimental results. This integration aims to enhance the robustness and applicability of the current modelling approaches.

6 Testing Methods

Throughout the last decades extensive work was made in the field for PC, and many shrinkage testing techniques were ready to use such as. Studies that were made in literature, for the vast majority, used PC norms and standards, as shown in Table 4.

As introduced previously, some testing methods developed for PC-based materials have been directly applied for AAMs. A description of testing methods for chemical and autogenous shrinkage used is given here below, as for PC the two were interconnected when it comes to the comprehension of the behaviors of the material.

6.1 Chemical Shrinkage

In the case of chemical shrinkage, three measurement techniques were developed for PC: dilatometry, initially proposed by Le Chatelier [239, 268–275], gravimetry [276, 277] and pycnometry [273], as shown in Fig. 19. Nevertheless, they are all based on the same basic principle. The cement paste is placed in a flask and the system is filled with water. As the hydration reaction takes place, initial mix water is consumed. Once the material sets, the extra amount of water must be available in sufficient amount in order to ensure the further development of the hydration of the anhydrous grains and to fill the voids created by the volume deficit.

The main factors affecting the chemical shrinkage measurement are: the thickness of the layer of paste which is introduced in the flask [274], the amount of water added at the surface of the sample (avoid leaching [274, 277, 278]), and the presence of air voids within the fresh paste [274, 278, 279]. The influence of the w/c ratio was also under discussion with some authors claiming that the chemical shrinkage varies with this parameter [268, 269, 274], while others claim that at early age (at least up to 24 h) the chemical shrinkage is constant and independent of the w/c used [280–282]. Regarding the thickness of the layer of cement paste which is introduced in the flask, if the sample is too thick, water will not penetrate the entire sample, and the chemical shrinkage can be underestimated.

Some of the measurements proposed in AAMs studies are either ASTM C1608 (for the majority) or the gravimetric method (Fig. 20 and Table 4). By contrast, Li et al. modified the gravimetric method by employing a thin layer (around 10 g) of alkali solution with the same concentration as activator and covering paraffin oil onto the surface of the alkali solution until the dish was nearly filled [107]. It is commented that during the testing of chemical shrinkage in AAMs, water can dilute the concentration of dissolved species, while an alkali solution might alter the reaction kinetics of the paste. Both of these methods produce errors, but they are unavoidable, similar to intrinsic inaccuracies encountered in the chemical shrinkage testing of PC. For example, sufficient additional water can invalidate chemical shrinkage studies conducted on systems with a low w/c ratio. Therefore, when measuring the chemical shrinkage of AAMs, variations in the thickness of the water

Table 4 Shrinkage testing methods for alkali activated cements/mortars

References	Material	Type of shrinkage	Testing method	Comments
[256]	AAS (sodium silicate, sodium hydroxide)	Drying shrinkage	Prismatic specimens with dimensions 25 × 25 × 285 mm ASTM C490 demoulded at 6 h	Effect of activator concentration and comprehension of mechanisms
		Autogenous shrinkage		
[257]	AASF paste and mortar	Chemical shrinkage	Volumetric method according to ASTM C1608	Comprehension of mechanisms (comparison with PC mortars)
		Autogenous shrinkage	ASTM C 490, Prismatic specimens 25 × 25 × 285 mm, demolded at final setting time	
		Drying shrinkage	ASTM C 490, Prismatic specimens 25 × 25 × 285 mm, demolded at 24 h	
[121]	AASF pastes	Autogenous shrinkage	70 × 70 × 70 mm specimen-shrinkage measured by laser sensor (displacement on a reflecting plate-linear)	Comprehension mechanisms
		Chemical shrinkage	ASTM C1608-12	
[48]	AAFA	Autogenous shrinkage (volumetric)	Corrugated tube method (according to ASTM C1698-09)—measurements start at final setting time	Comprehension mechanism: using ellipse ring test to correlate cracking risk to shrinkage
		Drying shrinkage	40 × 40 × 160 mm Measured with a comparator—measurements start after curing for 7 days	
		Restrained shrinkage	Ellipse ring test	
[258]	FA based geopolymer (activated by sodium hydroxide, sodium silicate and potassium silicate)	Chemical shrinkage	Capillary tube ASTM C1608-17	Effect of temperature and pressure on autogenous shrinkage comparison avec PC
		Autogenous shrinkage	API RP 10B-5 diaphragm accumulator test	

(continued)

Table 4 (continued)

References	Material	Type of shrinkage	Testing method	Comments
[259]	FA based geopolymer	Drying shrinkage	ASTM C157 10 mm × 10 mm × 60 mm	Comprehension mechanisms: link between shrinkage and cracking behaviour comparison with PC
		Restrained shrinkage	ASTM C1581 Ring test, H30mm, Øint100 mm, Øext150 mm	
[107]	MK based geopolymer	Chemical shrinkage	Gravimetry method (buoyancy method)	Comprehension of the chemical deformation of the material, linked to reactions and reaction products
[48]	AAS mortars	Autogenous shrinkage	Corrugated tube method (according to ASTM C 1698-09)—measurements start at final setting time	Comprehension of autogenous shrinkage mechanism and mitigation
[193]	AAS mortars	Autogenous shrinkage	50 × 50 × 300 mm by vibrating wire strain gage (Measurements start after final setting time)	Mitigation of autogenous shrinkage/ superabsorbent polymers
[260]	Geopolymer granulated blast-furnace slag	Chemical shrinkage	ASTM C1608-07	Shrinkage mitigation by expansive agents
		Autogenous shrinkage	Corrugated tube method using non-contact sensors	
		Drying shrinkage	JC/T 603-2004 25 × 25 × 280 mm	
[261]	AAS	Autogenous shrinkage	Corrugated tube method (according to ASTM C 1698-09)	Effect of hydrophobicity on autogenous shrinkage
[110]	AAS	Autogenous shrinkage	Corrugated tube method (according to ASTM C 1698-09)	Mitigating the autogenous shrinkage by MK
		Chemical shrinkage	Gravimetry method	
[181]	AASF pastes	Autogenous shrinkage	70 × 70 × 70 mm specimen-shrinkage measured by laser sensor (displacement on a reflecting plate-linear)	Mitigation of autogenous concrete by internal curing using SAP

(continued)

Table 4 (continued)

References	Material	Type of shrinkage	Testing method	Comments
		Chemical shrinkage	ASTM C1608-12-dilatometry	
[262]	AASF concrete	Autogenous shrinkage	ASTM C 1698-09-corrugated polyethylene tubes	Mitigation of autogenous shrinkage by air entraining admixtures Evaluation of the extent of microcracking in all concretes was done through petrographic examination
[176]	GGBFS activated by sodium hydroxide and sodium silicate	Autogenous shrinkage	Corrugated tubes	Mitigate self-desiccation by internal curing by SAP
		Restrained shrinkage	Dual ring test	
[263]	GGBFS activated with hydrated lime and gypsum	Drying shrinkage	ASTM C 490, Prismatic specimens 25 × 25 × 285 mm, demolded at 24 h	Effect of activator
		Autogenous shrinkage	25 × 25 × 285 mm	
[86]	AASF binary cements	Chemical shrinkage	Gravimetric technique/ buoyancy method	Effect of FA, slag proportions and type of activating solution
		Autogenous shrinkage (volumetric)	Corrugated tube method (ASTM C1698-09). L420 mm, Ø29 mm Tubes rotated until final setting to avoid bleeding Initial length measured at set time	
		Drying shrinkage	ASTM C157M-08 25,4 × 25,4 × 254 mm	
[264]	Geopolymer (MK based)	Autogenous shrinkage	NF P15-433 40 mm × 40 mm × 160 mm	Effect of formulation parameters on autogenous shrinkage
[265]	FA-based lightweight geopolymer	Autogenous shrinkage	25 mm × 25 mm × 285 mm	Effect of mix parameters
		Drying shrinkage	25 mm × 25 mm × 285 mm	

(continued)

Table 4 (continued)

References	Material	Type of shrinkage	Testing method	Comments
[123]	AAFA concrete	Drying shrinkage	ASTM C490	Influence of activators and their concentration (sodium silicate and sodium hydroxide)
		Autogenous shrinkage	ASTM C490	
[106]	Geopolymer (MK, sodium activated)	Chemical shrinkage	Capillary tube ASTM C1608-17	Comprehension mechanisms
		Autogenous shrinkage	ASTM C1698-09 corrugated tubes, L420 mm, Ø29 mm; rotated prior to setting	
[108]	AASF paste	Chemical shrinkage	Gravimetry	Effect of MK on the autogenous shrinkage
		Autogenous shrinkage	Corrugated tube method (according to ASTM C 1698-09)	
[126]	Carbonate activated slag	Autogenous shrinkage	ASTM C 1698-09—corrugated polyethylene tubes	Study of the shrinkage mechanism of sodium carbonate activated slag containing limestone powder
		Drying shrinkage	ASTM C490	
[266]	AASF mortar	Autogenous shrinkage	Corrugated mold according to ASTM C1698-09	Effect of the use of copper slag
		Drying shrinkage	40 mm × 40 mm × 160 mm prism samples according to Chinese standard JGJ70-2009	
[245]	AAS	Autogenous shrinkage (linear)	Prismatic specimens 25 × 25 × 285 mm	Comprehension: influence of surface tension (and capillary pore pressure) on autogenous shrinkage
		Autogenous shrinkage (volumetric)	Elastic membrane method	
[267]	AAS and AAFA	Autogenous shrinkage	Autogenous deformation testing machine (ADTM)—linear horizontal	Comprehension and link between material properties and cracking risks

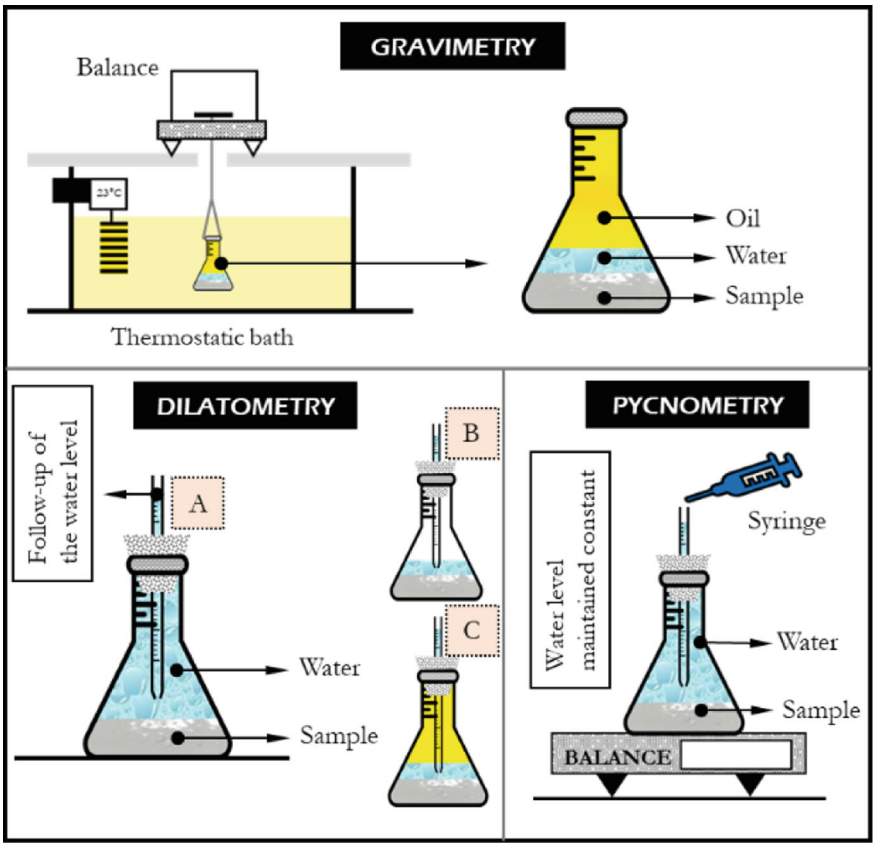

Fig. 19 Chemical shrinkage measurement methods. Modified based on [274, 283]

or alkali solution layer chosen by different researchers may affect direct comparisons between studies. Nonetheless, comparisons within a certain study under consistent experimental conditions remain valid.

6.2 Autogenous Shrinkage

In the case of autogenous shrinkage, measurements can be done on linear or gravimetric samples. Linear measurements correspond to a general principal, namely the monitoring of dimensional changes of a specimen on its longitudinal direction. The measurement can be made vertically by means of extensometers on the sample that has been removed from the mould and sealed [229, 285, 286], similar to the drying shrinkage method which consists in casting the material in prismatic steel moulds, which allow a screw to be embedded in the fresh material at each end. Metal inserts,

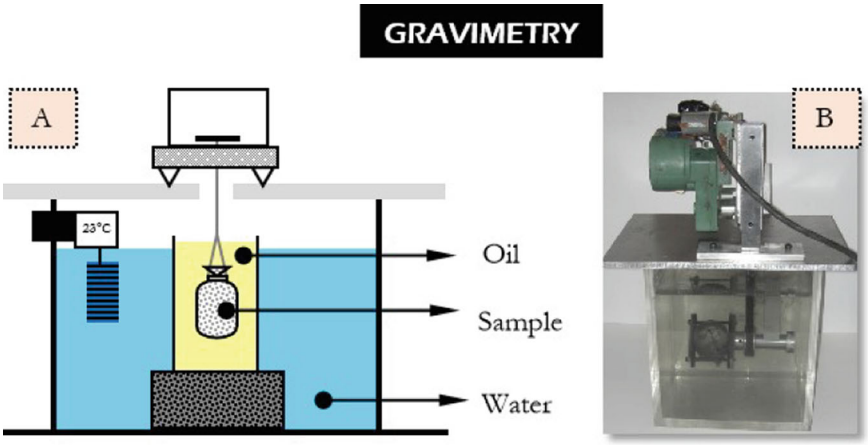

Fig. 20 Chemical shrinkage gravimetry method, **a** static samples; **b** rotated samples [107]

centred during casting, can be used, once the material has hardened, to install the test pieces in the measuring device. The test consists of measuring the deformation of mortar prisms having given dimensions which are function of the material (cement, mortar or concrete) and function of norms and standards used in different countries. The measuring device usually consists of a metal frame on which an extensometer is fixed. The measurements are taken each day, with a starting point of 24 h from the moment of liquid to solid contact, the first measurement indicating the initial length. The following measurements of the length of the mortar prisms allow us to calculate the deformations undergone by the material. Some authors proposed a variant of this measure but with a continuous acquisition of data, by using linear variable differential transformer sensors (LVDT's) [287, 288]. Measurements can also be taken horizontally, using LVDT's [289], gauges [290], inductive displacement transducers (IDT's) [291] or lasers [292]. Samples are commonly cast in a rigid module with a low friction.

Linear measures are prone to friction artefacts (mainly for horizontal methods) and to important settlement/sedimentation effects (mainly for vertical methods). In order to lessen the friction effect the use of lubricants on the substrate, plastic films and talcum powder is common practice [291, 293, 294].

Still many previous methods need demoulding of the samples before measurements start, so at the beginning of the tests samples are already hardened. Given that autogenous rate of autogenous shrinkage for PC is at its peak at early ages, measurement of the deformations before set time can give important information on the behaviour of the material. Jensen and Hansen [295] proposed the use of a flexible mould that does not prevent the deformation of the material, and that allows monitoring of the autogenous shrinkage as soon as the sample is cast. The measures can be made vertically or horizontally [280, 295–300]. Bouasker and al. [301] have shown that vertical devices are more likely to be influenced by bleeding, which leads

to an overestimation of the values measured. However it was shown that horizontal devices can be influenced by bleeding equally, and providing a rotating system for the samples can overcome the overestimation of values measured [302]. All this work resulted in standards and normalized measurement devices such as a new standard test method for autogenous strain measurement of cement paste and mortar using the corrugated tube method that was published by the American Society for Testing Materials [303]. Finally, some authors proposed improvements in the accuracy of the results by using non-contact sensors [304]. This corrugated tube method has been widely used to study AAMs [8, 31, 178].

Volumetric measurements set-up is very similar to chemical shrinkage gravimetric measurements [305, 306]. The main difference is that the system is sealed and no hydric exchange with the exterior is allowed in order to ensure the autogenous conditions required by the measure. The material is cast in a flexible waterproof membrane, able to follow the deformation of the sample. The sample is immersed in a thermostatically controlled water-filled container. Deformations are measured automatically immediately after casting. Usually no longer than 1 h will pass from the fabrication of the paste to the first acquired data. One of the main factors that influence the validity of the results is the bleeding of the material, giving rise to supplementary deformations at the moment when the water is re-absorbed. A solution was found by Le Roy et al. [287], who proposed a rotating system in order to avoid bleeding. Several studies show a neat improvement of precision of the measure when using the rotating system [273, 307–309]. Bleeding of the samples leads to an overestimation of the measured autogenous shrinkage, giving the same values of deformations as the chemical shrinkage within the first 24 h (see Fig. 21). It was shown that the set time coincides with the divergence between the chemical shrinkage and the autogenous shrinkage. Indeed, if no measurement artefacts are present, a divergence between the chemical and the autogenous shrinkage should be observed at liquid to solid transition moment. Till now, the number of published studies using volumetric method on AAMs are limited.

Several comparisons between the different measurement techniques were made [273, 280, 300, 310], including a RILEM round robin program [311]. The general trend show that linear horizontal measurements give the lowest values of deformations (due to friction), followed by the linear vertical measurements. Generally, if the values obtained are reinitialised at 24 h, the two measurements are quite similar. This is not the case with volumetric measurements which seem overestimated in most of the cases. Still, once the measurement artefacts are not present (mainly linked to the permeability of the membrane), that linear and volumetric measures can give similar results as shown by Sant et al. [278].

In the case of AAMs (Table 4), most of the authors applied for autogenous shrinkage measures the same linear method that is used to determine drying shrinkage (ASTM C490)—with the difference that the samples are being sealed once demolded. It should be noticed that most of autogenous shrinkage samples were demolded after set-time, whereas for drying shrinkage measurements begin at 24 h. Some authors use the corrugated test method developed for autogenous shrinkage monitoring at early ages. Few testing devices are developed just for AAMs: laser sensor [121] or

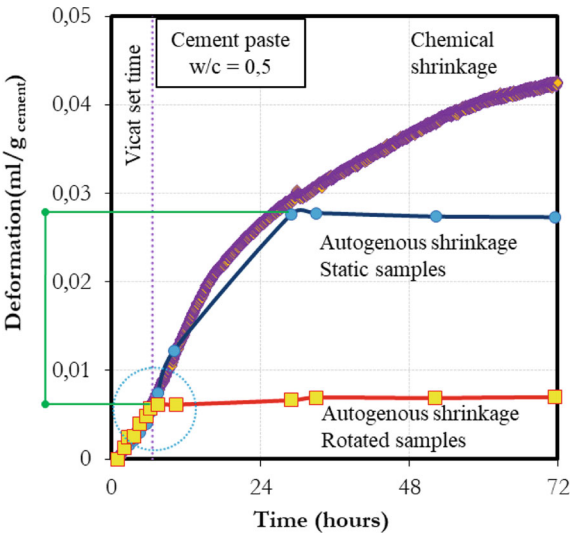

Fig. 21 Influence of the rotation of the samples for a w/c = 0.5 bleeding cement paste on the autogenous shrinkage value (volumetric setup) [312]

the autogenous deformation testing machine (ATDM) device, which is actually a version of a linear measurement [151].

The question that arises is that: are methods developed for PC directly transposable to alkali activated cements?

There is no doubt that the intense work and the numerous benchmarks that were made for PC systems in what concerns testing devices have provided sound measurement techniques, that can be applied to other cementitious materials, provided some verifications are previously made.

However, it has been shown that volumetric methods presented some bias that are intrinsic to the behaviour of the material. For example, bleeding is one of the most detrimental factors for autogenous measurements that monitor deformation starting from the moment the material is cast—rotating systems can mitigate these problems. This should probably be checked beforehand for AAMs, in order to assure a proper use of testing devices (although some authors specified using rotated samples, this is not a general trend that was observed for all the work done with AAMs). Some authors reported that a certain amount of pore solution is expelled for MK based formulations past setting, meaning that it is not bleeding water [107], and measurements of chemical shrinkage highlight a period of swelling instead contraction [106, 107]. These are factors that should be taken into account in the choice of the autogenous measurement technique, in order to avoid any experimental bias in the case of volumetric methods and corrugated tube setup.

Although chemical and autogenous shrinkage were already studied, the emergence of advances in laboratory work, enhanced measurement set-ups and modelling came with the development of high-performance building materials. These materials, with better mechanical properties and lower porosity that were gradually available on the market as they found various applications and became extensively used. Still,

the better performance of such materials came with a drawback: a higher occurrence of cracking risks at early ages due to a higher autogenous shrinkage [290, 313, 314]. This cracking risks at early ages occurs before any external load is applied on the structure. This naturally directed the work towards the comprehension of the phenomena triggering these higher values.

At early age, after setting, the material will simultaneously gain in stiffness and strength and will deform. Provided deformations are restrained, the greater they are, the higher the strains that will rise within the material and the higher the risk of cracking. For PC it has been shown that Young's modulus evolution at early ages happens at a faster kinetics than the evolution of mechanical strength [312, 315–319]. In other words, after final setting time, the material stiffens, and tends to oppose to the deformations that are imposed by the reaction of hydration, but the tensile strength is not yet high enough.

Yet, measurements of mechanical properties are possible once the material has set, and the samples can be demoulded. However, the material gains in stiffness as soon as initial setting begins and shrinkage of the material (a mix between chemical and autogenous shrinkage at this point) already induces stresses so some authors developed methods that allow to monitor the evolution of the material even before the final set of material [320, 321]. The procedure allows the determination of tensile strain capacity of the material and what was observed confirms previous results: during setting the tensile strength increases slowly whereas the tensile strain capacity decreases of several orders of magnitude, reaching a minimum value at final setting. The minimum values of tensile strain capacity are due to a shift between the development of the modulus and the tensile strength of concrete.

Thus, early age corresponds to a critical stage in terms of cracking for cementitious materials. Being identified as a main stress-inducing phenomenon, autogenous shrinkage has been widely studied and it had become quite clear that the moment at which measurements begin is crucial—which led to the evolution of experimental setups and to the definition of "time-zero" concept. This aimed to determine the best moment to start the acquisition of autogenous shrinkage data: if the measurements start too late it will lead to an underestimation of shrinkage values (and implicitly of cracking risks) whereas starting acquisition too soon might be of no interest as it does not have practical consequences in the stress developments. Time zero represents thus the transition from fluid to solid of the material—property that was normally identified by the normalized but still arbitrary Vicat setting time, but then several means of identification were proposed that were much closer linked to the microstructure changes and property evolution:

- superposing chemical and autogenous shrinkage data and identifying the deviation time between the two as shown in, method investigated by several authors [278, 312, 322–325];
- rate of change for electrical conductivity measurements of the pastes [322] or heat flow [284, 326, 327];
- ultrasonic measurements [284, 327–332].
- start of the acceleration period measured by calorimetry [116].

All this work aimed to determine an accurate time of set considered to be fundamental for acquiring correct data that can be used for the modelling of the cracking potential of PC or AAMs.

The purpose of developing novel methods of investigation was linked to the need of mitigate a structural problem linked to autogenous shrinkage.

7 Connections with Other Deformations

7.1 Autogenous Shrinkage and Chemical Shrinkage

Chemical shrinkage (also known as *Le Chatelier* contraction), is the driving force of autogenous shrinkage, and is originated from the absolute volume change due to chemical reaction in which the summed volume of all reacted products is less than the summed volume of all reactants (i.e., aluminosilicate precursors and activators). Chemical shrinkage of AAMs occur as activation proceeds and leads to macroscopic volume reduction of fresh AAMs in sealed conditions, manifested as autogenous shrinkage. As such, at the very early stages when AAMs have not solidified, the measured autogenous shrinkage is approximately the same as the chemical shrinkage, as illustrated in Fig. 22. However, as reaction continues and setting takes place due to precipitation and coalescence of reacted products, the increased stiffness of solidifying AAMs allow the formation of voids in the matrices. In other words, the chemical shrinkage (absolute volume reduction) past the setting moment, is manifested in the forms of internally distributed voids and pores in hardened matrices. As such, the autogenous shrinkage is usually less than the chemical shrinkage after the setting moment. Nevertheless, in addition to the *Le Chatelier* phenomena, capillary depression in the porous spaces formed in hardened cementitious matrices due to chemical shrinkage, can also contribute to the autogenous shrinkage. The pores formed in early-age AAMs under sealed condition are quickly drained and become partially saturated due to the consumption of free water in chemical reactions. This self-desiccation process in porous space results in the generation of meniscus at which capillary stress builds up, leading to contracting forces at pore walls. The capillary force acting on the solid skeleton of the porous matrices of AAMs results in additional macroscopic autogenous shrinkage. Therefore, the development of autogenous shrinkage of AAMs after setting is influenced by the magnitude of capillary force, stiffness, and viscoelasticity of porous matrices.

The magnitude of chemical shrinkage of cementitious materials affects the proportion of voids formed in hardening matrices, as well as the level of self-desiccation. Under an equivalent condition, lager chemical shrinkage tends to induce lager autogenous shrinkage, particularly at the early ages, as exemplified in Fig. 23. As such, the large autogenous shrinkage observed in slag-rich AAMs can be partially explained by its large chemical shrinkage. The chemical shrinkage of slag-rich AAMs can be measured using a similar approach as to PC systems (e.g., using dilatometry,

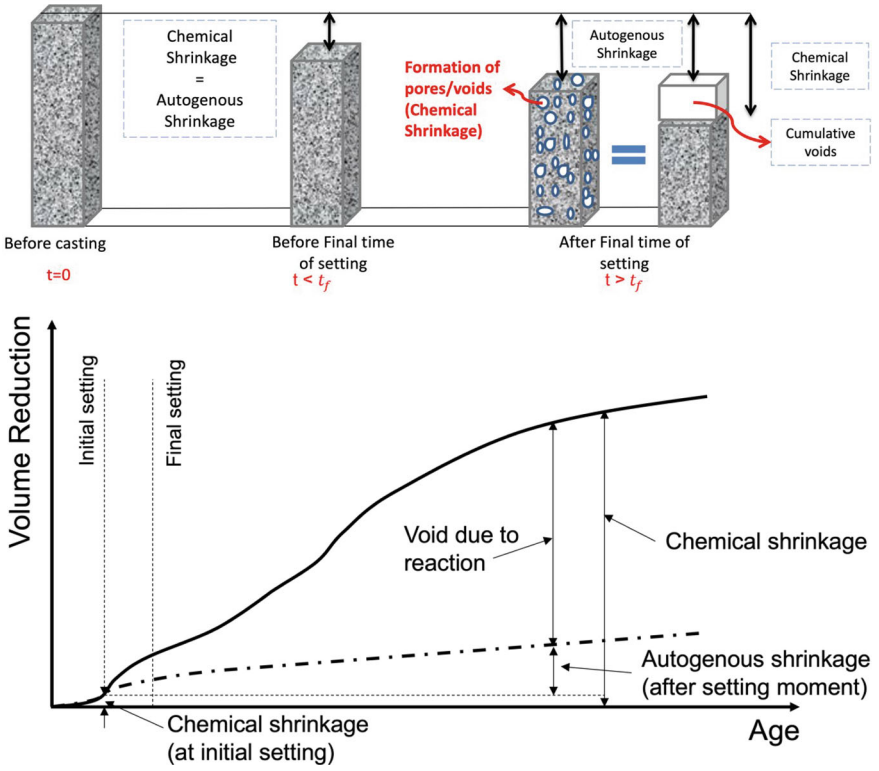

Fig. 22 The time-dependent relationship between chemical shrinkage and autogenous shrinkage of cementitious materials. Modified based on [333]

buoyancy method [334], small-angle neutron scattering [32]). The reported average chemical shrinkage of AAS paste is about 0.12 ml/g_{slag}, which is about twice larger than that of PC (0.06 ml/g_{cement}); however, the magnitude of chemical shrinkage is dependent on the activator type, as it affects phase assemblage and gel density. On the other hand, the development of reaction models of AAMs (simple stoichiometric models [335], thermodynamic models [336]), allows the theoretical estimation of chemical shrinkage, as shown in Fig. 24. The calculated chemical shrinkage of AAMs is close to the value of experimental measurements.

Another reason responsible for the large autogenous shrinkage of AAMs is attributed to the high alkalinity of the pore solution from the very beginning of alkaline activation. Different from PC systems, the alkali content in pore solution of AAMs can maintain at high levels even at late ages. The high alkali concentration of activator, regardless of using hydroxide or silicate-based solution, reduces the water activity and magnifies the surface tensions of the pore fluid in AAMs. Under the same level of self-desiccation and internal moisture content, the lower water activity

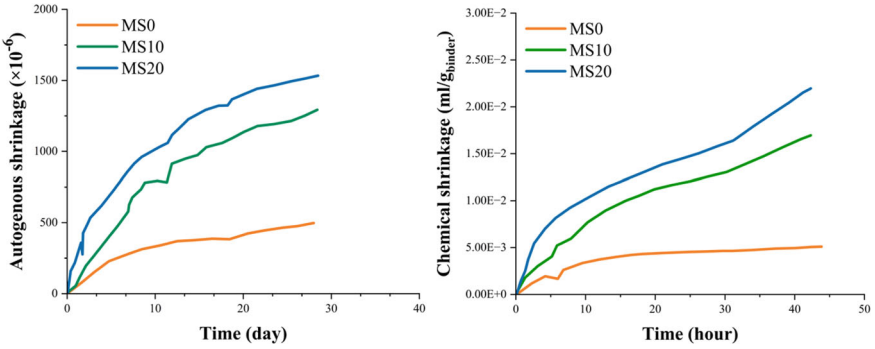

Fig. 23 Autogenous and chemical shrinkage of slag-fly ash based AAMs mortars (left) and pastes (right) with a constant water-to-binder ratio of 0.34. The data are from [257]

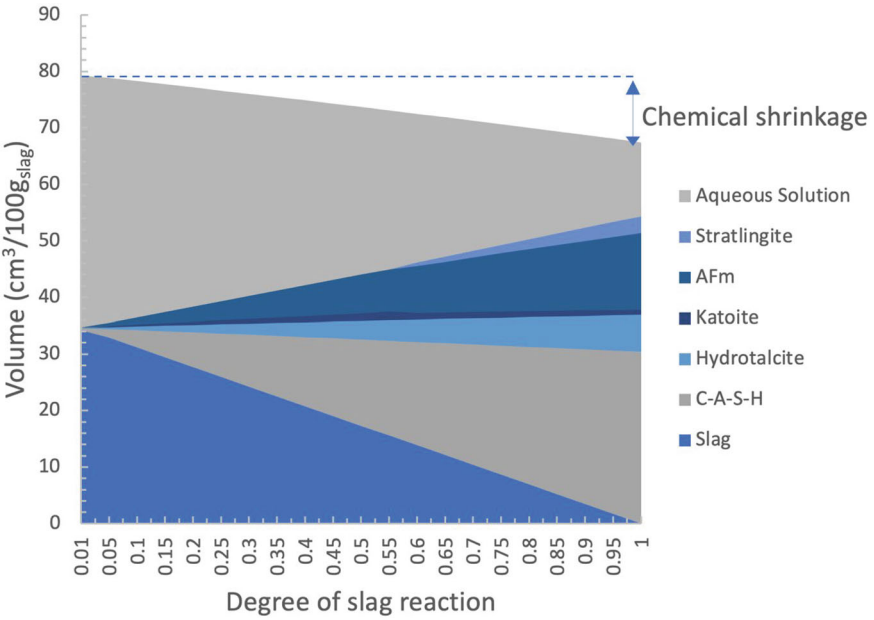

Fig. 24 Prediction of chemical shrinkage of AAS based on the phase evolution using thermodynamic modelling. Data are from [336]

and higher surface tension of the pore lead to higher capillary stresses at meniscus, thus resulting in higher autogenous shrinkage.

7.2 Autogenous Shrinkage and Thermal Deformation

The early-age alkaline activation is an exothermal process, which may lead to temperature rise of AAMs and hence induced thermal deformation. Therefore, in addition to autogenous shrinkage, simultaneous thermal deformation caused by heat release during activating reaction may occur in AAMs. Thus, some reported autogenous shrinkage results of AAMs in the literature results may include thermal deformation, if not separated properly. In case the time-dependent coefficient of thermal expansion of early-age AAMs is known, autogenous shrinkage can be simply distinguished from the thermal deformation. The temperature rise of AAMs during early-age reaction is usually less than 3 °C [256], and as such, the contribution of thermal deformation is considered to be relatively small for AAMs, as illustrated in Fig. 25. However, under semi-adiabatic condition, the temperature increase in slag-based AAMs can be up to 10 °C, which enhances autogenous shrinkage when cooled down [337].

7.3 Autogenous Shrinkage and Drying Shrinkage

The apparent difference between autogenous shrinkage and drying shrinkage of AAMs is that one occurs under a sealed condition while another is in an open system. However, such single apparent difference can lead to significant differences in shrinkage kinetics, magnitude, and underlying mechanisms. In addition, exposing AAMs to atmosphere results in carbonation and sometimes efflorescence, which can induced phase alteration and related volume change [338, 339]. As such, some reported drying shrinkage data of AAMs may include the component originated from surface carbonation, although its contribution may be trivial to large members. On the contrary, the measured autogenous shrinkage of AAMs may include the volume variation due to thermal effects at the very early ages.

In a sealed system, the magnitude and kinetics of shrinkage (i.e., autogenous shrinkage) of AAMs of a given formulation is theoretically irrespective of the specimen size, but highly influenced by the L/S ratio and activator type or composition. It is reasonable that lower L/S ratio can result in a higher autogenous shrinkage magnitude due to stronger self-desiccation, which increases capillary stress. The activator type or composition affects the kinetics of precursors dissolution and reaction, time-dependent evolution of internal RH, as well as the early-age properties (e.g., elastic modulus, viscosity) of solidifying AAMs materials, all of which are intimately relevant to autogenous shrinkage. As shown in Fig. 26, it was reported that the autogenous shrinkage of slag-based AAMs increases with the activator dosage, which may be explained by the faster reaction and higher alkalinity of pore fluid. Under the same alkali dosage, the autogenous shrinkage of sodium silicate-activated slag is influenced by the silica modulus ($n = SiO_2/Na_2O$). As shown in Fig. 27, the AAM with medium level of n ($n = 0.5$) shows the largest autogenous shrinkage, under which

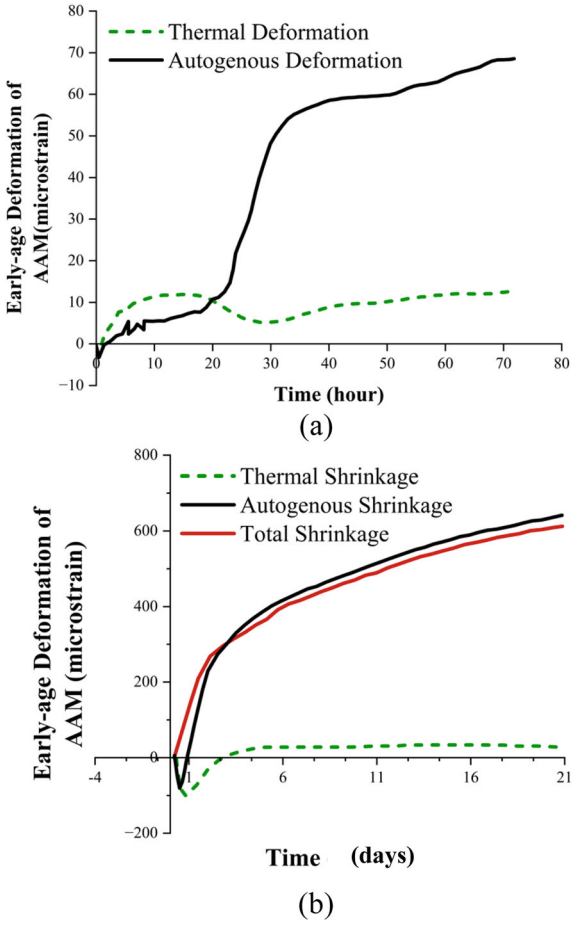

Fig. 25 **a** The contribution of thermal deformation to the early-age autogenous shrinkage of AAMs (The linear coefficient of thermal expansion of AAMs is assumed to be constant at 5 $\times$ 10^{-6}/°C) (data are from [247]); **b** Simulated autogenous, thermal and total deformations of slag-based AAMs concrete under semi-adiabatic condition. Data are from [337]

aqueous silicate composition the dissolution of slag may be most intensive. Similar observation was reported in FA-based AAMs, as illustrated in Fig. 28.

When hardened AAMs are exposed to an atmospheric condition (an unsealed system), shrinkage or swelling can occur depending on gradient direction of vapor pressure between internal and external environments (e.g., internal and external RH levels). Under a low ambient RH condition, evaporation of internal moisture in AAMs takes place, leading to loss of moisture and thus drying shrinkage. The rate of evaporation is dependent on the temperature, composition and properties of the pore solution, the gradient of vapor pressure, the rate of air flow, and the diffusion coefficient of hardened matrices. Therefore, in comparison with autogenous shrinkage, the magnitude of drying shrinkage of AAMs is not uniform, but depends on the level of evaporation. The drying surface has a higher capillary pressure and tends to shrink more than the interior regions. When the higher shrinkage at drying surface is restrained by the relative lower shrinkage at interior, tensile stress is formed at surface, which may induce

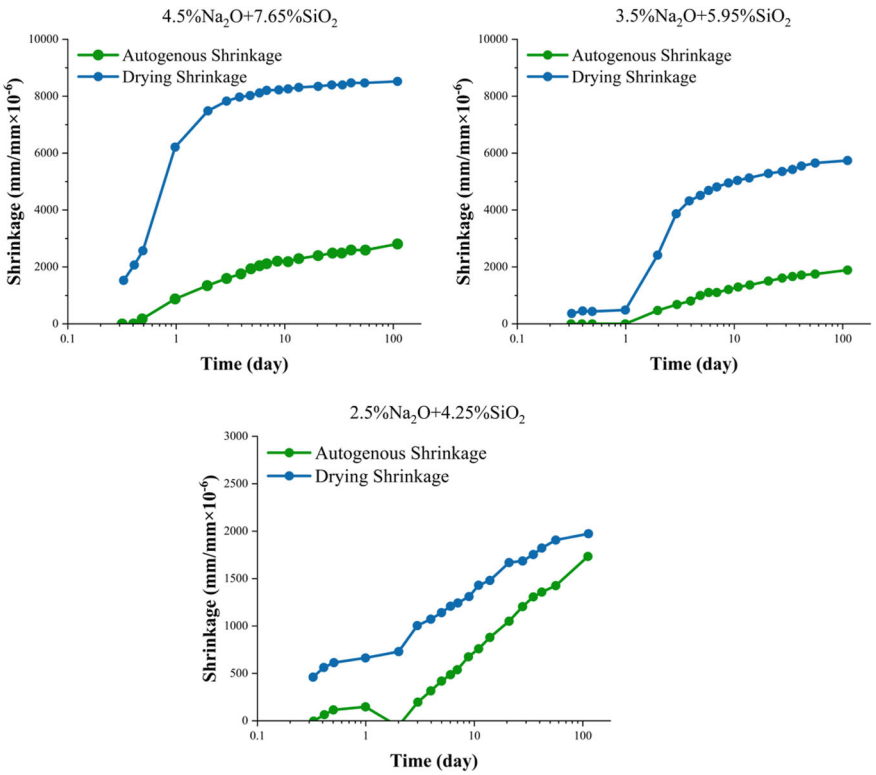

Fig. 26 The development of drying and autogenous shrinkage of sodium silicate-activated slag prepared using waterglass of different concentrations (with the same silica modulus). Data are from [256]

micro-cracking. In addition, the measured drying shrinkage of AAMs is affected by the size and shape of the specimens used. The kinetics of drying shrinkage in AAMs is also dependent on the rate of evaporation, properties of pore solution, pore structure, and sample geometry. Practically, the magnitude of drying shrinkage of AAMs is affected by the age at which measurement commences, since the diffusion-related properties and stiffness of hardened AAMs matrices evolves over curing.

Similar to the trends observed in autogenous shrinkage, the drying shrinkage of AAMs tend to be large for those prepared using a higher alkali content and silica modulus, as shown in Figs. 23, 24 and 25. The major reason behind this phenomenon may be related to the considerable variation of pore structure and viscoelastic performance of AAMs prepared using different activators. In particular, the AAMs with higher alkali and silicate dosages tend to have more densified pore structure but more reduced stiffness, both of which contributes to a higher drying-induced deformation. In addition, the high alkalinity of pore fluid in AAMs prepared using higher alkali dosage increases the capillary stress under a given RH condition, magnifying the capillary force.

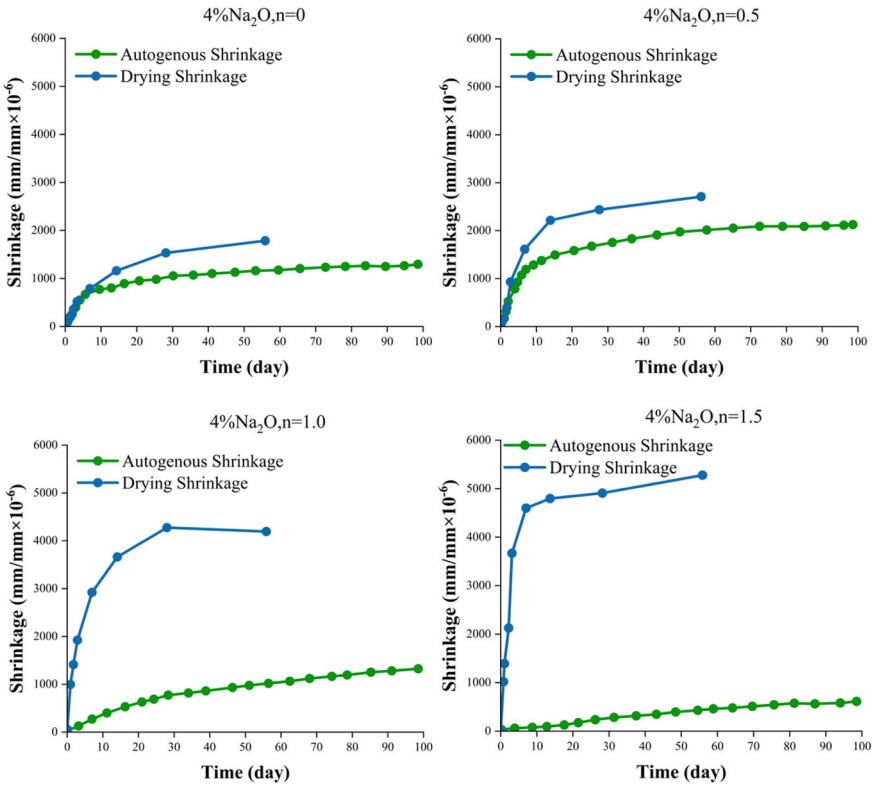

Fig. 27 The development of drying and autogenous shrinkage of slag-based AAMs prepared with the same alkali dosage (4% Na_2O) but different silica modulus ($n = 0$, 0.5, 1.0, and 1.5). Data are from [50]

When early-age AAMs is exposed to drying conditions, the scenario is even more complicated. The concurrence of self-desiccation and drying may result in a different kinetics and magnitude of overall shrinkage. In other words, the overall shrinkage may not be simply a sum of autogenous shrinkage and pure drying shrinkage. More specifically, early-age drying can interrupt the hydration process, modify the moisture distribution, and affect the development of C–(A)–S–H properties. Therefore, it is important to assess the time-dependent properties of young cementitious materials, as well as the influence of drying on the evolution of early age properties.

7.4 Autogenous Shrinkage and Creep

Creep is a material property defined as a time-dependent deformation under sustained forces. The forces acting on cementitious materials can be imposed externally or

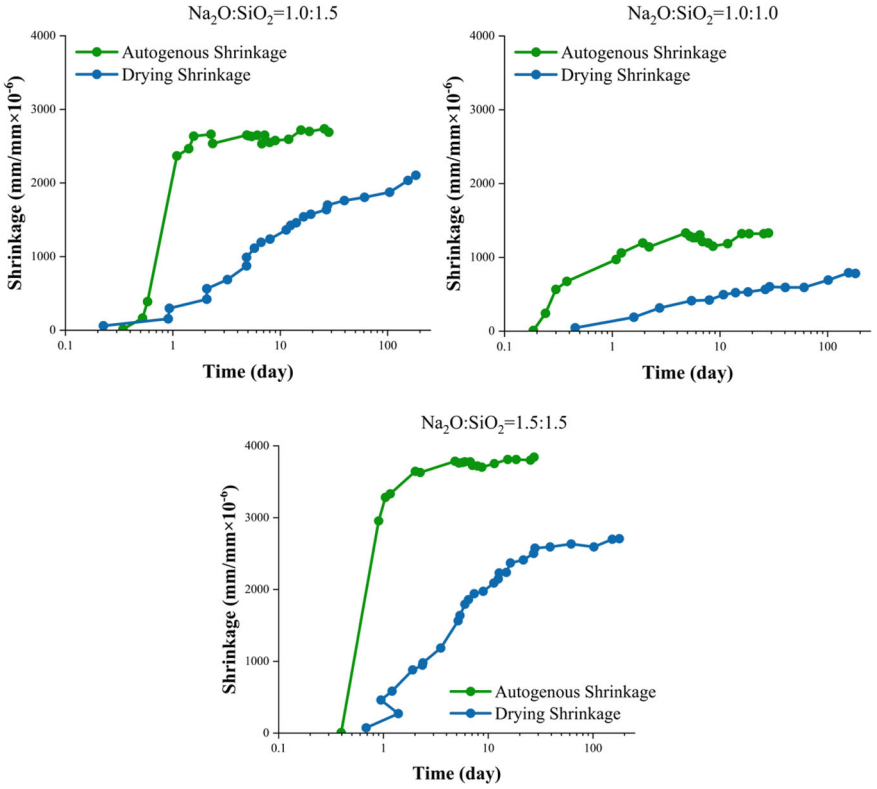

Fig. 28 The development of drying and autogenous shrinkage of FA-based AAMs prepared with the waterglass of different compositions. Data are from [48]

internally, including the forms of internal forces built up with the generation of capillary stresses in autogenous shrinkage, as mentioned earlier. In that context, the autogenous and drying shrinkage of cementitious materials may contain some creep deformation (i.e., the viscoelastic/viscoelastic deformation under sustained internal capillary forces), as exemplified in Fig. 29. The AAMs usually has relatively low elastic and creep modulus (more pronounced viscoelastic deformation) [149], and, thus, a substantial proportion of the autogenous deformation in AAMs may be originated from creep [116]. It should be noted that the creep phenomenon is not necessarily related to the drying condition. In fact, creep can be observed in sealed or immersed condition [88]. The origin of creep of AAMs is believed to be related to the reorganization and redistribution of gel products under internal stresses [57]. However, systematic investigation on the creep mechanism of AAMs is rare.

Based on the relationship between creep and autogenous shrinkage, one strategy to enhance the volumetric stability of AAMs is to improve its stiffness; however, large creep is beneficial to stress relaxation, while higher stiffness may impose larger restrained shrinkage stresses that increase the risk of cracking. Moreover, because

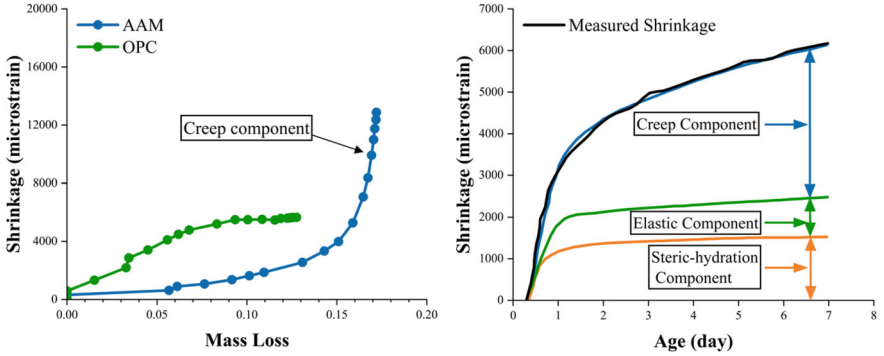

Fig. 29 (Left) Shrinkage development of PC and slag-based AAMs under constant moisture content (or degree of saturation) (data are from [57]); (right) Decomposition of the contribution of different components on autogenous shrinkage Data are from [116]

of the higher creep compliance of AAMs, its higher autogenous shrinkage does not always lead to higher cracking risk under restrained conditions.

8 Conclusions and Perspectives

Autogenous shrinkage of construction materials can lead to cracking under restrained conditions and then reduce the serviceability and lifetime of structures. Previous studies have shown that AAMs can show high autogenous shrinkage compared with PC. The value and kinetics of autogenous shrinkage differ with the types of precursors, alkali activators and the curing conditions. For AAS or slag dominating systems, one general consensus is that the autogenous shrinkage of the AAMs is higher than that of PC. The main difference in the deformation is spotted at the early ages. In AAFA or AAMK systems, the autogenous shrinkage turns to be similar and even lower than that of PC. When it comes to slag-FA/MK blended AAMs, higher autogenous shrinkage is observed with the higher amount of slag. Shrinkage behaviour in AAMs prepared with different widely used activators can also be concluded. The lowest autogenous shrinkage of AAMs is claimed in that with sodium carbonate. While being activated with sodium silicate, attributed to the extreme reaction rates both the magnitude and the kinetics of the autogenous shrinkage increased significantly. The key features for determining the autogenous shrinkage are Na_2O content and the alkali-activated modulus SiO_2/M_2O, the higher which the larger the autogenous shrinkage. As with the analysed weight ranking of influencing factors, the modulus of sodium silicate is the second important feature for autogenous shrinkage.

Over the past decades, numerous methods have been proposed to mitigate autogenous shrinkage of AAMs, e.g., use of shrinkage-reducing agents, water repelling

agents, expansive agents, internal curing, optimization of the mix design and addition of inert inclusions or polypropylene fibres. Each strategy has its own advantages and limitations, and the optimal approach will depend on the specific application and requirements of the AAS. However, by carefully considering these factors and selecting the appropriate strategy, it is possible to overcome the challenges associated with shrinkage and achieve high-performance AAS with excellent durability and strength.

To predict the early-age deformation and evaluate the cracking potential, different empirical models, analytical expressions and formulae of autogenous shrinkage of AAMs have been proposed in recent years. Although these proposed models or formulae can predict the trend of autogenous shrinkage of AAMs, there is still a significant discrepancy between measured and predicted results. Several critical areas necessitate further research, e.g., influence of curing temperature, consideration of additional mechanisms, definition of time zero and integration of new experimental results.

An accurate measurement of the autogenous shrinkage of AAMs and a clear comprehension of the mechanisms are important also to the understanding of other deformations that are related to autogenous shrinkage, such as thermal deformation, drying shrinkage, and creep. It is hoped that the information reviewed in the chapter can act as a stepping stone for future studies on the volume stability of sustainable building materials.

Acknowledgements Lavinia Stefan contributed to the writing of Sect. 6, but she cannot be listed as an author of this chapter since she has not been a RILEM member. Zhenming Li would like to acknowledge the Guangdong Provincial Key Laboratory of Intelligent and Resilient Structures for Civil Engineering (2023B1212010004) and Guangdong Basic and Applied Basic Research Foundation (2023A1515111138).

References

1. Jensen, O.M., Hansen, P.F.: Autogenous deformation and RH-change in perspective. Cem. Concr. Res. **31**, 1859–1865 (2001). https://doi.org/10.1016/S0008-8846(01)00501-4
2. Lura, P.: Autogenous Deformation and Internal Curing of Concrete. Ph.D. thesis. Delft University of Technology (2003)
3. Provis, J.L., Van Deventer, J.S.J.: Geopolymers: structures, Processing, Properties and Industrial Applications. Elsevier (2009)
4. Uppalapati, S.: Early-age structural development and autogenous shrinkage of alkali-activated slag/fly-ash cements. KU Leuven (2021)
5. Li, Z.: Autogenous shrinkage of alkali-activated slag and fly ash materials from mechanism to mitigating strategies. TU Delft University (2021)
6. Bakharev, T., Sanjayan, J.G., Cheng, Y.: Effect of admixtures on properties of alkali-activated slag concrete. **30** (2000)
7. Ballekere Kumarappa, D., Peethamparan, S., Ngami, M.: Autogenous shrinkage of alkali activated slag mortars: basic mechanisms and mitigation methods. Cem. Concr. Res. **109**, 1–9 (2018). https://doi.org/10.1016/j.cemconres.2018.04.004

8. Chen, W., Li, B., Wang, J., Thom, N.: Cement and concrete research effects of alkali dosage and silicate modulus on autogenous shrinkage of alkali-activated slag cement paste. **141** (2021). https://doi.org/10.1016/j.cemconres.2020.106322
9. Markandeya, A., Shanahan, N., Mapa, D., et al.: Influence of slag composition on cracking potential of slag-Portland cement concrete. Constr. Build. Mater. **164**, 820–829 (2018). https://doi.org/10.1016/j.conbuildmat.2017.12.216
10. Elahi, M.M.A., Hossain, M.M., Karim, M.R., et al.: A review on alkali-activated binders: materials composition and fresh properties of concrete. Constr. Build. Mater. **260**, 119788 (2020). https://doi.org/10.1016/j.conbuildmat.2020.119788
11. Nodehi, M., Taghvaee, V.M.: Alkali-activated materials and geopolymer: a review of common precursors and activators addressing circular economy. Circ. Econ. Sustain. **2**, 165–196 (2022). https://doi.org/10.1007/s43615-021-00029-w
12. Shi, C.: Strength, pore structure and permeability of alkali-activated slag mortars. Cem. Concr. Res. **26**, 1789–1799 (1996). https://doi.org/10.1016/S0008-8846(96)00174-3
13. Shi, C., Day, R.L.: Some factors affecting early hydration of alkali-slag cements. Cem. Concr. Res. **26**, 439–447 (1996)
14. Vafaei, B., Farzanian, K., Ghahremaninezhad, A.: The influence of superabsorbent polymer on the properties of alkali-activated slag pastes. Constr. Build. Mater. **236**, 117525 (2020). https://doi.org/10.1016/j.conbuildmat.2019.117525
15. Prabahar, J., Vafaei, B., Baffoe, E., Ghahremaninezhad, A.: The effect of biochar on the properties of alkali-activated slag pastes. 1–14 (2022)
16. Mastali, M., Kinnunen, P., Dalvand, A., et al.: Drying shrinkage in alkali-activated binders—A critical review. Constr. Build. Mater. **190**, 533–550 (2018). https://doi.org/10.1016/j.conbuildmat.2018.09.125
17. Wang, S.D., Pu, X.C., Scrivener, K.L., Pratt, P.L.: Alkali-activated slag cement and concrete: a review of properties and problems. Adv. Cem. Res. **7**, 93–102 (1995). https://doi.org/10.1680/adcr.1995.7.27.93
18. Li, Y., Sun, Y.: Preliminary study on combined-alkali-slag paste materials. Cem. Concr. Res. **30**, 963–966 (2000). https://doi.org/10.1016/S0008-8846(00)00269-6
19. Thomas, R.J., Lezama, D., Peethamparan, S.: On drying shrinkage in alkali-activated concrete: improving dimensional stability by aging or heat-curing. Cem. Concr. Res. **91**, 13–23 (2017). https://doi.org/10.1016/j.cemconres.2016.10.003
20. Puertas, F., Amat, T., Fernández-Jiménez, A., Vázquez, T.: Mechanical and durable behaviour of alkaline cement mortars reinforced with polypropylene fibres. Cem. Concr. Res. **33**, 2031–2036 (2003). https://doi.org/10.1016/S0008-8846(03)00222-9
21. Rakhimova, N.R., Rakhimov, R.Z.: A review on alkali-activated slag cements incorporated with supplementary materials. J. Sustain. Cem.-Based Mater. **3**, 61–74 (2014). https://doi.org/10.1080/21650373.2013.876944
22. Sun, B., Ye, G., de Schutter, G.: A review: reaction mechanism and strength of slag and fly ash-based alkali-activated materials. Constr. Build. Mater. **326**, 126843 (2022). https://doi.org/10.1016/j.conbuildmat.2022.126843
23. Li, Z., Chen, Y., Provis, J.L., et al.: Autogenous shrinkage of alkali-activated slag: a critical review. Cem. Concr. Res. **172**, 107244 (2023). https://doi.org/10.1016/j.cemconres.2023.107244
24. Awoyera, P., Adesina, A.: A critical review on application of alkali activated slag as a sustainable composite binder. Case Stud. Construct. Mater. **11**, e00268 (2019). https://doi.org/10.1016/j.cscm.2019.e00268
25. Provis, J.L.: Alkali-activated materials. Cem. Concr. Res. **114**, 40–48 (2018). https://doi.org/10.1016/j.cemconres.2017.02.009
26. Karim, R., Hossain, M., Elahi, M.A., et al.: Effects of source materials, fineness and curing methods on the strength development of alkali-activated binder. J. Build. Eng. **29**, 101147 (2020). https://doi.org/10.1016/j.jobe.2019.101147
27. Wang, P.Z., Trettin, R., Rudert, V.: Effect of fineness and particle size distribution of granulated blast-furnace slag on the hydraulic reactivity in cement systems. Adv. Cem. Res. **17**, 161–167 (2005)

28. Amer, I., Kohail, M., El-Feky, M.S., et al.: A review on alkali-activated slag concrete. Ain Shams Eng. J. **12**, 1475–1499 (2021). https://doi.org/10.1016/j.asej.2020.12.003
29. Wan, H., Shui, Z., Lin, Z.: Analysis of geometric characteristics of GGBS particles and their influences on cement properties. **34**, 133–137 (2004). https://doi.org/10.1016/S0008-8846(03)00252-7
30. Mohamed, O.A.: A review of durability and strength characteristics of alkali-activated slag concrete. Materials **12** (2019). https://doi.org/10.3390/ma12081198
31. Nedeljković, M., Li, Z., Ye, G.: Setting, strength, and autogenous shrinkage of alkali-activated fly ash and slag pastes: effect of slag content. Materials **11** (2018). https://doi.org/10.3390/ma11112121
32. Thomas, J.J., Allen, A.J., Jennings, H.M.: Density and water content of nanoscale solid C–S–H formed in alkali-activated slag (AAS) paste and implications for chemical shrinkage. Cem. Concr. Res. **42**, 377–383 (2012)
33. Pacheco-Torgal, F., Castro-Gomes, J., Jalali, S.: Alkali-activated binders: a review. Part 2. About materials and binders manufacture. Constr. Build. Mater. **22**, 1315–1322 (2008). https://doi.org/10.1016/j.conbuildmat.2007.03.019
34. Pan, Z., Cheng, L., Lu, Y., Yang, N.: Hydration products of alkali-activated slag–red mud cementitious material. Cem. Concr. Res. **32**, 357–362 (2002)
35. Talling, B., Brandstetr, J.: Present state and future of alkali-activated slag concretes. Spec. Publ. **114**, 1519–1546 (1989)
36. Wang, S.D., Scrivener, K.L., Pratt, P.L.: Factors affecting the strength of alkali-activated slag. Cem. Concr. Res. **24**, 1033–1043 (1994). https://doi.org/10.1016/0008-8846(94)90026-4
37. Suntharalingam, S., Takahashi, Y.: Experimental study on autogenous shrinkage behaviors of different Portland blast furnace slag cements. Constr. Build. Mater. **230**, 116980 (2020). https://doi.org/10.1016/j.conbuildmat.2019.116980
38. Hansen, W., Hansen, W., Mat, A.C.I., et al.: Unified shrinkage model for concrete from autogenous shrinkage test on paste with and without GGBFS related papers, Unified shrinkage model for concrete from autogenous shrinkage test on paste with and without ground-granulated blast-furnace slag (2013)
39. Zhang, W., Hama, Y., Hyun, S.: Drying shrinkage and microstructure characteristics of mortar incorporating ground granulated blast furnace slag and shrinkage reducing admixture. Constr. Build. Mater. **93**, 267–277 (2015). https://doi.org/10.1016/j.conbuildmat.2015.05.103
40. Bentz, D.P., Jensen, O.M., Hansen, K.K., et al.: Influence of cement particle-size distribution on early age autogenous strains and stresses in cement-based materials. **35**, 129–135 (2001)
41. Brough, A.R., Atkinson, A.: Sodium silicate-based, alkali-activated slag mortars—Part I. Strength, hydration and microstructure. Cem. Concr. Res. **32**, 865–879 (2002). https://doi.org/10.1016/S0008-8846(02)00717-2
42. He, J., Bai, W., Zheng, W., et al.: Influence of hydrated lime on mechanical and shrinkage properties of alkali-activated slag cement. Constr. Build. Mater. **289**, 123201 (2021). https://doi.org/10.1016/j.conbuildmat.2021.123201
43. Ye, H., Radlińska, A.: Shrinkage mitigation strategies in alkali-activated slag. Cem. Concr. Res. **101**, 131–143 (2017). https://doi.org/10.1016/j.cemconres.2017.08.025
44. Gong, J., Qu, Z.: Mechanical properties and drying shrinkage investigation of alkali-activated mortar using waste glass powder (2020)
45. Chen, W., Li, B., Wang, J., Thom, N.: Effects of alkali dosage and silicate modulus on autogenous shrinkage of alkali-activated slag cement paste. Cem. Concr. Res. **141**, 106322 (2021)
46. Kang, C., Kim, T.: Pore and strength characteristics of alkali-activated slag paste with seawater. Mag. Concr. Res. **72**, 499–508 (2020). https://doi.org/10.1680/jmacr.18.00390
47. Collins, F., Sanjayan, J.G.: Effect of pore size distribution on drying shrinkage of alkali-activated slag concrete. Cem. Concr. Res. **30**, 1401–1406 (2000). https://doi.org/10.1016/S0008-8846(00)00327-6
48. Ma, Y., Ye, G.: The shrinkage of alkali activated fly ash. Cem. Concr. Res. **68**, 75–82 (2015). https://doi.org/10.1016/j.cemconres.2014.10.024

49. Zhang, B., Zhu, H., Wei, K., et al.: Optimization of mix proportion of alkali-activated slag mortars prepared with seawater and coral sand. Constr. Build. Mater. **284**, 122805 (2021). https://doi.org/10.1016/j.conbuildmat.2021.122805
50. Hu, X., Shi, C., Zhang, Z., Hu, Z.: Autogenous and drying shrinkage of alkali-activated slag mortars. J. Am. Ceram. Soc. **102**, 4963–4975 (2019). https://doi.org/10.1111/jace.16349
51. Cartwright, C., Rajabipour, F., Radlińska, A.: Shrinkage characteristics of alkali-activated slag cements. J. Mater. Civ. Eng. **27**, 1–9 (2015). https://doi.org/10.1061/(asce)mt.1943-5533.0001058
52. Humad, A.M., Provis, J.L., Cwirzen, A.: Effects of curing conditions on shrinkage of alkali-activated high-MgO Swedish Slag concrete **6** (2019). https://doi.org/10.3389/fmats.2019.00287
53. Bakharev, T., Sanjayan, J.G., Cheng, Y.B.: Effect of elevated temperature curing on properties of alkali-activated slag concrete. Cem. Concr. Res. **29**, 1619–1625 (1999). https://doi.org/10.1016/S0008-8846(99)00143-X
54. Cai, Y., Yu, L., Yang, Y., et al.: Effect of early age-curing methods on drying shrinkage of alkali-activated slag concrete. Materials **12**, 1633 (2019)
55. Chi, M.: Effects of dosage of alkali-activated solution and curing conditions on the properties and durability of alkali-activated slag concrete. Constr. Build. Mater. **35**, 240–245 (2012). https://doi.org/10.1016/j.conbuildmat.2012.04.005
56. Ye, H., Cartwright, C., Rajabipour, F., Radlińska, A.: Understanding the drying shrinkage performance of alkali-activated slag mortars. Cem. Concr. Compos. **76**, 13–24 (2017). https://doi.org/10.1016/j.cemconcomp.2016.11.010
57. Ye, H., Radlińska, A.: Shrinkage mechanisms of alkali-activated slag. Cem. Concr. Res. **88**, 126–135 (2016). https://doi.org/10.1016/j.cemconres.2016.07.001
58. Zhang, B., Zhu, H., Cheng, Y., et al.: Shrinkage mechanisms and shrinkage-mitigating strategies of alkali-activated slag composites: a critical review. Constr. Build. Mater. **318**, 125993 (2022). https://doi.org/10.1016/j.conbuildmat.2021.125993
59. Melo, A.A., Alba, M., Repette, W.: Drying and autogenous shrinkage of pastes and mortars with activated slag cement. **38**, 565–574 (2008). https://doi.org/10.1016/j.cemconres.2007.11.002
60. Lin, F.: Modeling of hydration kinetics and shrinkage of Portland cement paste (2006)
61. Aili, A., Vandamme, M., Torrenti, J.-M., Masson, B.: Is long-term autogenous shrinkage a creep phenomenon induced by capillary effects due to self-desiccation? Cem. Concr. Res. **108**, 186–200 (2018)
62. Abate, S.Y., Park, S., Kim, H.K.: Parametric modeling of autogenous shrinkage of sodium silicate-activated slag. Constr. Build. Mater. **262**, 120747 (2020). https://doi.org/10.1016/j.conbuildmat.2020.120747
63. Yang, L.Y., Jia, Z.J., Zhang, Y.M., Dai, J.G.: Effects of nano-TiO2 on strength, shrinkage and microstructure of alkali activated slag pastes. Cement Concr. Compos. **57**, 1–7 (2015). https://doi.org/10.1016/j.cemconcomp.2014.11.009
64. Lee, N.K., Jang, J.G., Lee, H.-K.: Shrinkage characteristics of alkali-activated fly ash/slag paste and mortar at early ages. Cement Concr. Compos. **53**, 239–248 (2014). https://doi.org/10.1016/j.cemconcomp.2014.07.007
65. Wang, X., Wang, K., Bektas, F., et al.: Drying shrinkage of ternary blend concrete in transportation structures. 0373 (2012). https://doi.org/10.1080/21650373.2012.728566
66. Wang, S., Wang, S.: Review of recent research on alkali-activated concrete in China. 29–35 (1991)
67. Aydin, S., Baradan, B.: Effect of activator type and content on properties of alkali-activated slag mortars. Compos. B Eng. **57**, 166–172 (2014). https://doi.org/10.1016/j.compositesb.2013.10.001
68. Shi, C.-J., Day, R.L.: Comparison of the microstructure and performance of alkali-slag and Portland cement pastes. Int. Congr. Chem. Cem. 9 th, III pp. 298 (1992)
69. Kutti, T.: Hydration products of alkali activated slag. In: Ninth International Congress on Cement Chemistry, vol. 4, pp. 468–474 (1992)

70. Glukhovskij, V., Zaitsev, Y., Pakhomov, V.: Slag-alkaline cements and concretes-structure, properties, technological and economical aspects of the use. Silic. Indus. **48**, 197–200 (1983)
71. Krizan, D., Zivanovic, B.: Effects of dosage and modulus of water glass on early hydration of alkali-slag cements. Cem. Concr. Res. **32**, 1181–1188 (2002). https://doi.org/10.1016/S0008-8846(01)00717-7
72. Wang, S.D., Scrivener, K.L.: Hydration products of alkali activated slag cement. Cem. Concr. Res. **25**, 561–571 (1995). https://doi.org/10.1016/0008-8846(95)00045-E
73. Jiang, W., Silsbee, M.R., Roy, D.M.: Alkali activation reaction mechanism and its influence on microstructure of slag cement. In: Proceedings of the 10th International Congress on the Chemistry of Cement. Amarkai and Congrex Göteborg Gothenburg, pp. 1–9, Sweden (1997)
74. Richardson, I.G., Brough, A.R., Groves, G.W., Dobson, C.M.: The characterization of hardened alkali-activated blast-furnace slag pastes and the nature of the calcium silicate hydrate (C–S–H) phase. Cem. Concr. Res. **24**, 813–829 (1994). https://doi.org/10.1016/0008-8846(94)90002-7
75. Gruskovnjak, A., Lothenbach, B., Holzer, L., et al.: Hydration of alkali-activated slag: comparison with ordinary Portland cement. Adv. Cem. Res. **18**, 119–128 (2006). https://doi.org/10.1680/adcr.2006.18.3.119
76. Richardson, I.G., Groves, G.W.: The incorporation of minor and trace elements into calcium silicate hydrate (C–S–H) gel in hardened cement pastes. Cem. Concr. Res. **23**, 131–138 (1993)
77. Faucon, P., Delagrave, A., Petit, J.C., et al.: Aluminum incorporation in calcium silicate hydrates (C−S−H) depending on their Ca/Si ratio. J. Phys. Chem. B **103**, 7796–7802 (1999)
78. Jennings, H.M.: Model for the microstructure of calcium silicate hydrate in cement paste. Cem. Concr. Res. **30**, 101–116 (2000). https://doi.org/10.1016/S0008-8846(99)00209-4
79. Alcaide, J.S., Alcocel, E.G., Puertas, F., et al.: Comportamiento de morteros de escoria activada alcalinamente con adición de fibras de carbón. Materiales de Construccion **57**, 33–48 (2007). https://doi.org/10.3989/mc.2007.v57.i288.63
80. Thomas, J.J., Allen, A.J., Jennings, H.M.: Cement and concrete research density and water content of nanoscale solid C–S–H formed in alkali-activated slag (AAS) paste and implications for chemical shrinkage. Cem. Concr. Res. **42**, 377–383 (2012). https://doi.org/10.1016/j.cemconres.2011.11.003
81. Zhu, X., Tang, D., Yang, K., et al.: Effect of Ca (OH) 2 on shrinkage characteristics and microstructures of alkali-activated slag concrete. Constr. Build. Mater. **175**, 467–482 (2018). https://doi.org/10.1016/j.conbuildmat.2018.04.180
82. Zhang, B., Zhu, H., Shah, K.W., et al.: Performance evaluation and microstructure characterization of seawater and coral/sea sand alkali-activated mortars. Constr. Build. Mater. **259**, 120403 (2020). https://doi.org/10.1016/j.conbuildmat.2020.120403
83. Gu, Y., Fang, Y.: Shrinkage, cracking, shrinkage-reducing and toughening of alkali-activated slag cement—A short review. Kuei Suan Jen Hsueh Pao/J. Chinese Ceram. Soc. **40**, 76–84 (2012)
84. Ye, H., Radlińska, A.: A review and comparative study of existing shrinkage prediction models for Portland and non-Portland cementitious materials. Adv. Mater. Sci. Eng. **2016**, 10–14 (2016). https://doi.org/10.1155/2016/2418219
85. Kovler, K., Zhutovsky, S.: Overview and future trends of shrinkage research. 827–847 (2006). https://doi.org/10.1617/s11527-006-9114-z
86. Hojati, M., Radlin, A.: Shrinkage and strength development of alkali-activated fly ash-slag binary cements. **150**, 808–816 (2017). https://doi.org/10.1016/j.conbuildmat.2017.06.040
87. Lura, P., Jensen, O.M., Van Breugel, K.: Autogenous shrinkage in high-performance cement paste: an evaluation of basic mechanisms. Cem. Concr. Res. **33**, 223–232 (2003)
88. Ye, H., Cartwright, C., Rajabipour, F., Radlińska, A.: Understanding the drying shrinkage performance of alkali-activated slag mortars. Cement Concr. Compos. **76**, 13–24 (2017). https://doi.org/10.1016/j.cemconcomp.2016.11.010
89. Provis, J.L., Bernal, S.A.: Geopolymers and related alkali-activated materials. 299–329 (2014). https://doi.org/10.1146/annurev-matsci-070813-113515

90. Chen, B., Wang, J., Zhao, J.: Mitigating the drying shrinkage and autogenous shrinkage of alkali-activated slag by NaAlO2. Materials **13** (2020). https://doi.org/10.3390/MA13163499
91. Zhang, J., Pan, G., Yan, Y.: Early hydration, mechanical strength and drying shrinkage of low-carbon alkali-activated Ti-extracted residues-fly ash cement and mortars. Construct. Build. Mater. **293**, 123517 (2021). https://doi.org/10.1016/j.conbuildmat.2021.123517
92. Ma, Y.: Microstructure and engineering properties of alkali activated fly ash—As an environment friendly alternative to Portland cement. **141** (2013)
93. Hu, Z., Wyrzykowski, M., Lura, P.: Estimation of reaction kinetics of geopolymers at early ages. Cem. Concr. Res. **129**, 105971 (2020). https://doi.org/10.1016/j.cemconres.2020.105971
94. Powers, T.C.: Studies of the physical properties of hardened Portland cement paste. ACI J. Proc. **43**, 101–132 (1946). https://doi.org/10.14359/8745
95. Criado, M., Fernández-Jiménez, A., de la Torre, A.G., et al.: An XRD study of the effect of the SiO2/Na2O ratio on the alkali activation of fly ash. Cem. Concr. Res. **37**, 671–679 (2007). https://doi.org/10.1016/j.cemconres.2007.01.013
96. Brinker, C.J., Scherer, G.W.: Sol-Gel Science: the Physics and Chemistry of Sol-Gel Processing. Academic press (2013)
97. Provis, J.L., van Deventer, J.S.J.: Geopolymerisation kinetics. 2. Reaction kinetic modelling. Chem. Eng. Sci. **62**, 2318–2329 (2007). https://doi.org/10.1016/j.ces.2007.01.028
98. Provis, J.L., Lukey, G.C., van Deventer, J.S.J.: Do geopolymers actually contain nanocrystalline zeolites? A reexamination of existing results. Chem. Mater. **17**, 3075–3085 (2005)
99. Gevaudan, J.P., Campbell, K.M., Kane, T.J., et al.: Mineralization dynamics of metakaolin-based alkali-activated cements. Cem. Concr. Res. **94**, 1–12 (2017)
100. Duxson, P., Provis, J.L., Lukey, G.C., et al.: Understanding the relationship between geopolymer composition, microstructure and mechanical properties. Colloids Surf. A **269**, 47–58 (2005)
101. Palumbo, G., Iadicicco, A., Messina, F., et al.: Characterization of early age curing and shrinkage of metakaolin-based inorganic binders with different rheological behavior by fiber Bragg grating sensors. Materials **11**, 10 (2017)
102. Li, C., Sun, H., Li, L.: A review: the comparison between alkali-activated slag (Si+ Ca) and metakaolin (Si+ Al) cements. Cem. Concr. Res. **40**, 1341–1349 (2010)
103. Kuenzel, C., Vandeperre, L.J., Donatello, S., et al.: Ambient temperature drying shrinkage and cracking in metakaolin-based geopolymers. J. Am. Ceram. Soc. **95**, 3270–3277 (2012)
104. Li, Z., Ye, G.: Experimental study of the chemical deformation of metakaolin based geopolymer. In: SynerCrete'18 International Conference on Interdisciplinary Approaches for Cement-Based Materials and Structural Concrete, pp. 443–448 (2018)
105. Zhan, J., Li, H., Pan, Q., et al.: Effect of slag on the strength and shrinkage properties of metakaolin-based geopolymers. Materials **15**, 2944 (2022)
106. Lolli, F., Thomas, J.J., Kurtis, K.E., et al.: Early age volume changes in metakaolin geopolymers: insights from molecular simulations and experiments. Cem. Concr. Res. **144**, 106428 (2021)
107. Li, Z., Zhang, S., Zuo, Y., et al.: Chemical deformation of metakaolin based geopolymer. Cem. Concr. Res. **120**, 108–118 (2019). https://doi.org/10.1016/j.cemconres.2019.03.017
108. Li, Z., Liang, X., Chen, Y., Ye, G.: Effect of metakaolin on the autogenous shrinkage of alkali-activated slag-fly ash paste. Constr. Build. Mater. **278**, 122397 (2021)
109. Fu, B., Cheng, Z., Han, J., Li, N.: Understanding the role of metakaolin towards mitigating the shrinkage behavior of alkali-activated slag. Materials **14**, 6962 (2021)
110. Li, Z., Nedeljković, M., Chen, B., Ye, G.: Mitigating the autogenous shrinkage of alkali-activated slag by metakaolin. Cem. Concr. Res. **122**, 30–41 (2019). https://doi.org/10.1016/j.cemconres.2019.04.016
111. Van Jaarsveld, J.G.S., Van Deventer, J.S.J., Lukey, G.C.: The effect of composition and temperature on the properties of fly ash-and kaolinite-based geopolymers. Chem. Eng. J. **89**, 63–73 (2002)

112. Duxson, P., Fernández-Jiménez, A., Provis, J.L., et al.: Geopolymer technology: the current state of the art. J. Mater. Sci. **42**, 2917–2933 (2007)
113. Bílek, V., Jr., Novotný, R., Koplík, J., et al.: Philosophy of rational mixture proportioning of alkali-activated materials validated by the hydration kinetics of alkali-activated slag and its microstructure. Cem. Concr. Res. **168**, 107139 (2023)
114. Provis, J.L., Van Deventer, J.S.J.: Alkali Activated Materials: state-of-the-Art Report, RILEM TC 224-AAM. Springer Science & Business Media (2013)
115. Caron, R., Patel, R.A., Dehn, F.: Extension of the fib MC 2010 for basic and drying shrinkage of alkali-activated slag concretes. Struct. Concr. **23**, 3960–3973 (2022)
116. Li, Z., Lu, T., Liang, X., et al.: Mechanisms of autogenous shrinkage of alkali-activated slag and fly ash pastes. Cem. Concr. Res. **135**, 106107 (2020). https://doi.org/10.1016/j.cemconres.2020.106107
117. Nguyen, T.H.Y., Cao, N.T., Ngoc, T.D.M., Huynh, T.P.: Experimental evaluation on engineering properties and drying shrinkage of no-cement mortar produced by alkaline activation of fly ash-slag mixtures. Eng. J. **26**, 17–28 (2022). https://doi.org/10.4186/ej.2022.26.3.17
118. Wang, G., Ma, Y.: Drying shrinkage of alkali-activated fly ash/slag blended system. J. Sustain. Cem.-Based Mater. **7**, 203–213 (2018)
119. Ma, Y., Yang, X., Hu, J., et al.: Accurate determination of the "time-zero" of autogenous shrinkage in alkali-activated fly ash/slag system. Compos. B Eng. **177**, 107367 (2019)
120. Uppalapati, S., Cizer, Ö.: Assessing the Autogenous Shrinkage of Alkali-Activated Slag/Fly Ash Mortar Blends. ACI Spec Publ, American Concrete Institute (2017)
121. Fang, G., Bahrami, H., Zhang, M.: Mechanisms of autogenous shrinkage of alkali-activated fly ash-slag pastes cured at ambient temperature within 24 h. Constr. Build. Mater. **171**, 377–387 (2018). https://doi.org/10.1016/j.conbuildmat.2018.03.155
122. Humad, A.M., Kothari, A., Provis, J.L., Cwirzen, A.: The effect of blast furnace slag/fly ash ratio on setting, strength, and shrinkage of alkali-activated pastes and concretes. Front. Mater. **6**, 9 (2019)
123. Ruengsillapanun, K., Udtaranakron, T., Pulngern, T., et al.: Mechanical properties, shrinkage, and heat evolution of alkali activated fly ash concrete. Constr. Build. Mater. **299**, 123954 (2021)
124. Puertas, F., Martínez-Ramírez, S., Alonso, S., Vázquez, T.: Alkali-activated fly ash/slag cements: Strength behaviour and hydration products. Cem. Concr. Res. **30**, 1625–1632 (2000)
125. Uppalapati, S., Vandewalle, L., Cizer, Ö.: Autogenous shrinkage of slag-fly ash blends activated with hybrid sodium silicate and sodium sulfate at different curing temperatures. Constr. Build. Mater. **265**, 121276 (2020)
126. Yuan, B., Yu, Q.L., Dainese, E., Brouwers, H.J.H.: Autogenous and drying shrinkage of sodium carbonate activated slag altered by limestone powder incorporation. Constr. Build. Mater. **153**, 459–468 (2017)
127. Avila, Y., Silva, R.V., de Brito, J.: Alkali-activated materials with pre-treated municipal solid waste incinerator bottom ash. Appl. Sci. **12**, 3535 (2022)
128. Cao, R., Li, B., You, N., et al.: Properties of alkali-activated ground granulated blast furnace slag blended with ferronickel slag. Constr. Build. Mater. **192**, 123–132 (2018)
129. Yin, K., Jiang, Y., He, H., et al.: Characterization of one-part alkali-activated slag with rice straw ash. Construct. Build. Mater. **345**, 128403. https://doi.org/10.1016/j.conbuildmat.2022.128403
130. Li, Z., Alfredo Flores Beltran, I., Chen, Y., et al.: Early-age properties of alkali-activated slag and glass wool paste. Constr. Build. Mater. **291**, 123326 (2021). https://doi.org/10.1016/j.conbuildmat.2021.123326
131. Zhu, C., Zhou, Y., Guo, Y., et al.: Resistivity Measurements to study the early chemical and autogenous shrinkage of a binary alkali-activated slag-metakaolin system. IOP Conf. Ser.: Earth Environ. Sci. (IOP Publishing) 12146 (2021)
132. You, N., Li, B., Cao, R., et al.: The influence of steel slag and ferronickel slag on the properties of alkali-activated slag mortar. Constr. Build. Mater. **227**, 116614 (2019)
133. Štěpánková, E., Kalina, L., Bílek, V., Jr., Bartoníčková, E.: Utilization of by-pass cement kiln dust in alkali-activated materials. Key Eng. Mater. **761**, 23–26 (2018)

134. Kim, H.-J., Tafesse, M., Lee, H.K., Kim, H.-K.: Incorporation of CFBC ash in sodium silicate-activated slag system: modification of microstructures and its effect on shrinkage. Cem. Concr. Res. **123**, 105771 (2019)
135. Dueramae, S., Tangchirapat, W., Chindaprasirt, P., et al.: Autogenous and drying shrinkages of mortars and pore structure of pastes made with activated binder of calcium carbide residue and fly ash. Constr. Build. Mater. **230**, 116962 (2020)
136. Suttiprapa, P., Tangchirapat, W., Jaturapitakkul, C., et al.: Strength behavior and autogenous shrinkage of alkali-activated mortar made from low-calcium fly ash and calcium carbide residue mixture. Constr. Build. Mater. **312**, 125438 (2021)
137. Liang, G., Liu, T., Li, H., Wu, K.: Shrinkage mitigation, strength enhancement and microstructure improvement of alkali-activated slag/fly ash binders by ultrafine waste concrete powder. Compos. B Eng. **231**, 109570 (2022)
138. Wang, D., Wang, Q., Zhuang, S., Yang, J.: Evaluation of alkali-activated blast furnace ferronickel slag as a cementitious material: reaction mechanism, engineering properties and leaching behaviors. Constr. Build. Mater. **188**, 860–873 (2018)
139. Navarro, R., Alcocel, E.G., Sánchez, I., et al.: Mechanical properties of alkali activated ground SiMn slag mortars with different types of aggregates. Constr. Build. Mater. **186**, 79–89 (2018)
140. Sturm, P., Gluth, G.J.G., Jäger, C., et al.: Sulfuric acid resistance of one-part alkali-activated mortars. Cem. Concr. Res. **109**, 54–63 (2018). https://doi.org/10.1016/j.cemconres.2018.04.009
141. Luukkonen, T., Abdollahnejad, Z., Yliniemi, J., et al.: One-part alkali-activated materials: a review. Cem. Concr. Res. **103**, 21–34 (2018). https://doi.org/10.1016/j.cemconres.2017.10.001
142. Elzeadani, M., Bompa, D.V., Elghazouli, A.Y.: One part alkali activated materials: a state-of-the-art review Ordinary Portland cement. J. Build. Eng. **57**, 104871 (2022). https://doi.org/10.1016/j.jobe.2022.104871
143. Moelich, G.M., Kruger, J., Combrinck, R.: Plastic shrinkage cracking in 3D printed concrete. Compos. B Eng. **200** (2020). https://doi.org/10.1016/j.compositesb.2020.108313
144. Osmanovic, Z., Haračić, N., Zelić, J.: Properties of blastfurnace cements (CEM III/A, B, C) based on Portland cement clinker, blastfurnace slag and cement kiln dusts. Cement Concr. Compos. **91** (2018). https://doi.org/10.1016/j.cemconcomp.2018.05.006
145. Qu, Z.Y., Yu, Q., Ji, Y.D., et al.: Mitigating shrinkage of alkali activated slag with biofilm. Cem. Concr. Res. **138** (2020). https://doi.org/10.1016/j.cemconres.2020.106234
146. Carneiro, G.O., Santana, H.A., Ribeiro, D.V., et al.: One-part alkali-activated binder produced from inertized asbestos cement waste. J. Clean. Prod. **367** (2022). https://doi.org/10.1016/j.jclepro.2022.132966
147. Pan, S., Zheng, Z., Guo, Z., Luo, H.: An optimized XGBoost method for predicting reservoir porosity using petrophysical logs. J. Petrol. Sci. Eng. **208**, 109520 (2022). https://doi.org/10.1016/j.petrol.2021.109520
148. Trincal, V., Multon, S., Benavent, V., et al.: Shrinkage mitigation of metakaolin-based geopolymer activated by sodium silicate solution. Cem. Concr. Res. **162**, 106993 (2022)
149. Hojati, M., Rajabipour, F., Radlińska, A.: Creep of alkali-activated cement mixtures. Case Stud. Construct. Mater. **16**, e00954 (2022)
150. Lee, H., Vimonsatit, V., Chindaprasirt, P., et al.: Creep properties of cement and alkali activated fly ash materials using nanoindentation technique. Constr. Build. Mater. **168**, 547–555 (2018). https://doi.org/10.1016/j.conbuildmat.2018.02.166
151. Li, Z., Zhang, S., Liang, X., Ye, G.: Cracking potential of alkali-activated slag and fly ash concrete subjected to restrained autogenous shrinkage. Cement Concr. Compos. **114**, 103767 (2020). https://doi.org/10.1016/j.cemconcomp.2020.103767
152. Senft, S., Gallegos, S., Manson, D.P., Gonzales, C.: Chemical Admixtures for Concrete. CRC Press (1999)
153. Palacios, M., Puertas, F.: Effect of superplasticizer and shrinkage-reducing admixtures on alkali-activated slag pastes and mortars. **35**, 1358–1367 (2005). https://doi.org/10.1016/j.cemconres.2004.10.014

154. Zhang, W., Xue, M., Lin, H., et al.: Effect of polyether shrinkage reducing admixture on the drying shrinkage properties of alkali-activated slag. Cem. Concr. Compos. **136**, 104865 (2023). https://doi.org/10.1016/j.cemconcomp.2022.104865
155. Rosen, M.J., Kunjappu, J.T.: Surfactants and Interfacial Phenomena. Wiley (2012)
156. Wang, X., Yuan, S., Jiang, B.: Wetting process and adsorption mechanism of surfactant solutions on coal dust surface. J. Chem. **2019**, 1–9 (2019)
157. Möbius, D., Miller, R., Fainerman, V.B.: Surfactants: chemistry, Interfacial Properties, Applications. Elsevier (2001)
158. Hinze, W.L., Singh, H.N., Baba, Y., Harvey, N.G.: Micellar enhanced analytical fluorimetry. TrAC Trends Anal. Chem. **3**, 193–199 (1984)
159. Lu, T., Liang, X., Liu, C., et al.: Experimental and numerical study on the mitigation of autogenous shrinkage of cementitious material. Cement Concr. Compos. **141**, 105147 (2023). https://doi.org/10.1016/j.cemconcomp.2023.105147
160. Mobili, A., Belli, A., Giosuè, C., et al.: Metakaolin and fly ash alkali-activated mortars compared with cementitious mortars at the same strength class. Cem. Concr. Res. **88**, 198–210 (2016). https://doi.org/10.1016/j.cemconres.2016.07.004
161. Ben, H.M., Le Saout, G., Winnefeld, F., Lothenbach, B.: Influence of activator type on hydration kinetics, hydrate assemblage and microstructural development of alkali activated blast-furnace slags. Cem. Concr. Res. **41**, 301–310 (2011)
162. Gao, X., Yu, Q.L., Brouwers, H.J.H.: Development of alkali activated slag-fly ash mortars: mix design and performance assessment. In: Fourth International Conference on Sustainable Construction Materials and Technologies, Las Vegas, USA (2016)
163. Herb, H., Gerdes, A., Brenner-Weiß, G.: Characterization of silane-based hydrophobic admixtures in concrete using TOF-MS. Cem. Concr. Res. **70**, 77–82 (2015)
164. Zhang, M., Zang, Y., Shan, L.: Enhancing volumetric stability of Metakaolin-based geopolymer composites with organic modifiers WER and SCA. Buildings **14**, 586 (2024)
165. Ruan, S., Chen, S., Liu, Y., et al.: Early-age deformation of hydrophobized metakaolin-based geopolymers. Cem. Concr. Res. **169**, 107168 (2023)
166. Kurdowski, W.: Cement and Concrete Chemistry. Springer Science & Business (2014)
167. Taylor, H.F.W: Cement Chemistry. Thomas Telford, London (1997)
168. Steiger, M.: Crystal growth in porous materials—I: the crystallization pressure of large crystals. J. Cryst. Growth **282**, 455–469 (2005)
169. Mehta, P.K.: Mechanism of expansion associated with ettringite formation. Cem. Concr. Res. **3**, 1–6 (1973)
170. Bernall, D., Rebinder, P.: Some recent concepts on Portland cement hydration and hardening. Special Report-Highway Research Board 447 (1966)
171. Jin, F., Gu, K., Al-Tabbaa, A.: Strength and drying shrinkage of reactive MgO modified alkali-activated slag paste. Constr. Build. Mater. **51**, 395–404 (2014). https://doi.org/10.1016/j.conbuildmat.2013.10.081
172. Jia, Z., Yang, Y., Yang, L., et al.: Hydration products, internal relative humidity and drying shrinkage of alkali activated slag mortar with expansion agents. Constr. Build. Mater. **158**, 198–207 (2018). https://doi.org/10.1016/j.conbuildmat.2017.09.162
173. Akturk, B., Kizilkanat, A.B.: Improvement of durability and drying shrinkage of sodium carbonate activated slag through the incorporation of calcium hydroxide and sodium hydroxide. Constr. Build. Mater. **243** (2020). https://doi.org/10.1016/j.conbuildmat.2020.118260
174. Choi, S., Ryu, G.-S., Koh, K.-T., et al.: Experimental study on the shrinkage behavior and mechanical properties of AAM mortar mixed with CSA expansive additive. Materials **12**, 3312 (2019)
175. Zhang, B., Zhu, H., Feng, P., Zhang, P.: A review on shrinkage-reducing methods and mechanisms of alkali-activated/geopolymer systems: effects of chemical additives. J. Build. Eng. **49**, 104056 (2022)
176. Li, Z., Wyrzykowski, M., Dong, H., et al.: Internal curing by superabsorbent polymers in alkali-activated slag. Cem. Concr. Res. **135**, 106123 (2020). https://doi.org/10.1016/j.cemconres.2020.106123

177. Oh, S., Choi, Y.C.: Superabsorbent polymers as internal curing agents in alkali activated slag mortars. Constr. Build. Mater. **159**, 1–8 (2018). https://doi.org/10.1016/j.conbuildmat.2017.10.121
178. Sakulich, A.R., Bentz, D.P.: Mitigation of autogenous shrinkage in alkali activated slag mortars by internal curing. Mater. Struct./Materiaux et Construct. **46**, 1355–1367 (2013). https://doi.org/10.1617/s11527-012-9978-z
179. Liu, C., Wu, H., Li, Z., et al.: Effect of curing condition on mechanical properties and durability of alkali-activated slag mortar. Construct. Build. Mater. **439**, 137376 (2024). https://doi.org/10.1016/j.conbuildmat.2024.137376
180. Yang, J., Snoeck, D., De, B.N., Sun, Z.: Comparison of liquid absorption-release of superabsorbent polymers in alkali-activated slag and Portland cement systems: an NMR study combined with additional methods. Cem. Concr. Res. **142**, 106369 (2021). https://doi.org/10.1016/j.cemconres.2021.106369
181. Tu, W., Zhu, Y., Fang, G., et al.: Internal curing of alkali-activated fly ash-slag pastes using superabsorbent polymer. Cem. Concr. Res. **116**, 179–190 (2019). https://doi.org/10.1016/j.cemconres.2018.11.018
182. Li, Z., Yao, X., Chen, Y., et al.: A low-autogenous-shrinkage alkali-activated slag and fly ash concrete. Appl. Sci. **10**, 6092 (2020)
183. Xiang, J., He, Y., Liu, L., et al.: Exothermic behavior and drying shrinkage of alkali-activated slag concrete by low temperature-preparation method. Constr. Build. Mater. **262**, 120056 (2020). https://doi.org/10.1016/j.conbuildmat.2020.120056
184. Geiker, M.R, Bentz, D.P, Jensen, O.M.: Mitigating autogenous shrinkage by internal curing. ACI Spec. Publ. 143–154 (2004)
185. Bentur, A., Igarashi, S., Kovler, K.: Prevention of autogenous shrinkage in high-strength concrete by internal curing using wet lightweight aggregates. Cem. Concr. Res. **31**, 1587–1591 (2001)
186. Snoeck, D., Jensen, O.M., De Belie, N.: The influence of superabsorbent polymers on the autogenous shrinkage properties of cement pastes with supplementary cementitious materials. Cem. Concr. Res. **74**, 59–67 (2015)
187. Justs, J., Wyrzykowski, M., Bajare, D., Lura, P.: Internal curing by superabsorbent polymers in ultra-high performance concrete. Cem. Concr. Res. **76**, 82–90 (2015)
188. Lura, P., Durand, F., Jensen, O.M.: Autogenous strain of cement pastes with superabsorbent polymers. In: International RILEM conference on volume changes of hardening concrete: testing and mitigation, pp. 57–65. RILEM Publications SARL Paris, France (2006)
189. Mechtcherine, V., Gorges, M., Schroefl, C., et al.: Effect of internal curing by using superabsorbent polymers (SAP) on autogenous shrinkage and other properties of a high-performance fine-grained concrete: results of a RILEM round-robin test. Mater. Struct. **47**, 541–562 (2014)
190. Yang, L., Shi, C., Wu, Z.: Mitigation techniques for autogenous shrinkage of ultra-high-performance concrete–a review. Compos. B Eng. **178**, 107456 (2019)
191. Jensen, O.M., Hansen, P.F.: Water-entrained cement-based materials: I. Principles and theoretical background. Cem. Concr. Res. **31**, 647–654 (2001)
192. Lee, N.K., Abate, S.Y., Kim, H.-K.: Use of recycled aggregates as internal curing agent for alkali-activated slag system. Constr. Build. Mater. **159**, 286–296 (2018)
193. Song, C., Choi, Y.C., Choi, S.: Effect of internal curing by superabsorbent polymers—Internal relative humidity and autogenous shrinkage of alkali-activated slag mortars. Constr. Build. Mater. **123**, 198–206 (2016). https://doi.org/10.1016/j.conbuildmat.2016.07.007
194. Della, V.P., Kühn, I., Hotza, D.: Rice husk ash as an alternate source for active silica production. Mater. Lett. **57**, 818–821 (2002)
195. Van Tuan, N., Ye, G., Van Breugel, K., et al.: The study of using rice husk ash to produce ultra high performance concrete. Constr. Build. Mater. **25**, 2030–2035 (2011)
196. Weiss, J., Bentz, D., Schindler, A., Lura, P.: Internal curing. Structure **12**, 10–14 (2012)
197. Kim, H.-J., Tafesse, M., Lee, H.K., Kim, H.-K.: Incorporation of CFBC ash in sodium silicate-activated slag system: modification of microstructures and its effect on shrinkage. Cem. Concr. Res. **123**, 105771 (2019). https://doi.org/10.1016/j.cemconres.2019.05.016

198. Xiang, J., Liu, L., Cui, X., et al.: Effect of limestone on rheological, shrinkage and mechanical properties of alkali—Activated slag/fly ash grouting materials. Construct. Build. Mater. **191**:1285–1292 (2018). https://doi.org/10.1016/j.conbuildmat.2018.09.209
199. Chen, W., Xie, Y., Li, B., et al.: Role of aggregate and fibre in strength and drying shrinkage of alkali-activated slag mortar. Constr. Build. Mater. **299** (2021). https://doi.org/10.1016/j.conbuildmat.2021.124002
200. Dheyaaldin, M.H., Mosaberpanah, M.A., Alzeebaree, R.: Shrinkage behavior and mechanical properties of alkali activated mortar incorporating nanomaterials and polypropylene fiber. Ceram. Int. **48**, 23159–23171 (2022)
201. El-Yamany, H.E., El-Salamawy, M.A., El-Assal, N.T.: Microstructure and mechanical properties of alkali-activated slag mortar modified with latex. Constr. Build. Mater. **191** (2018). https://doi.org/10.1016/j.conbuildmat.2018.09.200
202. Delsaute, B., Staquet, S.: Testing concrete since setting time under free and restrained conditions. In: Advanced Techniques for Testing of Cement-Based Materials. pp. 177–209 (2020)
203. Wyrzykowski, M., Hu, Z., Ghourchian, S., et al.: Corrugated tube protocol for autogenous shrinkage measurements: review and statistical assessment. Mater. Struct. **50**, 57 (2017). https://doi.org/10.1617/s11527-016-0933-2
204. Delsaute, B., Staquet, S.: Monitoring of the thermal and autogenous strain, pp. 135–176 (2020)
205. Jiang, C., Yang, Y., Wang, Y., et al.: Autogenous shrinkage of high performance concrete containing mineral admixtures under different curing temperatures. Constr. Build. Mater. **61**, 260–269 (2014). https://doi.org/10.1016/j.conbuildmat.2014.03.023
206. Delsaute, B., Staquet, S.: Impact of recycled sand and gravels in concrete on volume change. Constr. Build. Mater. **232**, 117279 (2020). https://doi.org/10.1016/j.conbuildmat.2019.117279
207. Shen, D., Wen, C., Zhu, P., et al.: Influence of Barchip fiber on early-age autogenous shrinkage of high-strength concrete internally cured with super absorbent polymers. Constr. Build. Mater. **264**, 119983 (2020). https://doi.org/10.1016/j.conbuildmat.2020.119983
208. fib.: Code-type models for structural behaviour of concrete: background of the constitutive relations and material models in the fib Model Code for Concrete Structures 2010 (2013)
209. JSCE.: Standard specifications for concrete structures (2007)
210. Wendner, R., Hubler, M.H., Bažant, Z.P.: The B4 model for multi-decade creep and shrinkage prediction. In: Mechanics and Physics of Creep, Shrinkage, and Durability of Concrete, pp. 429–436. American Society of Civil Engineers, Reston, VA (2013)
211. Qureshi, H.J., Saleem, M.U., Javed, M.F., et al.: Prediction of autogenous shrinkage of concrete incorporating super absorbent polymer and waste materials through individual and ensemble machine learning approaches. Materials **15**, 7412 (2022). https://doi.org/10.3390/ma15217412
212. Hilloulin, B., Tran, V.Q.: Using machine learning techniques for predicting autogenous shrinkage of concrete incorporating superabsorbent polymers and supplementary cementitious materials. J. Build. Eng. **49**, 104086 (2022). https://doi.org/10.1016/j.jobe.2022.104086
213. D'Aloia, L.: Activation energy, maturity and equivalent age. In: Early Age Cracking in Cementitious Systems—Report of RILEM Technical Committee 181-EAS Early age shrinkage induced stresses and cracking in cementitious systems us systems, Report of RILEM Technical Committee TC 181-EAS, pp. 127–148 (2003)
214. Benboudjema, F., Torrenti, J.M.: Early-age behaviour of concrete nuclear containments. Nucl. Eng. Des. **238**, 2495–2506 (2008). https://doi.org/10.1016/j.nucengdes.2008.04.009
215. Wadso, L.: The study of cement hydration by isothermal calorimetry, pp. 99–101 (1985)
216. Boulay, C., Torrenti, J.M., Andre, J., Saintilan, R.: Quasi-adiabatic calorimetry for concretes: Influential factors. Bulletin des Laboratoires des Ponts et Chauss ees 19–36 (2010)
217. Darquennes, A., Espion, B., Staquet, S.: How to assess the hydration of slag cement concretes? Constr. Build. Mater. **40**, 1012–1020 (2013). https://doi.org/10.1016/j.conbuildmat.2012.09.087

218. Darquennes, A., Staquet, S., Delplancke-Ogletree, M.-P., Espion, B.: Effect of autogenous deformation on the cracking risk of slag cement concretes. Cement Concr. Compos. **33**, 368–379 (2011)
219. Delsaute, B., Staquet, S.: Decoupling thermal and autogenous strain of concretes with different water/cement ratios during the hardening process. Adv. Civil Eng. Mater. **6**, 22 (2017). https://doi.org/10.1520/ACEM20160063
220. Carette, J., Joseph, S., Cizer, Ö., Staquet, S.: Decoupling the autogenous swelling from the self-desiccation deformation in early age concrete with mineral additions: micro-macro observations and unified modelling. Cement Concr. Compos. **85**, 122–132 (2018). https://doi.org/10.1016/j.cemconcomp.2017.10.008
221. Delsaute, B., Torrenti, J., Staquet, S.: Prediction of the basic creep of concrete with high substitution of Portland cement by mineral additions at early age. Struct. Concr. 201900313 (2020). https://doi.org/10.1002/suco.201900313
222. Carette, J., Staquet, S.: Unified modelling of the temperature effect on the autogenous deformations of cement-based materials. Cement Concr. Compos. **94**, 62–71 (2018). https://doi.org/10.1016/j.cemconcomp.2018.08.008
223. Lura, P., Jensen, O.M., Van Breugel, K.: Autogenous shrinkage in high-performance cement paste : an evaluation of basic mechanisms modeling of autogenous relative humidity change and autogenous. Cem. Concr. Res. **33**(2), 223–232 (2003)
224. Jensen, O.M., Hansen, P.F.: Influence of temperature on autogenous deformation and relative humidity change in hardening cement paste. Cem. Concr. Res. **29**, 567–575 (1999). https://doi.org/10.1016/S0008-8846(99)00021-6
225. Hu, Z., Wyrzykowski, M., Scrivener, K., Lura, P.: A novel method to predict internal relative humidity in cementitious materials by 1 H NMR. Cem. Concr. Res. **104**, 80–93 (2018). https://doi.org/10.1016/j.cemconres.2017.11.001
226. Bentz, D.P., Garboczi, E.J., Quenard, D.: Modelling drying shrinkage in reconstructed porous materials: application to porous Vycor glass. Modell. Simul. Mater. Sci. Eng. **6**, 211–236 (1998). https://doi.org/10.1088/0965-0393/6/3/002
227. Königsberger, M., Hlobil, M., Delsaute, B., et al.: Hydrate failure in ITZ governs concrete strength: A micro-to-macro validated engineering mechanics model. Cem. Concr. Res. (2017). https://doi.org/10.1016/j.cemconres.2017.10.002
228. Delsaute, B., Staquet, S.: Monitoring the viscoelastic behaviour of cement based materials by means of repeated minute-scale-duration loadings. In: Advanced Techniques for Testing of Cement-Based Materials, pp 99–134 (2020)
229. Irfan-ul-Hassan, M., Pichler, B., Reihsner, R., Hellmich, C.: Elastic and creep properties of young cement paste, as determined from hourly repeated minute-long quasi-static tests. Cem. Concr. Res. **82**, 36–49 (2016). https://doi.org/10.1016/j.cemconres.2015.11.007
230. Delsaute, B., Boulay, C., Granja, J., et al.: Testing concrete e-modulus at very early ages through several techniques: an inter-laboratory comparison. Strain **52**, 91–109 (2016). https://doi.org/10.1111/str.12172
231. Gabrijel, I., Staquet, S., Krüger, M., et al.: Ultrasonic techniques for determination and monitoring various properties of cementitious materials at early ages. In: Advanced Techniques for Testing of Cement-Based Materials, pp. 23–68 (2020)
232. Grasley, Z.C., Leung, C.K.: Desiccation shrinkage of cementitious materials as an aging, poroviscoelastic response. Cem. Concr. Res. **41**, 77–89 (2011). https://doi.org/10.1016/j.cemconres.2010.09.008
233. Delsaute, B., Torrenti, J.-M., Staquet, S.: Modeling basic creep of concrete since setting time. Cem. Concr. Compos. (2016)
234. Torrenti, J.-M., Le Roy, R.: Analysis of some basic creep tests on concrete and their implications for modeling. Struct. Concr. (2017). https://doi.org/10.1002/suco.201600197
235. Pickett, G.: Effect of aggregate on shrinkage of concrete and a hypothesis concerning shrinkage. J. Proc. 581–590 (1956)
236. Lu, T., Li, Z., Huang, H.: Restraining effect of aggregates on autogenous shrinkage in cement mortar and concrete. Constr. Build. Mater. **289**, 123166 (2021)

237. Delsaute, B.: New approach for Monitoring and Modelling of the Creep and Shrinkage behaviour of Cement Pastes, Mortars and Concretes since Setting Time. Université Libre de Bruxelles (BATir), Université Paris Est (IFSTTAR) (2016)
238. Pichler, C., Lackner, R., Mang, H.A.: A multiscale micromechanics model for the autogenous-shrinkage deformation of early-age cement-based materials. Eng. Fract. Mech. **74**, 34–58 (2007). https://doi.org/10.1016/j.engfracmech.2006.01.034
239. Le Chatelier, H.: Sur le changement de volume qui accompagne le durcissement des ciments. Bulletin de la Société de l'encouragement pour l'industrie nationale **5**, 54–57 (1900)
240. Huang, H., Ye, G.: Examining the "time-zero" of autogenous shrinkage in high/ultra-high performance cement pastes. Cem. Concr. Res. **97**, 107–114 (2017). https://doi.org/10.1016/j.cemconres.2017.03.010
241. Tenório Filho, J.R., Gomes, P., de Araújo, M.A., Snoeck, D., De Belie, N.: Discussing different approaches for the time-zero as start for autogenous shrinkage in cement pastes containing superabsorbent polymers. Materials **12**, 2962 (2019). https://doi.org/10.3390/ma12182962
242. Carette, J., Delsaute, B., Milenković, N., et al.: Advanced characterisation of the early age behaviour of bulk hydrophobic mortars. Constr. Build. Mater. **267**, 120904 (2021). https://doi.org/10.1016/j.conbuildmat.2020.120904
243. Saleh, M., Carette, J., Delsaute, B., Staquet, S.: Applicability of ultrasonic measurement on the monitoring of the setting of cement pastes: effect of water content and mineral additions. Adv. Civil Eng. (2017)
244. Zhang, J., Hou, D., Han, Y.: Micromechanical modeling on autogenous and drying shrinkages of concrete. Constr. Build. Mater. **29**, 230–240 (2012). https://doi.org/10.1016/j.conbuildmat.2011.09.022
245. Li, Z., Delsaute, B., Lu, T., et al.: A comparative study on the mechanical properties, autogenous shrinkage and cracking proneness of alkali-activated concrete and ordinary Portland cement concrete. Constr. Build. Mater. **292**, 123418 (2021)
246. Uppalapati, S.: Early-age structural development and autogenous shrinkage of alkali-activated slag/fly ash cements. KU Leuven (2020)
247. Ma, J., Dehn, F.: Shrinkage and creep behavior of an alkali-activated slag concrete. Struct. Concr. **18**, 801–810 (2017)
248. Lacante, M., Delsaute, B., Gambacorta, J., et al.: Development of early age autogenous and thermal strains of alkali-activated slag-fly ash pastes. Front. Built Environ. **8** (2022). https://doi.org/10.3389/fbuil.2022.1085912
249. Shen, J., Li, Y., Lin, H., Li, Y.: Development of autogenous shrinkage prediction model of alkali-activated slag-fly ash geopolymer based on machine learning. J. Build. Eng. **71**, 106538 (2023). https://doi.org/10.1016/j.jobe.2023.106538
250. Delsaute, B., Gambacorta, J., Staquet, S.: Influence of the Ms-modulus on the early-age volume change and heat release of slag and fly ash pastes activated by sodium hydroxide and sodium silicate. In: 4th International RILEM conference on Microstructure Related Durability of Cementitious Composites, Pp. 781–787 (2020)
251. Lacante, M., Delsaute, B., Staquet, S.: Effect of internal and external factors on the volume changes of slag binder activated by sodium hydroxide at early-age, pp. 350–361 (2023)
252. Naqi, A., Delsaute, B., Königsberger, M., Staquet, S.: Monitoring early age elastic and viscoelastic properties of alkali-activated slag mortar by means of repeated minute-long loadings. Dev. Built Environ. **16**, 100275 (2023). https://doi.org/10.1016/j.dibe.2023.100275
253. Li, Z., Lu, T., Chen, Y., et al.: Prediction of the autogenous shrinkage and microcracking of alkali-activated slag and fly ash concrete. Cem. Concr. Compos. **117**, 103913 (2021). https://doi.org/10.1016/j.cemconcomp.2020.103913
254. Naqi, A., Delsaute, B., Königsberger, M., Staquet, S.: Effect of solution-to-binder ratio and alkalinity on setting and early-age properties of alkali-activated slag-fly ash binders. Materials **16**, 373 (2022). https://doi.org/10.3390/ma16010373
255. Jiang, D., Li, X., Lv, Y., et al.: Autogenous shrinkage and hydration property of alkali activated slag pastes containing superabsorbent polymer. Cem. Concr. Res. **149**, 106581 (2021). https://doi.org/10.1016/j.cemconres.2021.106581

256. Melo Neto, A.A., Cincotto, M.A., Repette, W.: Drying and autogenous shrinkage of pastes and mortars with activated slag cement. Cem. Concr. Res. **38**, 565–574 (2008). https://doi.org/10.1016/J.CEMCONRES.2007.11.002
257. Lee, N.K., Jang, J.G., Lee, H.-K.: Shrinkage characteristics of alkali-activated fly ash/slag paste and mortar at early ages. Cement Concr. Compos. **53**, 239–248 (2014)
258. Panchmatia, P., Olvera, R., Genedy, M., et al.: Shrinkage behavior of Portland and geopolymer cements at elevated temperature and pressure. J. Petrol. Sci. Eng. **195**, 107884 (2020)
259. Ling, Y., Wang, K., Fu, C.: Shrinkage behavior of fly ash based geopolymer pastes with and without shrinkage reducing admixture. Cement Concr. Compos. **98**, 74–82 (2019)
260. Yang, Y., Chen, Z., Feng, W., et al.: Shrinkage compensation design and mechanism of geopolymer pastes. Constr. Build. Mater. **299**, 123916 (2021)
261. Qu, Z.Y., Gauvin, F., Wang, F.Z., et al.: Effect of hydrophobicity on autogenous shrinkage and carbonation of alkali activated slag. Construct. Build. Mater. **264**, 120665 (2020). https://doi.org/10.1016/j.conbuildmat.2020.120665
262. Rodrigue, A., Duchesne, J., Fournier, B., Bissonnette, B.: Influence of added water and fly ash content on the characteristics, properties and early-age cracking sensitivity of alkali-activated slag/fly ash concrete cured at ambient temperature. Constr. Build. Mater. **171**, 929–941 (2018)
263. Neto, A.A.M., Cincotto, M.A., Repette, W.: Mechanical properties, drying and autogenous shrinkage of blast furnace slag activated with hydrated lime and gypsum. Cement Concr. Compos. **32**, 312–318 (2010)
264. Archez, J., Farges, R., Gharzouni, A., Rossignol, S.: Influence of the geopolymer formulation on the endogeneous shrinkage. Constr. Build. Mater. **298**, 123813 (2021)
265. Mermerdaş, K., Algın, Z., Ekmen, Ş: Experimental assessment and optimization of mix parameters of fly ash-based lightweight geopolymer mortar with respect to shrinkage and strength. J. Build. Eng. **31**, 101351 (2020)
266. You, N., Liu, Y., Gu, D., et al.: Rheology, shrinkage and pore structure of alkali-activated slag-fly ash mortar incorporating copper slag as fine aggregate. Constr. Build. Mater. **242**, 118029 (2020). https://doi.org/10.1016/j.conbuildmat.2020.118029
267. Kalina, L., Bílek, V., Bartoníčková, E., et al.: Doubts over capillary pressure theory in context with drying and autogenous shrinkage of alkali-activated materials. Constr. Build. Mater. **248**, 118620 (2020). https://doi.org/10.1016/j.conbuildmat.2020.118620
268. Powers, T.: Absorption of water by Portland cement paste during the hardening process. Ind. Eng. Chem. **27**, 790–794 (1935)
269. Buil, M.: Contribution à l'étude du retrait de la pâte de ciment durcissante. RAPP RECH LPC (1979)
270. Buil, M.: Comportement physico-chimique du système ciment-fumées de silice. In: Annales de l'ITBTP (1990)
271. Justnes, H., Reyniers, B., Sellevold, E.J.: An evaluation of methods for measuring chemical shrinkage of cementitious pastes. Nordic Concr. Res. **14**, 45–61 (1994)
272. Tazawa, E., Miyazawa, S., Kasai, T.: Chemical shrinkage and autogenous shrinkage of hydrating cement paste. Cem. Concr. Res. **25**, 288–292 (1995)
273. Harald, J.: Chemical shrinkage of cement pastes with plasticizing admixtures. Nordic Concr. Res. **24**, 39–44 (2000)
274. Garcia-Boivin, S.: Retrait au jeune âge du béton: Développement d'une méthode expérimentale et contribution à l'analyse physique du retrait endogène. Thèse de doctorat, École Nationale des Ponts et Chaussées (1999)
275. Costoya Fernández, M.M.: Effect of particle size on the hydration kinetics and microstructural development of tricalcium silicate. EPFL (2008)
276. Rey, M.: Nouvelle méthode de mesure de l'hydratation des liants hydrauliques. Publication technique du CERILH **31** (1950)
277. Geiker, M., Knudsen, T.: Chemical shrinkage of Portland cement pastes. Cem. Concr. Res. **12**, 603–610 (1982)
278. Sant, G., Lura, P., Weiss, J.: Measurement of volume change in cementitious materials at early ages: review of testing protocols and interpretation of results. Transp. Res. Rec. **1979**, 21–29 (2006)

279. Mounanga, P.: Comportement des matrices cimentaires au jeune âge: relation entre évolution chimique et déformations chimique et endogène. XXIIEME rencontre Universitaires de Génie Civil (2003)
280. Bouasker, M., Mounanga, P., Khelidj, A., Coué, R.: Free autogenous strain of early-age cement paste: metrological development and critical analysis. Adv. Cem. Res. **20**, 75–84 (2008)
281. Holt, E.E.: Early Age Autogenous Shrinkage of Concrete. University of Washington (2001)
282. Justnes, H., Van Gemert, A., Verboven, F., Sellevold, E.J.: Total and external chemical shrinkage of low w/c ratio cement pastes. Adv. Cem. Res. **8**, 121–126 (1996)
283. Bouasker, M., Mounanga, P., Turcry, P., et al.: Chemical shrinkage of cement pastes and mortars at very early age: effect of limestone filler and granular inclusions. Cement Concr. Compos. **30**, 13–22 (2008)
284. Stefan, L.: Étude expérimentale et modélisation de l'évolution des propriétés mécaniques au jeune âge dans les matériaux cimentaires (2009)
285. Baroghel-Bouny, V.: Caractérisation des pâtes de ciment et des bétons-Méthodes, analyse, interprétations (1994)
286. ASTM C490-07.: ASTM: C490 standard practice for use of apparatus for the determination of length change of hardened cement paste, Mortar, and Concrete. ASTM International, pp. 1–5 (2008)
287. Le Roy, R.: Déformations instantanées et différées des bétons à hautes performances (1995)
288. Loukili, A., Khelidj, A., Richard, P.: Hydration kinetics, change of relative humidity, and autogenous shrinkage of ultra-high-strength concrete. Cem. Concr. Res. **29**, 577–584 (1999)
289. Charron, J.P., Marchand, J., Bissonnette, B.: Early-age deformations of hydrating cement systems: comparison of linear and volumetric shrinkage measurements. Concr. Sci. Eng. **3**, 168–173 (2001)
290. Baroghel-Bouny, V., Mounanga, P., Khelidj, A., et al.: Autogenous deformations of cement pastes: part II. W/C effects, micro–macro correlations, and threshold values. Cem. Concr. Res. **36**, 123–136 (2006)
291. Bjøntegaard, Ø., Hammer, T.A., Sellevold, E.J.: On the measurement of free deformation of early age cement paste and concrete. Cem. Concr. Compos. **26**, 427–435 (2004)
292. Fourdrin, E., Guigou, C., Chappuis, J.: Early age shrinkage of mortars: conception of a new device and detailed analysis of a typical experimental curve. In: PRO 17: international RILEM Workshop on Shrinkage of Concrete-'Shrinkage 2000', p. 387. RILEM Publications (2001)
293. Toma, G., Pigeon, M., Marchand, J., et al.: Earlyage autogenous restrained shrinkage: stress build up and relaxation. Concr. Sci. Eng. **2**, 129–133 (2000)
294. Charron, J.-P.: Contribution à l'étude du comportement au jeune âge des matériaux cimentaires en conditions de déformations libre et restreinte. Université Laval (2003)
295. Mejlhede Jensen, O., Freiesleben Hansen, P.: A dilatometer for measuring autogenous deformation in hardening Portland cement paste. Mater. Struct. **28**, 406–409 (1995)
296. Miao, B.: A new method to measure the early—Age deformation of cement based materials. In: Proceeding of the International RILEM Workshop, p. 381. RILEM Publications (2001)
297. Laplante, P., Boulay, C.: Evolution du coefficient de dilatation thermique du béton en fonction de sa maturité aux tout premiers âges. Mater. Struct. **27**, 596–605 (1994)
298. Boulay, C.: Test rig for early age measurements of the autogenous shrinkage of a concrete. In: RILEM-JCI International Workshop ConCrack, vol. 3. p. 111 (2012)
299. Boulay, C.: Test rig for early age measurements of the autogenous shrinkage of concretes (2007)
300. Bouasker, M.: Étude numérique et expérimentale du retrait endogène au très jeune âge des pâtes de ciment avec et sans inclusions (2007)
301. Bouasker, M., Mounanga, P., Khelidj, A., Coué, R.: Déformations endogènes de pâtes de ciment au très jeune âge: Analyse critique et développement métrologique. Eur. J. Environ. Civ. Eng. **12**, 347–365 (2008)
302. Mohr, B.J., Hood, K.L.: Influence of bleed water reabsorption on cement paste autogenous deformation. Cem. Concr. Res. **40**, 220–225 (2010)

303. Standards A book of A.: American Society for Testing and Materials (ASTM). ASTM C 1698 Standard test method for autogenous strain of cement paste and mortar (2009)
304. Gao, P., Zhang, T., Luo, R., et al.: Improvement of autogenous shrinkage measurement for cement paste at very early age: corrugated tube method using non-contact sensors. Constr. Build. Mater. **55**, 57–62 (2014)
305. Neville, H.A., Jones, H.C.: The study of hydration changes by a volume-change method. In: Colloid Symposium Monograph, vol. VI, pp. 309–318
306. Del Campo, M.: A new method to study the early volume changes on the neat cement paste. Bull. RILEM **4**, 18–23 (1959)
307. Baroghel-Bouny, V., Kheirbek, A.: Effect of mix-parameters on autogenous deformations of cement pastes-microstructural interpretations. Aıtcin, P-C(Hrsg) 115–142 (2000)
308. Mounanga, P.: Etude expérimentale du comportement de pâtes de ciment au très jeune âge: hydratation, retraits, propriétés thermophysiques (2003)
309. Mounanga, P., Baroghel-Bouny, V., Loukili, A., Khelidj, A.: Autogenous deformations of cement pastes: part I. Temperature effects at early age and micro–macro correlations. Cem. Concr. Res. **36**, 110–122 (2006)
310. Barcelo, L., Boivin, S., Rigaud, S., et al.: Linear vs. volumetric autogenous shrinkage measurement: material behaviour or experimental artefact. In: Proceedings of Self-dessiccation and Its Importance in Concrete Technology (1999)
311. Bjøntegaard, Ø., Budelmann, H., Krauss, M., Martius-Hammer, T.A.: RILEM Technical Committee 195-DTD Recommendation for test methods for AD and TD of Early Age Concrete, vol. 10, pp. 978–994. Dordrecht, Springer Netherlands (RILEM State-of-the-Art Reports) (2015)
312. Stefan, L., Boulay, C., Torrenti, J.-M., et al.: Influential factors in volume change measurements for cementitious materials at early ages and in isothermal conditions. Cem. Concr. Compos. **85**, 105–121 (2018)
313. Tazawa, E., Miyazawa, S.: Influence of constituents and composition on autogenous shrinkage of cementitious materials. Mag. Concr. Res. **49**, 15–22 (1997)
314. Bjøntegaard, Ø.: Thermal dilation and autogenous deformation as driving forces to self-induced stresses in high performance concrete. Norges Teknisk-Naturvitenskapelige Universitet (1999)
315. De Schutter, G., Taerwe, L.: Degree of hydration-based description of mechanical properties of early age concrete. Mater. Struct. **29**, 335–344 (1996)
316. Bisschop, J.: Report 25: early Age Cracking in Cementitious Systems-Report of RILEM Technical committee TC 181-EAS: early Age Cracking Shrinkage Induced Stresses and Cracking in Cementitious Systems, vol. 25, p. 27 (Evolution of solid behavior) (2003)
317. Kanstad, T., Hammer, T.A., Bjřntegaard, Ř., Sellevold, E.J.: Mechanical properties of young concrete-evaluation of test methods for tensile strength and modulus of elasticity-determination of models parameters. NOR-IPACS Report STF22 A99762 (1999)
318. Khan, A.A., Cook, W.D., Mitchell, D.: Tensile strength of low, medium, and high-strength concretes at early ages. Mater. J. **93**, 487–493 (1996)
319. Kasai, Y., Vokoyama, K., Matsui, I.: Tensile properties of early-age concrete. In: Proceedings of Conference on Mechanical Behaviour of Materials (1972)
320. Roziere, E., Loukili, A.: Tensile strength of concrete at early-age: new experimental procedure and influence of mix-design parameters. In: 10th International Conference on Fracture Mechanics of Concrete and Concrete Structures (2019)
321. Roziere, E., Cortas, R., Loukili, A.: Tensile behaviour of early age concrete: new methods of investigation. Cem. Concr. Compos. **55**, 153–161 (2015)
322. Sant, G., Lura, P., Weiss, J.: A discussion of analysis approaches for determining 'time-zero' from chemical shrinkage and autogenous strain measurements in cement paste. In: Proceedings of International RILEM Conference on Volume Changes of Hardening Concrete: testing and Mitigation, pp. 20–23 (2006)
323. Hammer, T.A.: Test methods for linear measurement of autogenous shrinkage before setting. In: Tazawa, E. (ed.) Autoshrink'98—Proceedings International Workshop on Autogenous Shrinkage of Concrete, pp. 141–152. Japan Concrete Institute, Hiroshima, Japan (1998)

324. Boivin, S., Acker, P., Rigaud, S., Clavaud, B.: Experimental assessment of chemical shrinkage of hydrating cement pastes. In: Autogenous Shrinkage of Concrete, pp. 81–92 (1999)
325. Sant, G., Rajabipour, F., Fishman, P., et al.: Electrical conductivity measurements in cement paste at early ages: a discussion of the contribution of pore solution conductivity, volume, and connectivity to the overall electrical response. In: International RILEM Workshop on Advanced Testing of Fresh Cementitious Materials (2006)
326. Weiss, J.: Experimental determination of the 'Time Zero', t0 ("Maturity-Zero", M0). In: Early Age Cracking in Cementitious Systems, RILEM Report, vol. 25, pp. 195–206 (2003)
327. Sant, G., Dehadrai, M., Bentz, D., et al.: Detecting the fluid-to-solid transition in cement pastes. Concr. Int. **31**, 53–58 (2009)
328. Staquet, S., Boulay, C., Robeyst, N., De Belie, N.: Ultrasonic monitoring of setting and autogenous shrinkage development of high performance concrete. In: International Conference: CONCREEP, pp. 321–327 (2008)
329. Reinhardt, H.W., Grosse, C.U.: Continuous monitoring of setting and hardening of mortar and concrete. Constr. Build. Mater. **18**, 145–154 (2004)
330. Robeyst, N., Gruyaert, E., Grosse, C.U., De Belie, N.: Monitoring the setting of concrete containing blast-furnace slag by measuring the ultrasonic p-wave velocity. Cem. Concr. Res. **38**, 1169–1176 (2008)
331. Boumiz, A., Vernet, C., Tenoudji, F.C.: Mechanical properties of cement pastes and mortars at early ages: evolution with time and degree of hydration. Adv. Cem. Based Mater. **3**, 94–106 (1996)
332. De Belie, N., Grosse, C.U., Kurz, J., Reinhardt, H.-W.: Ultrasound monitoring of the influence of different accelerating admixtures and cement types for shotcrete on setting and hardening behaviour. Cem. Concr. Res. **35**, 2087–2094 (2005)
333. Tazawa, E.: Autogenous Shrinkage of Concrete. CRC Press (1999)
334. Cartwright, C.P., Rajabipour, F., Radlińska, A.: Measuring the chemical shrinkage of alkali-activated slag cements using the buoyancy method. In: Mechanics and Physics of Creep, Shrinkage, and Durability of Concrete 308–315 (2013)
335. Chen, W., Brouwers, H.J.H.: The hydration of slag, part 1: reaction models for alkali-activated slag. J. Mater. Sci. **42**, 428–443 (2007)
336. Ye, H., Radlińska, A.: Quantitative analysis of phase assemblage and chemical shrinkage of alkali-activated slag. J. Adv. Concr. Technol. **14**, 245–260 (2016)
337. Li, Z., Liang, X., Liu, C., et al.: Thermal deformation and stress of alkali-activated slag concrete under semi-adiabatic condition: experiments and simulations. Cem. Concr. Res. **159**, 106887 (2022)
338. Ye, H., Radlińska, A.: Carbonation-induced volume change in alkali-activated slag. Construct. Build. Mater. **144** (2017)
339. Liu, C., Li, Z., Ye, G.: Mechanisms of efflorescence of alkali-activated slag. Cement Concr. Compos. **155**, 105811 (2025). https://doi.org/10.1016/j.cemconcomp.2024.105811